THE VIBRATIONAL AND ELECTRONIC SPECTRUM, AND THE POTENTIAL FIELD OF VARIOUS MANGANESE CARBONYL COMPLEXES

Thesis by

David Keith Ottesen

In Partial Fulfillment of the Requirements

For the Degree of

Doctor of Philosophy

California Institute of Technology

Pasadena, California

1971

(Submitted September 16, 1970)

To Jo Ann

ACKNOWLEDGMENTS

I thank Dr. J. Michael Smith who first suggested this topic of research to me. I am especially grateful to Professor Harry B. Gray at Caltech and Dr. Llewellyn Jones at the Los Alamos Scientific Laboratory for their continued interest and aid in the course of my studies.

I am grateful to my colleagues, especially Mr. D. Titus, for their assistance in my research and many enlightening discussions.

My thanks are given to my parents for their devotion and support, and to Professors Latimer Evans and Robert Rowan at New Mexico State University for their encouragement of my early scientific endeavors.

I am most grateful to my wife, Jo Ann, for her aid in typing the majority of this thesis.

Finally I wish to acknowledge the financial support of this Institute, the Atomic Energy Commission through three summers spent at the Los Alamos Scientific Laboratory, and the National Science Foundation.

ABSTRACT

I.

The infra-red and Raman spectra of $Mn(CO)_5Br$ as both solid and CH_2Cl_2 solution from 50 to 2150cm $^{-1}$ are presented for the normal isotopic compound, and the ^{13}CO and $C^{18}O$ substituted molecules. The observed bands are assigned, and the force constants and compliance constants of a general quadratic potential field are calculated using the FG method of Wilson, Decius, and Cross.

II.

The infra-red and Raman spectra of both $Mn_2(^{12}CO)_{10}$ and $Mn_2(^{13}CO)_{10}$ as solids and in CH_2Cl_2 solutions from 50 to 2150cm^{-1} are presented and are assigned. Potential constants are calculated using values transferred from the $Mn(CO)_5Br$ calculations. Special attention is paid to splitting interactions across the Mn--Mn bond and to the Mn--Mn stretching potential constants.

III.

Raman intensities and the electronic absorption spectrum of $M(CO)_5X^{n-}$ compounds are presented and discussed.

TABLE OF CONTENTS

I.

VIBRATIONAL ANALYSIS OF MANGANESE PENTACARBONYL BROMIDE

CHAPTER 1

INTRODUCTION -- THE INTERPRETATION OF CHEMICAL BONDING IN METAL CARBONYL COMPLEXES VIA THEIR OBSERVED VIBRATIONAL SPECTRA

In the past few years a large number of vibrational analyses dealing with metal-carbonyl complexes have appeared in the literature; some of the more thorough of these investigations are (1-14). For the main part, however, these studies dealt with assignments of infra-red frequencies which are primarily C--O stretching vibrations and the calculation of force fields of greater or lesser complexity for these vibrational coordinates. These simple calculations have proved quite useful in the interpretation of bonding changes when one or more ligands is substituted for a CO group or groups. (8, 15)

We may infer the nature of the substituted ligand-to-metal bond by observing changes in the C--O stretching frequencies on the basis of the synergic $d\pi \rightarrow \pi^*$CO "back-bonding" model. This is illustrated below in figure 1.

A brief explanation is that in the case of octahedrally substituted complexes (with which this work deals exclusively) a given CO ligand will be in competition with the substituted ligand trans to itself for the d-π electrons in the metal orbital which may combine with the

π^* antibonding orbitals of the ligands.

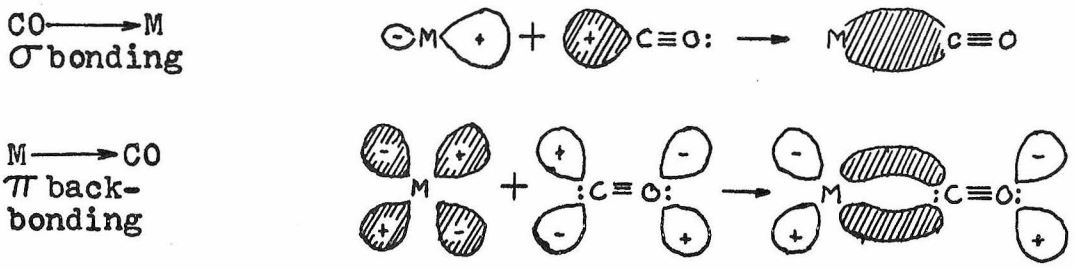

Figure 1. Synergic Model of Metal-CO Bonding (16)

As a first approximation it is considered (1) that the trans interaction will be twice that of a cis interaction simply because the metal may back-bond to two trans-ligands through two d-orbitals, while only one d-orbital of the appropriate symmetry for back-bonding is common to two cis-ligands.

From this postulate we reason that a ligand of less π-accepting character than a CO group will have the effect of increasing the $d\pi \rightarrow \pi^*$ bonding in the CO group trans to itself while exerting a much smaller effect in those ligands cis to itself. As the bond order of the trans M--C bond rises however, the trans C--O bond order will decrease due to the increasing population of electrons

in the π^* anti-bonding orbital.

This should have the net effect of lowering the trans CO stretching frequency and raising the trans MC stretching frequency relative to the unsubstituted compound.

A second effect will be changes in the electron density of the sigma bonding system due to differences in the electronegative character of the substituted ligand. The two effects are by no means separable; however, the predominance of one effect over the other is believed responsible for systematic variations in frequency and intensity of the Raman active M--C stretching modes of the $M(CO)_5X^{n-}$ (M = Cr or Mn) systems. This is discussed in conjunction with the electronic spectra of these molecules in Part III.

Part I of this thesis is devoted to a complete vibrational analysis and normal coordinate calculation of the molecule $Mn(CO)_5Br$. The motivation for this work was to accurately and fully assign the observed vibrational spectrum of this molecule and from this to calculate a potential field which could be compared with simpler force constant calculations.

We may gain by this a knowledge of the accuracy and limitations inherent in previous work concerned only with "C--O stretching" vibrations.

A further extension of this work is the transfer of

the calculated force field to the more complicated $Mn_2(CO)_{10}$ system; the remaining interaction constants in this binuclear complex will define the splitting of vibrations whose symmetry coordinates differ from each other only in regard to the rotation axes perpendicular to the metal-metal bond; i.e.,

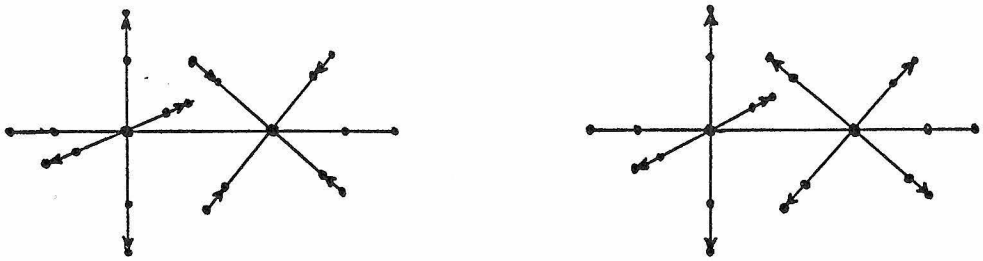

The magnitude and sign of these interaction constants may give information concerning the electronic structure of the metal-metal bond system. These approximate transfer calculations will be discussed in Part II.

CHAPTER 2

THE VIBRATIONAL SPECTRUM OF $Mn(CO)_5Br$

This compound was prepared in accordance with the literature method (17) by the reaction of Br_2 in CCl_4 solution with commercially available $Mn_2(CO)_{10}$ at room temperature for about 15 minutes. The yellow-orange product is considerably less soluble in CCl_4 than the parent carbonyl and it precipitates out of the reaction mixture.

The initial product usually showed only traces of $Mn_2(CO)_{10}$ or $Mn_2(CO)_8Br_2$ present. The former could be extracted by a suitable hydrocarbon solvent such as cyclohexane while the latter, being even less soluble than $Mn(CO)_5Br$ in halocarbons, could be removed by recrystallization from a solvent such as $CHCl_3$ or CH_2Cl_2.

This procedure yielded the pure monomeric compound whose CCl_4 solution I. R. spectrum from 2150 to 1950cm^{-1} agreed with the literature values (6). This was taken as the criterion for purity when accurate spectral measurements were taken.

The intense bands in both the I. R. and Raman spectra were found to fall into three energy groups; they are 2150 to 1950cm^{-1}, 650 to 200cm^{-1}, and 150 to 50cm^{-1}. The highest energy vibrations may be assigned to modes involving principally C--O stretching motion and these

are discussed below.

C--O Stretching Vibrations

The symmetry of this molecule is C_{4v} and the geometry along with the internal vibration coordinates are shown in figure 2. The observed I. R. and Raman spectra are illustrated in figures 3 and 4 and consist of one moderate band, one very strong band, and one strong band in the infrared in order of decreasing energy; in the Raman spectrum there are two strong bands followed by a moderate band in order of decreasing energy.

Group theory predicts the symmetry of the CO stretching modes to be $2A_1 + B_1 + E$. Of these the B_1 mode will I. R. inactive, and all four modes should be Raman active. These "symmetry" coordinates are shown in figure 11.

It should be emphasized firmly at this point that these coordinates do not describe exactly the vibrations involved but merely serve as useful approximations. The calculations in the following chapter will yield the amount of other symmetry coordinates which is mixed with each of these in determining the molecule's normal coordinates of vibration. The neglecting of mixing is precisely the approximation in simpler force field calculations which were mentioned in Chapter 1.

The assignment of these CO bands has been well established (6,18) and is as follows. The mode at 2085 in

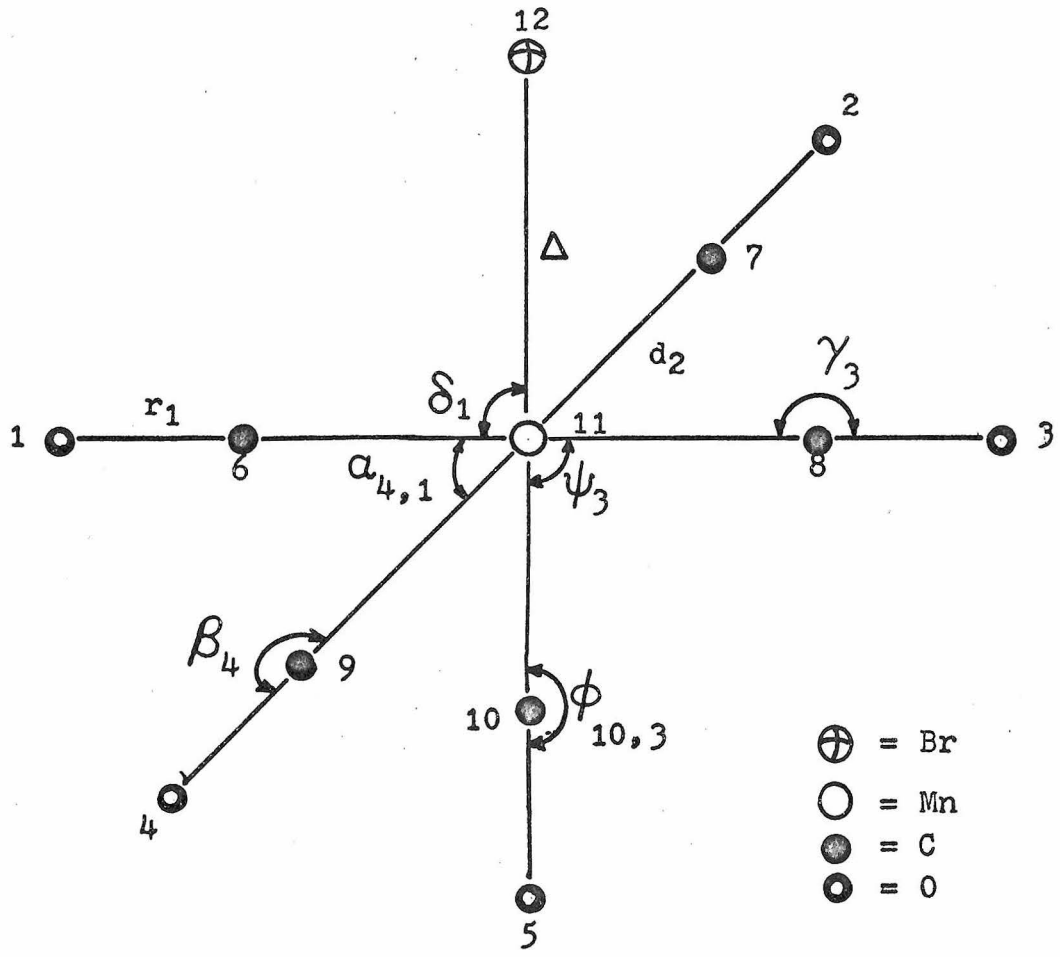

Figure 2. Internal Coordinates for $Mn(CO)_5Br$

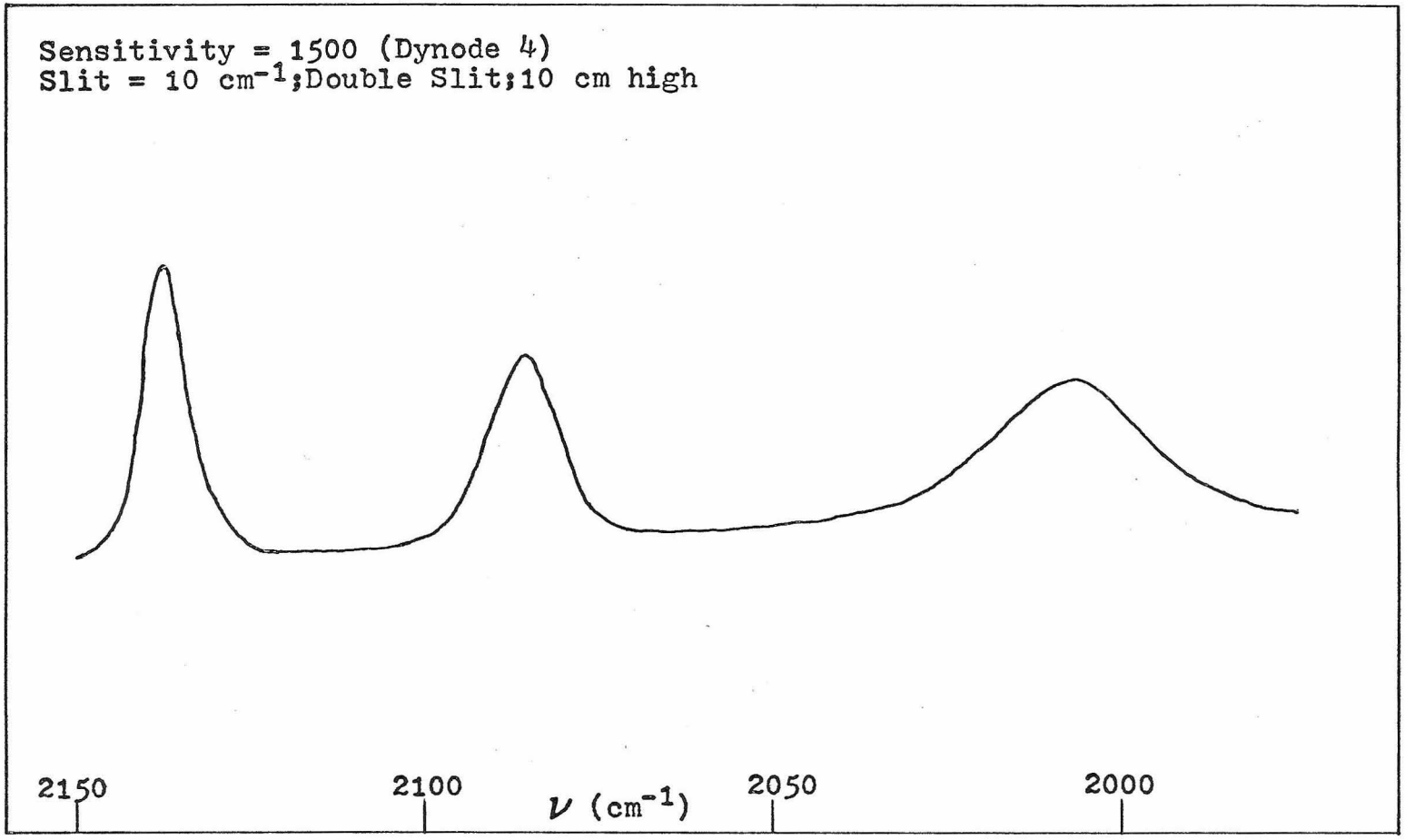

Figure 3. Raman Spectrum of $Mn(CO)_5Br$ in CH_2Cl_2 Solution

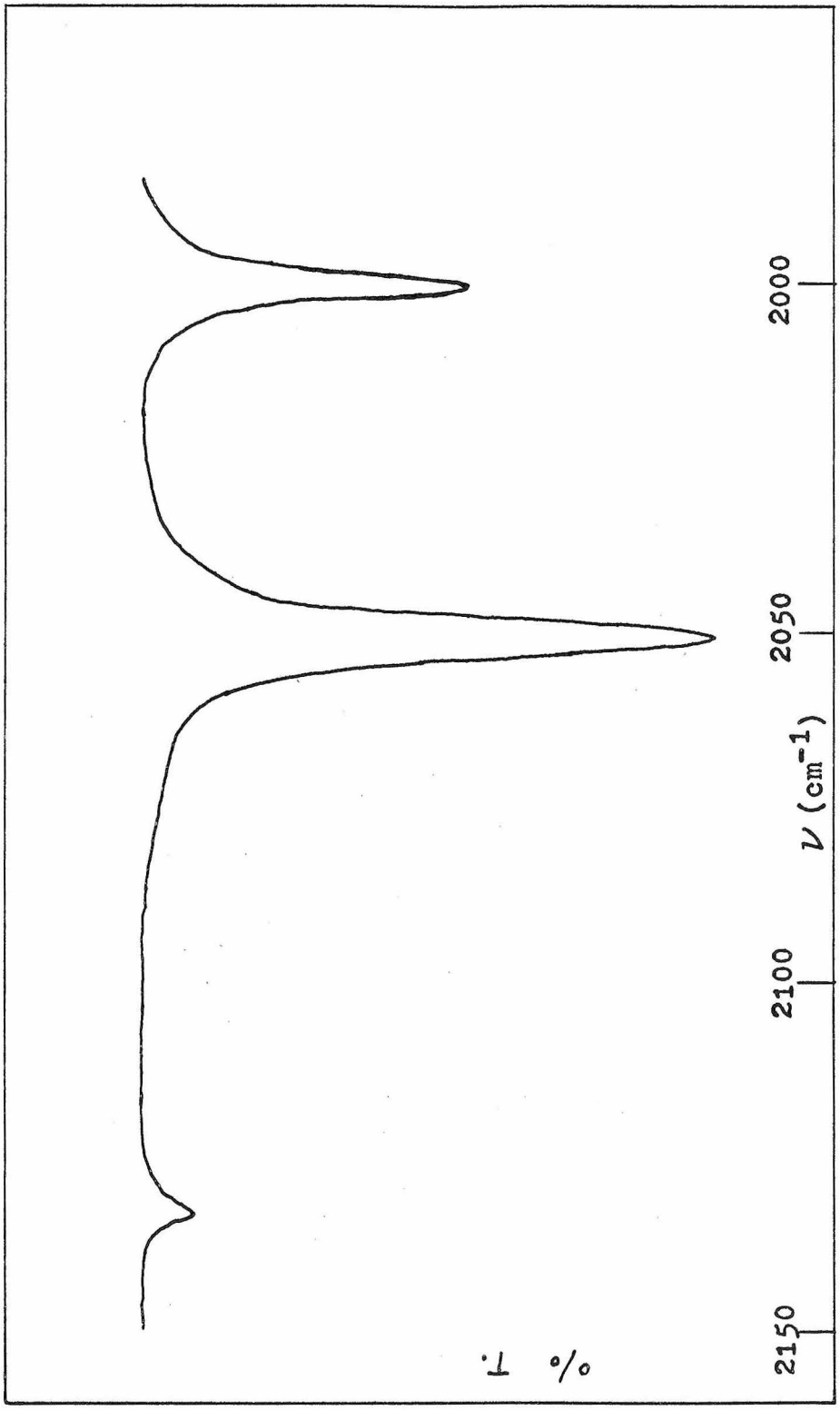

Figure 4. I.R. Spectrum of $Mn(CO)_5Br$ in C_6H_{12} Solution

the Raman is assigned as $(B_1)_{CO\text{-}r_i}$ as it appears to be I. R. inactive.

The weak band at 2138 in the I. R. is assigned as $(A_1)_{CO\text{-}r_i}$ as this band is expected to have the lowest intensity of the three I. R. modes. If the radial-CO ligands were actually planar and if this mode were unmixed with the A_1 axial-CO stretch, this band should have zero intensity.

The very intense I. R. band at 2052 is assigned as $(E)_{CO\text{-}r_i}$ as it does not appear in the Raman spectrum. This is reasonable as the Raman intensity of the E mode arises from the α_{zx} and α_{yz} terms of the polarizability tensor which are expected to be considerably smaller than the α_{zz} diagonal term responsible for the intensity of the A_1 axial mode.

This assignment leaves the band at 2007 as the $(A_1)_{CO\text{-}r_o}$ vibration. The synergic back-bonding model in the introduction agrees entirely with these assignments requiring that the (A_1) axial-CO mode occur at lowest energy. As Br^- is a considerably poorer π-electron acceptor than a CO ligand, it is expected that the $d\pi$-$p\pi^*$ electron density will increase for the axial Mn--C bond, and the order of the C--O axial bond will thus decrease relative to the radial C--O bonds.

Mn--C--O bending, Mn--C and Mn--Br stretching Vibrations

The next highest energy-group of bands is found between 650 and 200cm^{-1} and these are shown in figures 5, 6, 7, and 8. From studies on the Cr subgroup hexacarbonyls (14) and by comparison with spectra of other pentacarbonyl halide derivatives of Mn (19 - 21) these bands may be assigned as Mn--C--O bending modes from 650 to 400cm^{-1} and Mn--C stretching modes from 500 to 350cm^{-1}; the Mn--Br stretching mode should be found between 200 and 250cm^{-1}.

The symmetry of these modes is:

MCO Bend = $A_1 + A_2 + B_1 + B_2 + E$

MC Stretch = $2A_1 + B_1 + E$; MBr Stretch = A_1

The internal symmetry coordinates for these vibrations are in figure 11. A very helpful tool in the assignment of these modes to observed frequencies is the phenomenon of Raman depolarization ratios for solution spectra. Experimentally this involves the use of a polaroid film and a linearly polarized exciting source (which is satisfied by the available He-Ne laser instrumentation). Two readings are taken for a given band intensity, first with the analyzer film's electric vector perpendicular to the laser light's electric vector, and second with these vectors parallel.

Raman intensity theory (22) predicts a ratio of

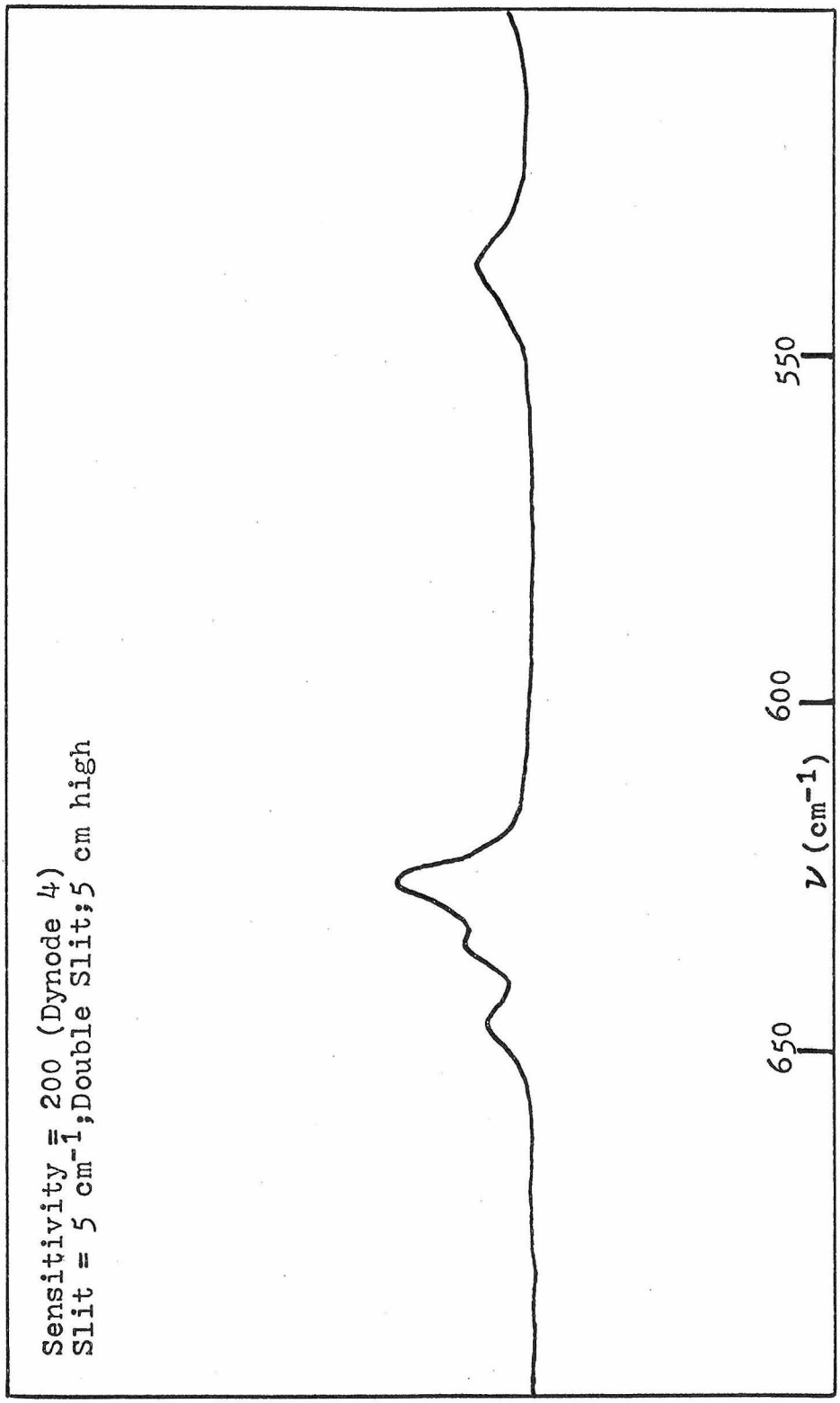

Figure 5. Raman Spectrum of Solid $Mn(CO)_5Br$

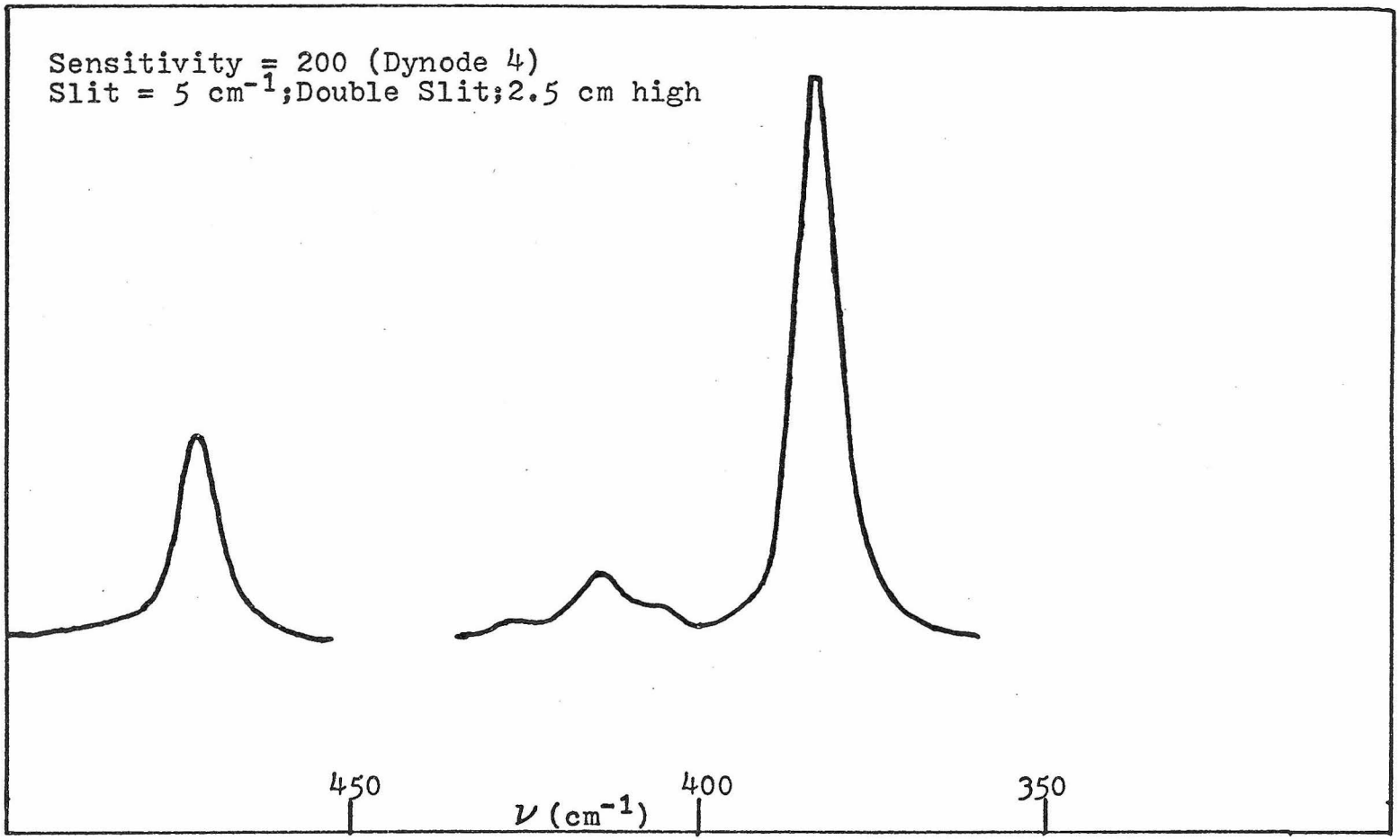

Figure 6. Raman Spectrum of Solid $Mn(CO)_5Br$

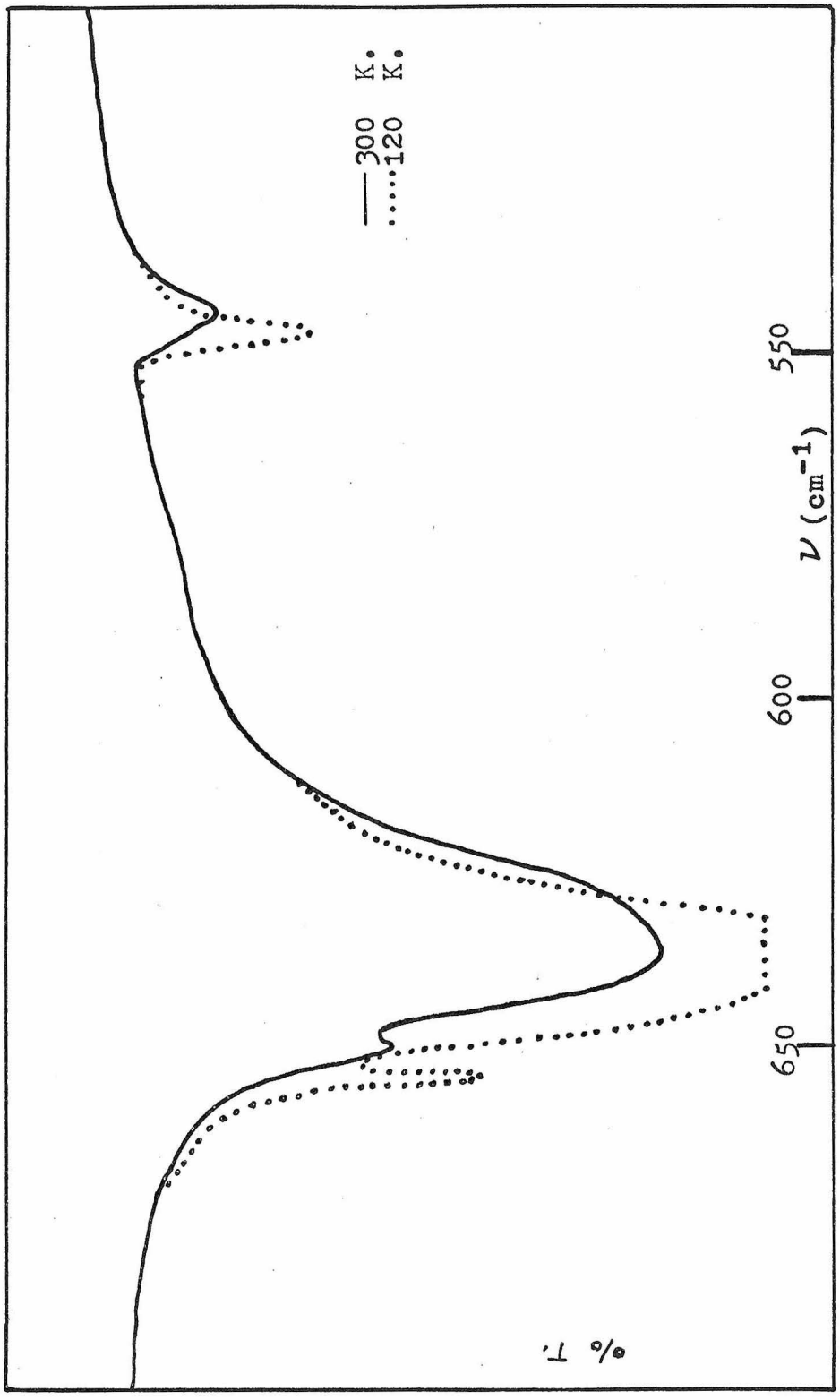

Figure 7. I.R. Spectrum of $Mn(CO)_5Br$ in a KBr Pressed Disc

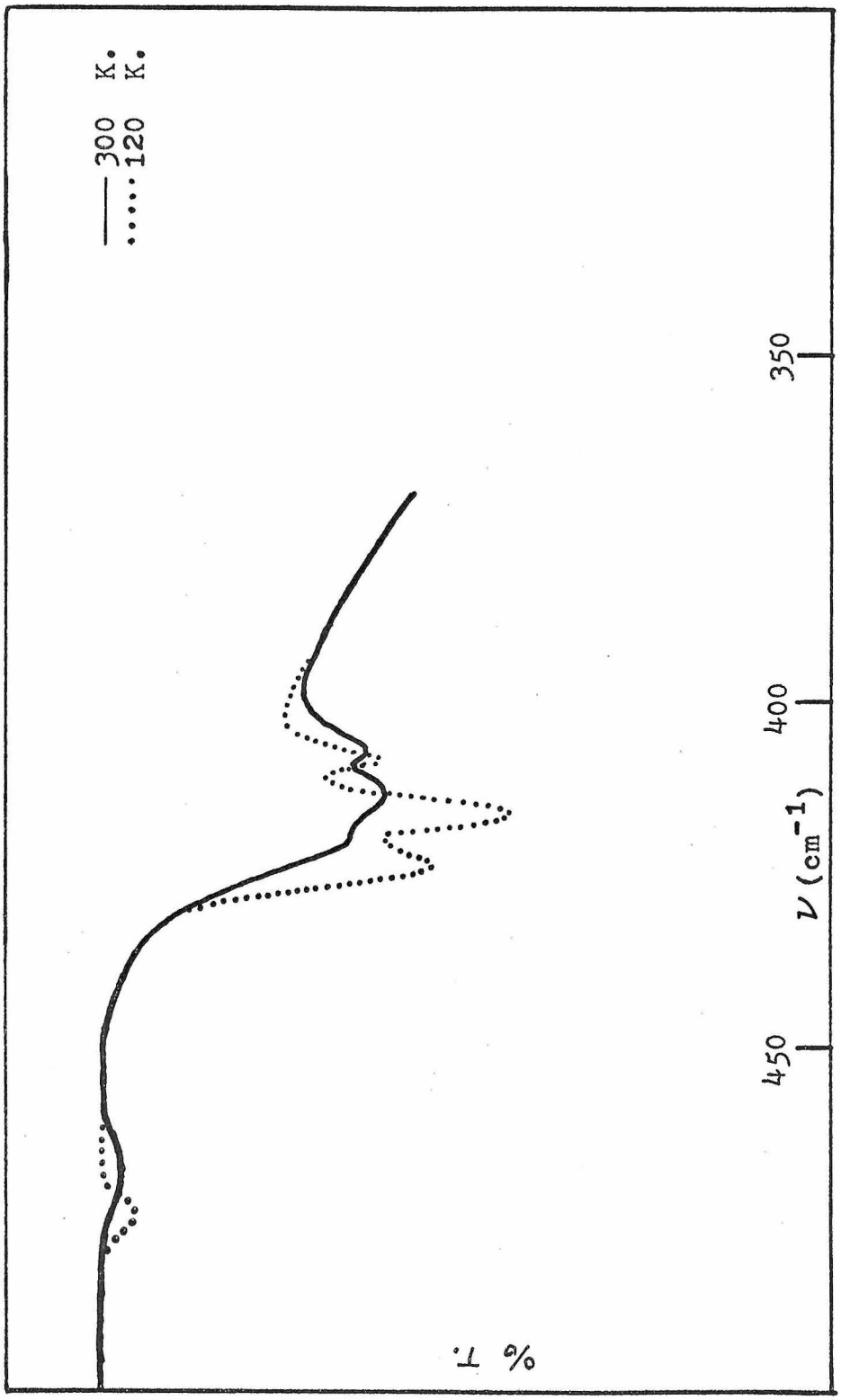

Figure 8. I.R. Spectrum of $Mn(CO)_5Br$ in a KBr Pressed Disc

.75 for all peaks except those modes which are totally symmetric (in this case, A_1 vibrations) which may have a ratio somewhere between 0 and .75.

Three strongly polarized bands were observed in CH_2Cl_2 solution at 222, 381, and 470cm^{-1}. The lowest of these A_1 modes is assigned to $(A_1)_\Delta$, the Mn--Br stretching vibration. In accordance with the bonding model and the studies on $M(CO)_6$, the axial Mn--C stretching vibration should occur at higher energy than the radial Mn--C stretch, and both should fall between 350 and 500cm^{-1}. Thus ν_{381} is assigned to $(A_1)_{d_i}$ and ν_{470} to $(A_1)_{d_o}$.

There remains one polarized Raman band in this energy range which was not observed; this is the A_1 Mn--C--O out-of-plane bending mode. This has previously been assigned to the 470cm^{-1} frequency (*19*) but this is deemed highly unreasonable in view of the recent studies on $M(CO)_6$ compounds (*14*). For these octahedral complexes the vibration corresponding to $(A_1)_\gamma$ is the I. R. active F_{1u} mode observed at 665cm^{-1} for $Cr(CO)_6$ in CCl_4 solution. Thus the assignment of the two observed Raman polarized bands as Mn--C stretches is retained as the most reasonable.

The moderate I. R. peak at 417cm^{-1} is assigned as the $(E)_{d_i}$ mode, and the moderately weak Raman band in the solid at 414cm^{-1} is assigned to $(B_1)_{d_i}$.

When the symmetry of octahedral $M(CO)_6$ is lowered

from O_h to C_{4v} in $M(CO)_5X$, the F_{1u} MCO bend is split into components of A_1 and E symmetry. This is diagrammed along with the changes in symmetry for the other MCO bending modes in figure 12. We therefore take the bands at 638 and 645cm^{-1} in the I. R. CH_2Cl_2 solution spectrum as $(A_1)_\gamma$ and $(E)_\beta$. The band at 638cm^{-1} is the more intense in the I. R. and the less intense in the Raman; further, the highest energy MCO bend for $Mn_2(CO)_{10}$ in CH_2Cl_2 solution has been observed as a <u>polarized</u> Raman band at 670cm^{-1} and is the A_1 mode analagous to $(A_1)_\gamma$ for $Mn(CO)_5Br$. From these facts we take the ordering $\nu_{645} \longrightarrow (A_1)_\gamma$ and $\nu_{638} \longrightarrow (E)_\beta$.

The remaining two I. R. peaks at 604cm^{-1} and 545cm^{-1} must be $(E)_\gamma$ and $(E)_\phi$ while the Raman active peaks at 627cm^{-1} and 535cm^{-1} in the solid are assigned as the $(B_1)_\gamma$ and $(B_2)_\beta$ modes. To obtain the proper ordering of these modes we make use of the synergic back-bonding model to predict changes in these frequencies between $Cr(CO)_6$ and $Mn(CO)_5Br$.

From the symmetry correlation diagram in figure 12 it is seen that both B_1 and B_2 modes should lie around 530cm^{-1}; from the observed spectra it is obvious that one of the modes has been shifted to considerably higher energy. The bonding model predicts a higher

electron density in the d_{zx} and d_{yz} orbitals between the Mn atom and axial-CO group than in the d_{xy} orbital shared by the radial-CO groups. The B_1 bending mode involves the γ, out-of-plane, coordinate, and the main effect of this motion (as illustrated by the isotopic shifts in Chapter 3) is the displacement of a radial C atom in an axial direction. The B_2 bending mode will move the same C atom in the in-plane direction perpendicular to the M--C--O axis. Thus the B_1 mode will involve primarily distortion of the π bonding in the d_{zx} and d_{yz} to CO-π* orbitals, while the B_2 mode will cause distortions mainly in the d_{zx} or d_{yz} and the less occupied d_{xy} to CO-π* systems.

This implies the restoring force will be greater for the out-of-plane B_1 mode than the in-plane B_2 mode and we assign $\nu_{627} \longrightarrow (B_1)_\gamma$ and $\nu_{535} \longrightarrow (B_2)_\beta$.

The two remaining E modes have apparently both shifted to higher energy from the analogous modes in $Cr(CO)_6$ indicating that considerable mixing of these two internal coordinates is occurring. Calculations on both possible assignments for ν_{604} and ν_{545} with $(E)_\gamma$ and $(E)_\phi$ have been carried out.

The inactive $(A_2)_\beta$ mode was not observed and its position is calculated from the potential field described in Chapter 3.

C--Mn--C and C--Mn--Br Bending Vibrations

These vibrations are expected to occur between 200 and 50cm^{-1} and are shown in figures 9 and 10. A complicating factor might be the presence of lattice modes in the spectra of the solid compound. Due to the rather low solubility of $Mn(CO)_5Br$ in even CH_2Cl_2 it was necessary to obtain data in the solid phase as only one band was observed for Raman solution spectra and no bands were observable in I. R. solution spectra. Fortunately the $Mn(CO)_5Br$ molecule is neutral and it is reasonable that the intermolecular forces are quite small. Thus the optically active lattice modes may quite reasonably be assumed to lie below 50cm^{-1} with the result that all observed bands may be assigned to internal vibrations.

Not only did solubility problems limit any information which could be obtained from Raman depolarization experiments, but also the solid I. R. and Raman spectrum proved to be quite complex; further, a lack of trends between the spectra of the Cl, Br, and I pentacarbonyl compounds (19-21) indicates that a large amount of mixing is occurring among the symmetry coordinates chosen to describe the vibrational modes. This simply means that changing the halogen ligand will affect not

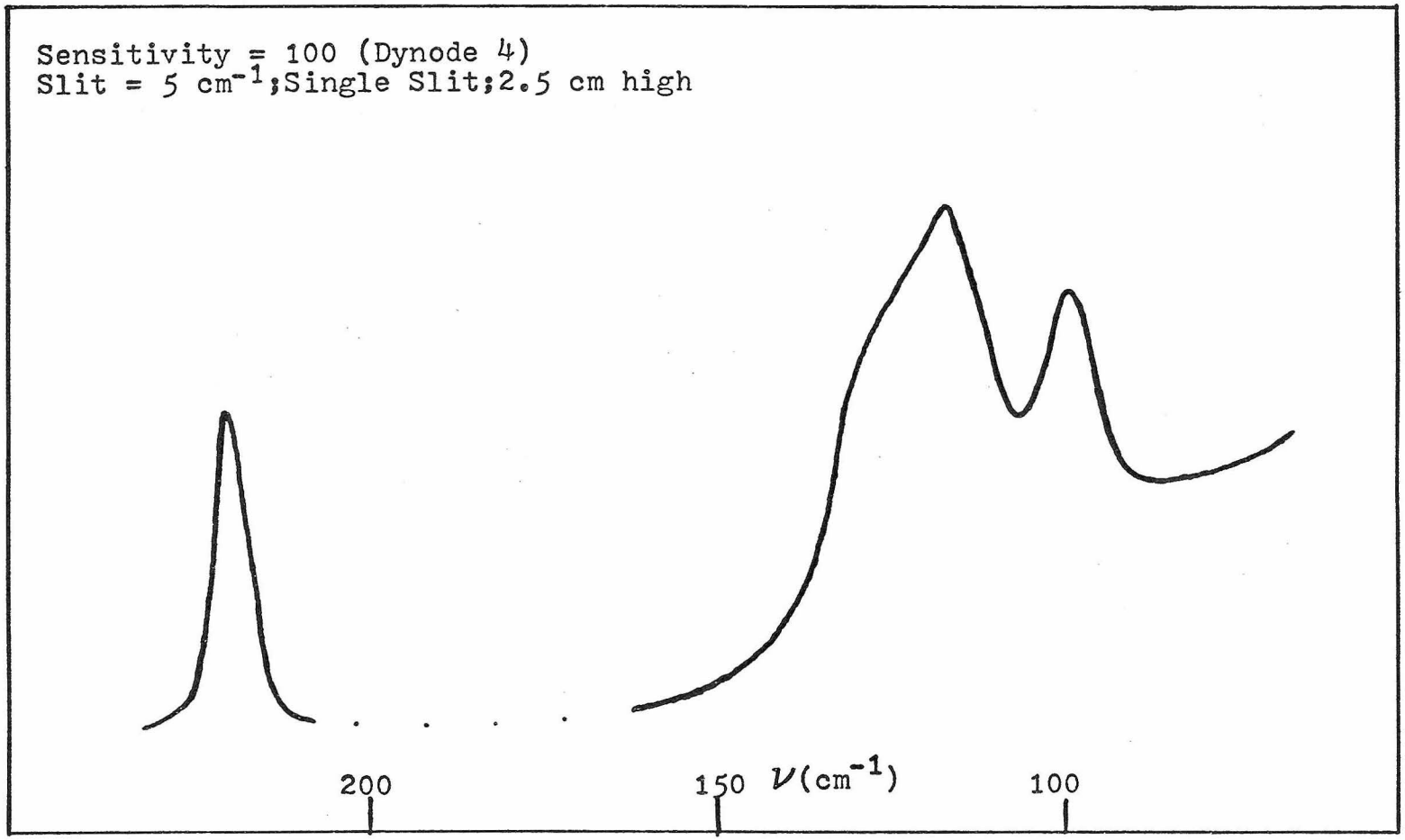

Figure 9. Raman Spectrum of Solid $Mn(CO)_5Br$

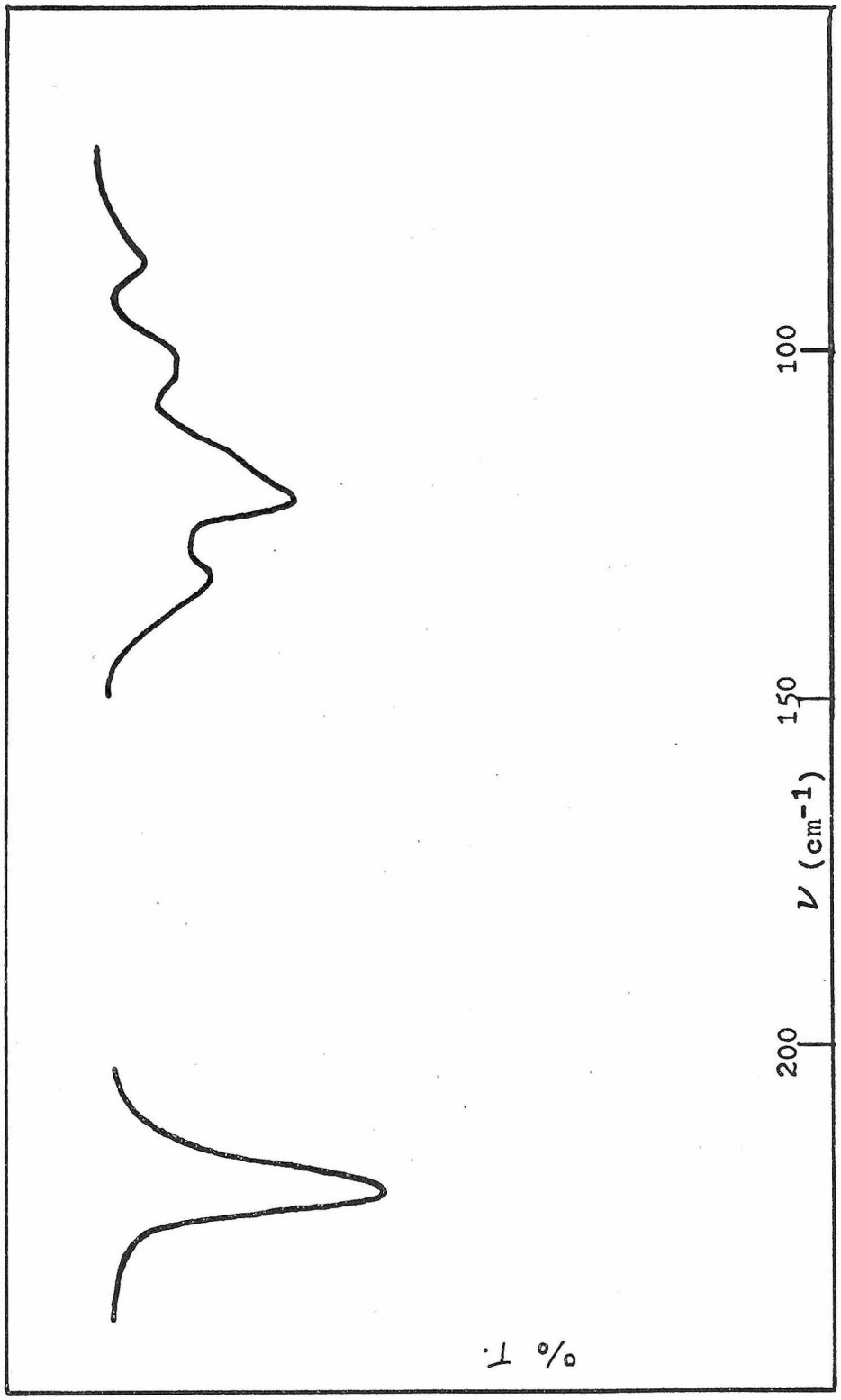

Figure 10. I.R. Spectrum of Mn(CO) Br in a Concentrated Nujol Mull

only the frequency having to do with C--Mn--X bending, but will perturb, to a certain extent, all the deformation modes of the same symmetry.

The symmetry of the modes in this energy range is:

C--Mn--C bend = $A_1 + B_1 + B_2 + 2E$

C--Mn--Br bend = E.

These are shown in figure 11. Experiments on $Mn_2(CO)_{10}$ in CH_2Cl_2 indicate the totally symmetric C--Mn--C bend lies around $111cm^{-1}$; this is analogous to $(A_1)_{\psi-\delta}$ and thus this band is assigned to the very intense Raman mode at $116cm^{-1}$. The I. R. band at $133cm^{-1}$ seems to be very weak in the Raman and is thus assigned as a C--Mn--C bend of E symmetry; due to the weaker bonding and the heavier atom involved, it is expected that the $(E)_\delta$ mode involving mostly C--Mn--Br bending will be at considerably lower energy than $133cm^{-1}$, thus this band is either $(E)_\psi$ or $(E)_\alpha$. The intense Raman bands at $129cm^{-1}$ and $99cm^{-1}$ are assigned to $(B_2)_\alpha$ and $(B_1)_{\psi-\delta}$ on the basis of a symmetry correlation diagram with $Cr(CO)_6$ (figure 12). The weak I. R. band at $100cm^{-1}$ coincident with the Raman frequency at $99cm^{-1}$ is judged to be the I. R. forbidden $(B_1)_{\psi-\delta}$ mode; this mode is slightly allowed under the different selection rules prevailing for the lower factor-group symmetry of $Mn(CO)_5Br$ in the solid state.

The I. R. active—only band at $87cm^{-1}$ is the other member of the $(E)_{\psi}$ - $(E)_{\alpha}$ pair with the peak at $133cm^{-1}$. This leaves the very weak Raman and I. R. band at $\sim 53cm^{-1}$ as the $(E)_{\delta}$ mode.

While these assignments are certainly only tentative, it will be seen in Chapter 3 that a quite good agreement of the calculated potential field compared with values transferred from $Cr(CO)_6$ (14) is obtained for this assignment.

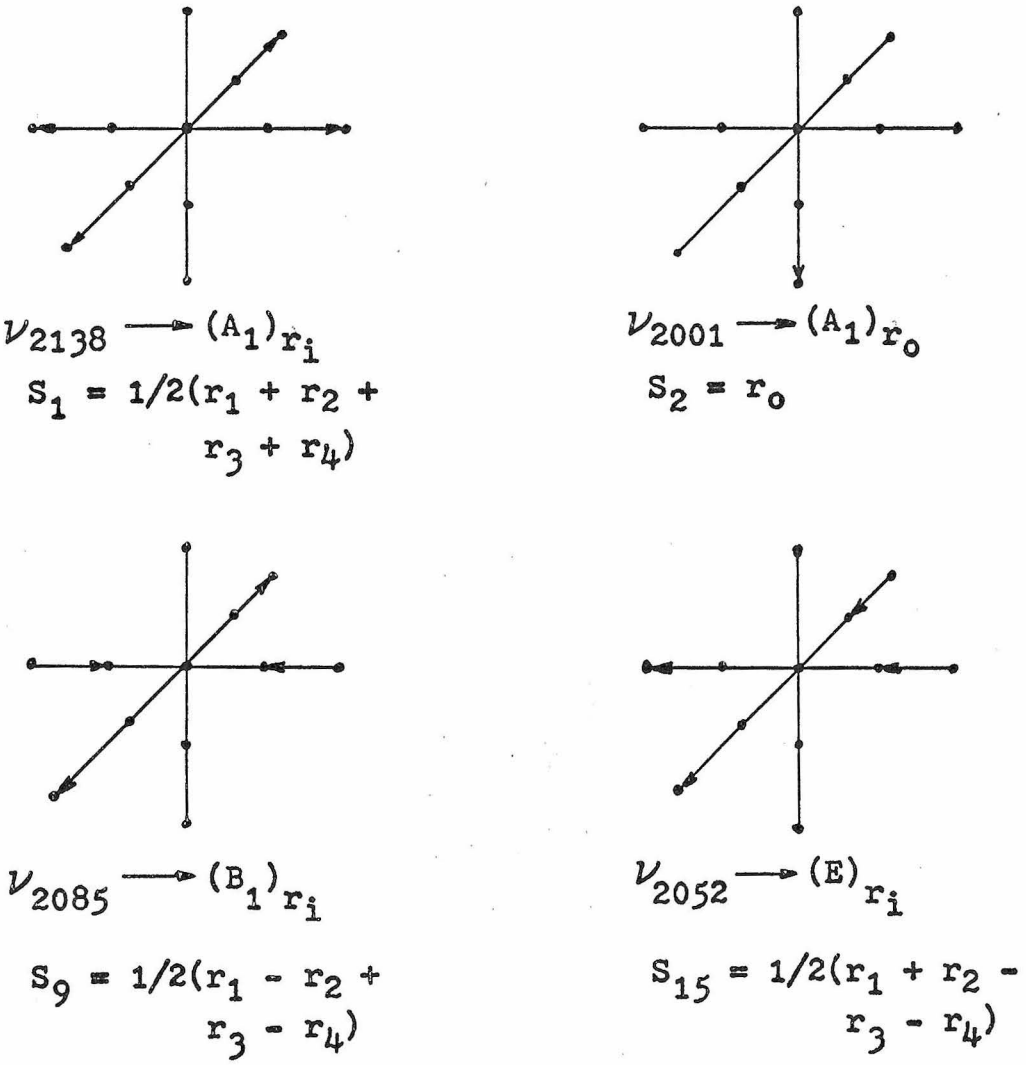

Figure 11. Internal Symmetry Coordinates and Frequency Assignments for C--O Stretching Modes

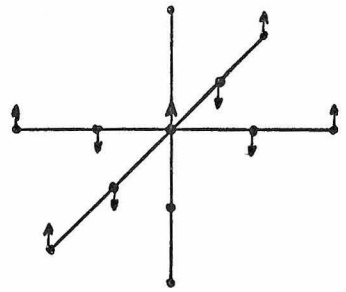

$\nu_{645} \rightarrow (A_1)_\gamma$

$S_3 = 1/2(\gamma_1 + \gamma_2 + \gamma_3 + \gamma_4)$

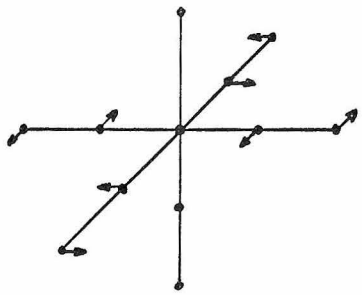

not obsd. $\rightarrow (A_2)_\beta$

$S_8 = 1/2(\beta_1 + \beta_2 + \beta_3 + \beta_4)$

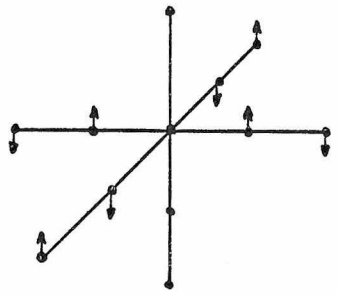

$\nu_{627} \rightarrow (B_1)_\gamma$

$S_{10} = 1/2(\gamma_1 - \gamma_2 + \gamma_3 - \gamma_4)$

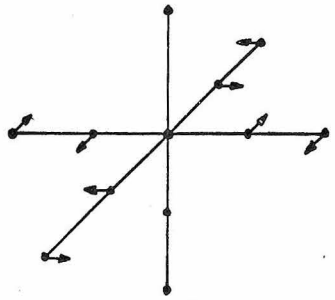

$\nu_{535} \rightarrow (B_2)_\beta$

$S_{13} = 1/2(\beta_1 - \beta_2 + \beta_3 - \beta_4)$

Figure 11. Internal Symmetry Coordinates and Frequency Assignments for M--C--O Bending Modes

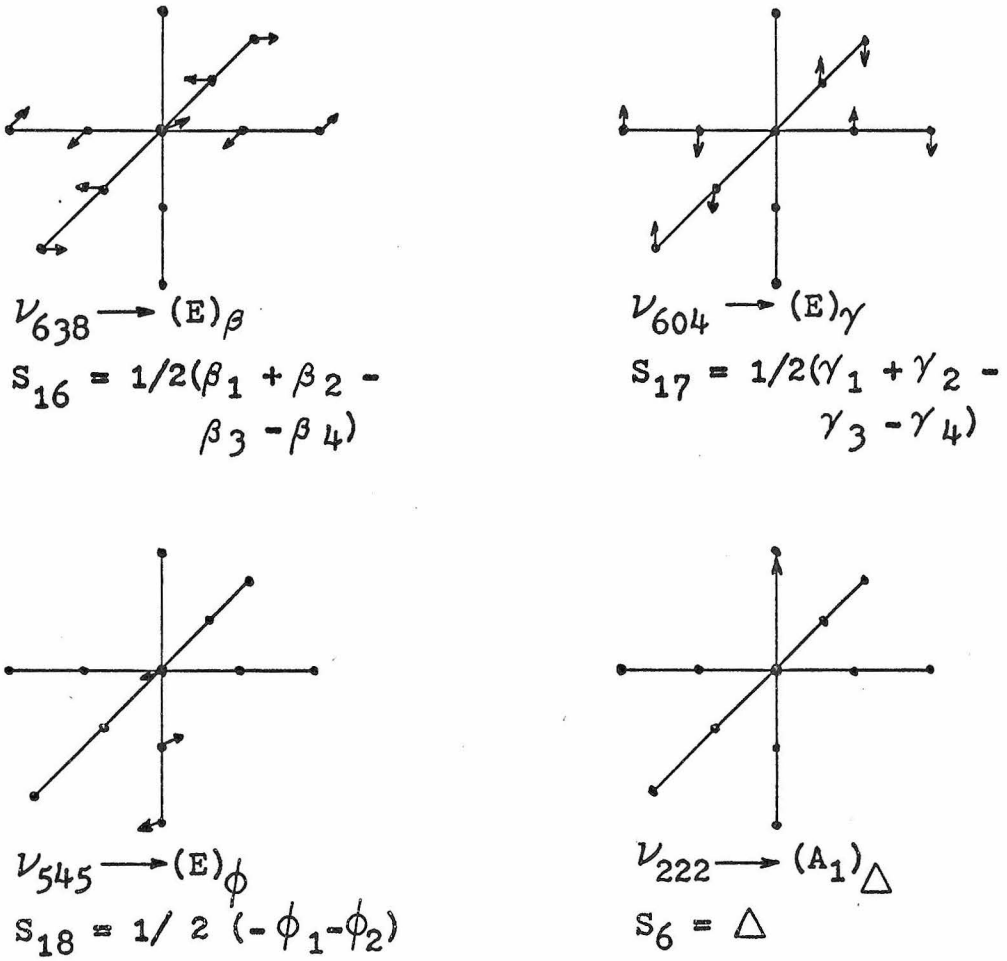

Figure 11. Internal Symmetry Coordinates and Frequency Assignments for M--C--O Bending Modes and M--Br Stretching Mode

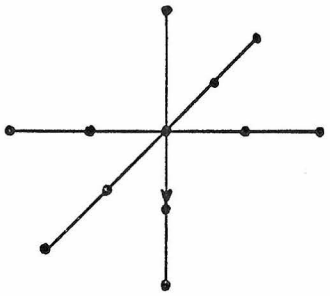

$\nu_{470} \longrightarrow (A_1)_{d_o}$

$S_4 = d_o$

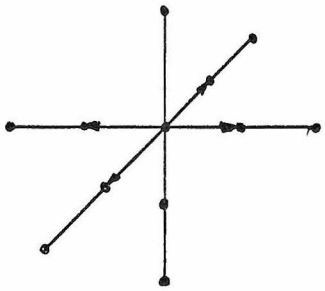

$\nu_{381} \longrightarrow (A_1)_{d_i}$

$S_5 = 1/2(d_1 + d_2 + d_3 + d_4)$

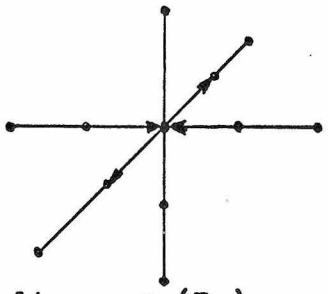

$\nu_{414} \longrightarrow (B_1)_{d_i}$

$S_{11} = 1/2(d_1 - d_2 + d_3 - d_4)$

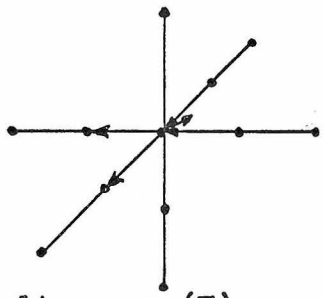

$\nu_{417} \longrightarrow (E)_{d_i}$

$S_{19} = 1/2(d_1 + d_2 - d_3 - d_4)$

Figure 11. Internal Symmetry Coordinates and Frequency Assignments for M--C Stretching Modes

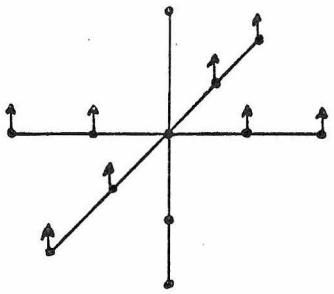

$\nu_{116} \longrightarrow (A_1)_{\psi-\delta}$

$S_7 = 1/2\ 2\ (\psi_1+\psi_2+\psi_3+\psi_4-\delta_5-\delta_6-\delta_7-\delta_8)$

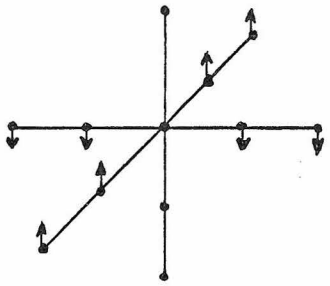

$\nu_{99} \longrightarrow (B_1)_{\psi-\delta}$

$S_{12} = 1/2\ 2\ (\psi_1-\psi_2+\psi_3-\psi_4-\delta_5+\delta_6-\delta_7+\delta_8)$

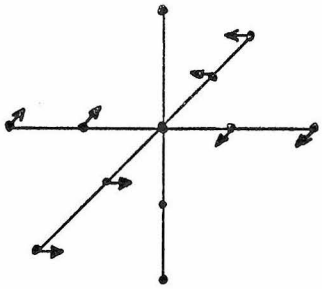

$\nu_{129} \longrightarrow (B_2)_{\alpha}$

$S_{14} = 1/2(\alpha_{12}-\alpha_{23}+\alpha_{34}-\alpha_{41})$

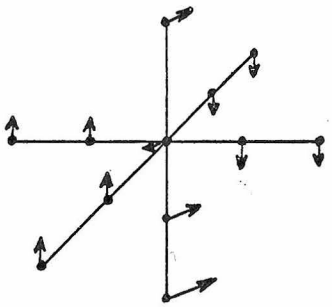

$\nu_{133} \longrightarrow (E)_{\psi}$

$S_{20} = 1/2(\psi_1+\psi_2-\psi_3-\psi_4)$

Figure 11. Internal Symmetry Coordinates and Frequency Assignments for C--M--C Bending Modes

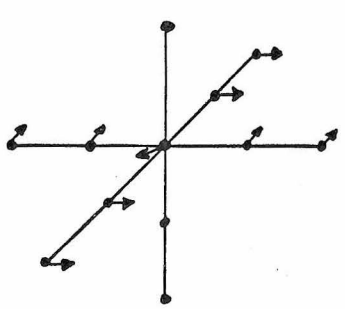

$\nu_{87} \longrightarrow (E)_{\alpha}$

$S_{21} = 1/\sqrt{2}\ (\alpha_{12} - \alpha_{34})$

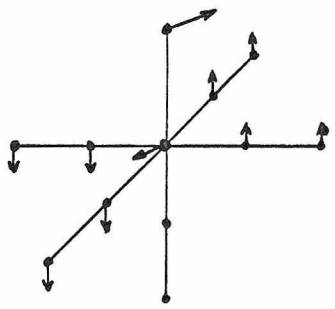

$\nu_{53} \longrightarrow (E)_{\delta}$

$S_{22} = 1/2(\delta_1 + \delta_2 - \delta_3 - \delta_4)$

Figure 11. Internal Symmetry Coordinates and Frequency Assignments for C--M--C and C--M--Br Bending Modes

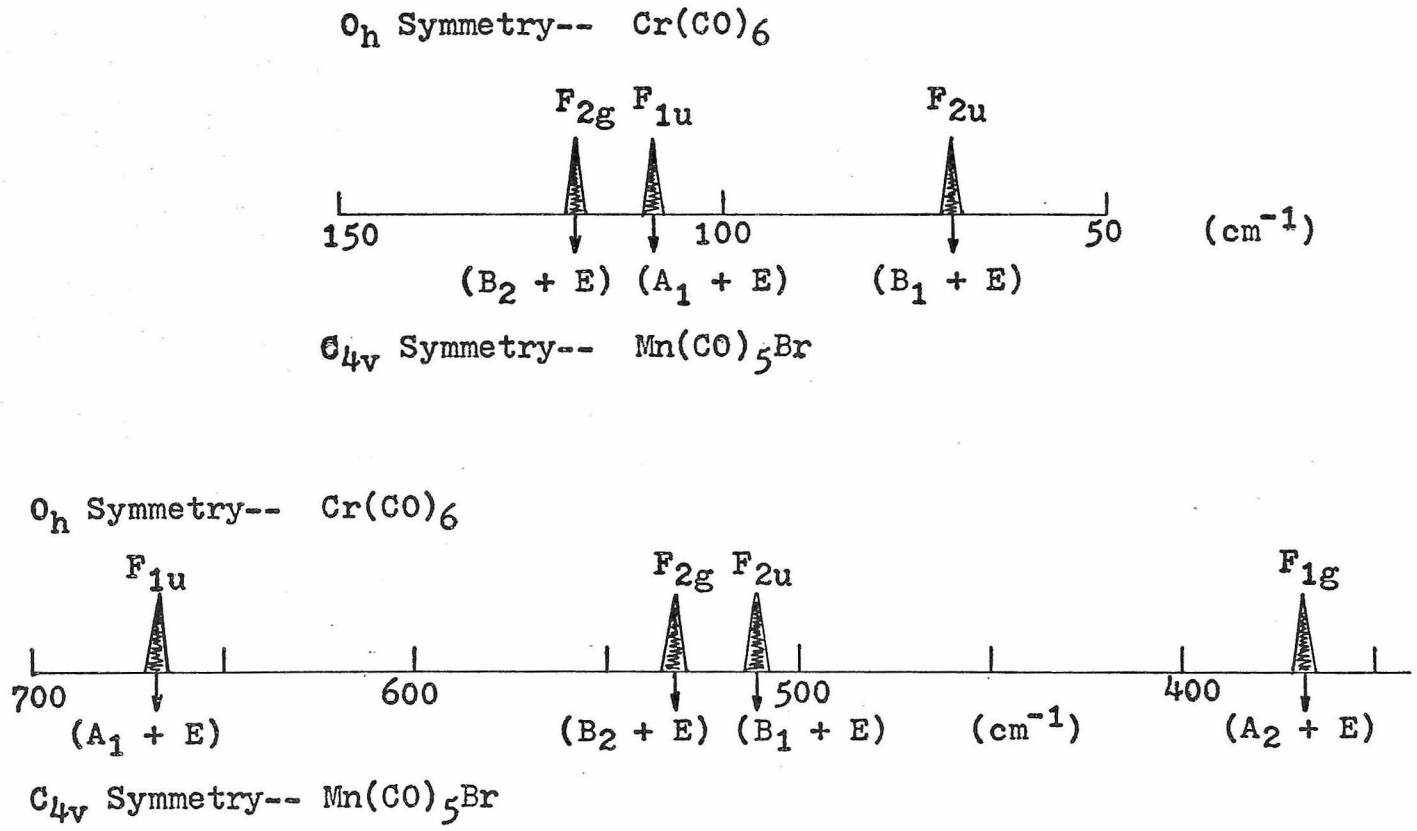

Figure 12. Correlation Diagram for $Cr(CO)_6$ and $Mn(CO)_5Br$

CHAPTER 3

ISOTOPIC SUBSTITUTION AND THE POTENTIAL FIELD OF $Mn(CO)_5Br$

Instrumentation

The vibrational spectra of $Mn(CO)_5Br$ and the other systems discussed in Part II were obtained with four instruments: I. R. spectra in the range 3000 to 200cm^{-1} were produced on Perkin-Elmer grating spectrometers #225 and #521. Most of these data were reproducible within the limit $\pm$ .5cm^{-1}. Similar accuracy (except for very weak or poorly resolved bands) was obtainable for the Raman spectra with a Cary 81 monochromator with a 100 mw. He-Ne laser (6328 A.) as an exciting source. Far I. R. spectra were obtained with an accuracy of $\sim \pm$ 1cm^{-1} on a Beckmann IR-11 grating spectrometer.

Isotopic Substitution

It has been found that the potential field of a given molecule will be invariant to isotopic substitution. This has been a tremendous aid in determining the potential fields of the simpler molecules; a simple change in the kinetic energy expressions to account for the presence of heavier or lighter nuclei together with

observed frequency shifts will furnish additional equations to solve for the unknown potential constants in the vibrational secular equation.

When as large a molecule as $Mn(CO)_5Br$ is being dealt with, the number of independent potential constants has risen to 78. There are, however, only 22 equations (from the 22 fundamental frequencies) to solve for these 78 constants, and without additional information the situation would be desperate to say the least.

Fortunately in the three summers I have spent at the Los Alamos Scientific Laboratory (LASL) I have had 95% $Mn(^{12}C^{18}O)_5Br$ (prepared by Mr. Maxwell Goldblatt at LASL) and 93% $Mn(^{13}C^{16}O)_5Br$ (prepared by myself at Caltech from $Mn_2(^{13}C^{16}O)_{10}$ on loan from LASL) made available to me during my research program.

It was attempted to obtain both I. R. and Raman spectra for these molecules in the common solvent, CH_2Cl_2. This proved impossible for the weaker Raman bands and in the far I. R. where CH_2Cl_2 absorbed too greatly (and where the compound also proved to be insufficienty soluble in non polar CCl_4 to show a spectrum). In these cases spectral data from the polycrystalline solid and nujol mull, respectively, were used. These data with their approximate error limits are presented in Tables 1, 2, and 3.

TABLE 1

Observed Intense Raman and Infra-red Bands for $Mn(CO)_5Br$ in CH_2Cl_2 Solutions

$Mn(^{12}C^{16}O)_5Br$		$Mn(^{13}C^{16}O)_5Br$		$Mn(^{12}C^{18}O)_5Br$	
Raman	Infra-red	Raman	Infra-red	Raman	Infra-red
222.4 ± 1	223.8 ± 1	221.6 ± .5	not obsvd.	220.6 ± .5	not obsvd.
380.5 ± .3	not obsvd.	374.8 ± .2	not obsvd.	366.5 ± .2	not obsvd.
not obsvd.	408.5 ± 1	not obsvd.	396.8 ± 1	not obsvd.	402.7 ± 1
not obsvd.	417.2 ± 1	not obsvd.	411.7 ± 1	not obsvd.	411.2 ± 1
not obsvd.	422.3 ± 2	not obsvd.	not obsvd.	not obsvd.	416.1 ± 2
470.4 ± .4	not obsvd.	462.3 ± .2	not obsvd.	459.8 ± .6	not obsvd.
not obsvd.	545.5 ± .2	not obsvd.	527.1 ± .2	not obsvd.	542.8 ± .2
not obsvd.	604.2 ± .2	not obsvd.	591.3 ± 1	not obsvd.	600.8 ± .2
not obsvd.	not obsvd.	605 ± 2	not obsvd.	not obsvd.	not obsvd.
not obsvd.	638.4 ± .7	not obsvd.	622.0 ± .7	not obsvd.	636.2 ± .7
not obsvd.	645.0 ± 1.5	631 ± 2	632.0 ± 1.5	not obsvd.	641.3 ± 1.5
2007.0 ± 1.0	2007.3 ± .2	1962.0 ± .4	1962.6 ± .2	obsvd. wkly.	1961.8 ± .2

TABLE 1 continued

$Mn(^{12}C^{16}O)_5Br$		$Mn(^{13}C^{16}O)_5Br$		$Mn(^{12}C^{18}O)_5Br$	
Raman	Infra-red	Raman	Infra-red	Raman	Infra-red
not obsvd.	2052.2 ± .2	not obsvd.	2007.0 ± .2	not obsvd.	2004.0 ± .2
not obsvd.	not obsvd.	not obsvd.	2053.1 ± .5	not obsvd.	not obsvd.
2085.4 ± .2	not obsvd.	2038.3 ± .2	not obsvd.	2038.1 ± .4	not obsvd.
2137.7 ± .2	2137.9 ± .2	2088.9 ± .6	2088.2 ± .3	2090.6 ± .3	2090.6 ± .2
not obsvd.	not obsvd.	not obsvd.	2107.6 ± .2	not obsvd.	not obsvd.

TABLE 2

Observed Intense Raman Bands for Solid $Mn(CO)_5Br$[a]

$Mn(^{12}C^{16}O)_5Br$	$Mn(^{13}C^{16}O)_5Br$	$Mn(^{12}C^{18}O)_5Br$
52.9 ± .1	not obsvd.	51.0 ± .2
99.0 ± .1	98.5 ± .1	95.6 ± .1
115.8 ± .6*	not	109.9 ± .6*
124.3 ± 1.5*	resolved	116.9 ± 1.5*
129.6 ± 2.0*	by hand	122.8 ± 2.0*
218.5 ± .1	217.4 ± .1	216.6 ± .1
383.9 ± .1	378.1 ± .1	370.4 ± .1
407.0 ± .4	395.5 ± .4	389.5 ± 1.5
414.3 ± .2	407.7 ± .3	397.2 ± .3
427.1 ± .3	418.5 ± .5	410.1 ± 1.0
473.2 ± .1	464.5 ± .1	462.1 ± .1
537.4 ± .2	517.4 ± .2	534.7 ± .8
obsvd. wkly.	527.8 ± .6	obsvd. wkly.
626.8 ± .2	613.4 ± .1	623.2 ± .3
635.4 ± .2	624.2 ± .2	632.2 ± .3
647.4 ± .3	634.2 ± .3	644.0 ± .6

[a] * denotes bands lying close together which were resolved by hand.

TABLE 3

Observed Far I. R. Bands for $Mn(^{12}C^{16}O)_5Br$[a] in Nujol Mull

ν (cm^{-1})	Intensity
133.0	medium (broad)
121.1	medium
114.3	weak
101.7	weak (broad)
87	weak
53	very weak

[a] Bands were obtained only for the plentiful normal species due to the exorbitant amount of sample necessary for each mull.

Two of the more interesting isotopic effects are illustrated in figures 13 through 18; the first three drawings indicate the different behavior of the two bending modes around 640cm^{-1}. These were assigned as the out-of-plane $(A_1)_\gamma$ bend and the in-plane $(E)_\beta$ bend in order of decreasing energy.

Both these bands shift more with ^{13}CO substitution than with $C^{18}O$ substitution; this is a general trait of MCO bending modes for all metal carbonyls (10, 14) and is a consequence of the large motion of the carbon atoms in the bending movement relative to the oxygen atoms.

However, it is also noticed that the splitting of these bands is greatest for ^{13}CO substitution and least for $C^{18}O$ substitution. As both shifts occur to lower energy, this indicates that the $(E)_\beta$ band has more MCO bending character than does $(A_1)_\gamma$.

It is also general behavior that M--C stretching modes shift further upon $C^{18}O$ substitution than ^{13}CO substitution (10,14).

Thus one immediately gains the information that the $(A_1)_\gamma$ vibration is more highly mixed with M--C stretching modes (mainly $(A_1)_{d_o}$ at 470cm^{-1}) than $(E)_\beta$ is, say with $(E)_{d_i}$ at 417cm^{-1}.

The next three spectra show that the splitting

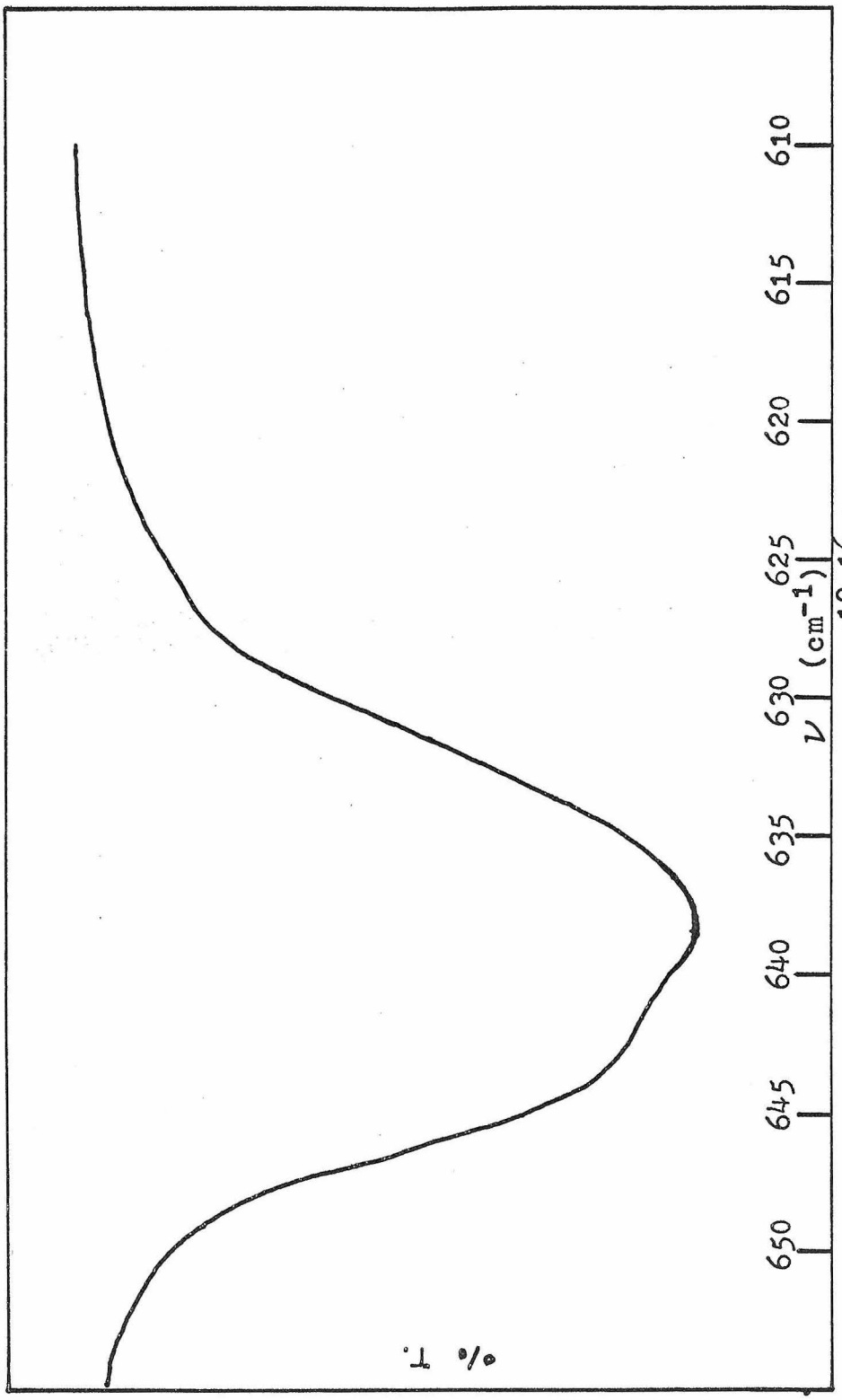

Figure 13. I.R. Spectrum of $Mn(^{12}C^{16}O)_5Br$ in CH_2Cl_2 Solution

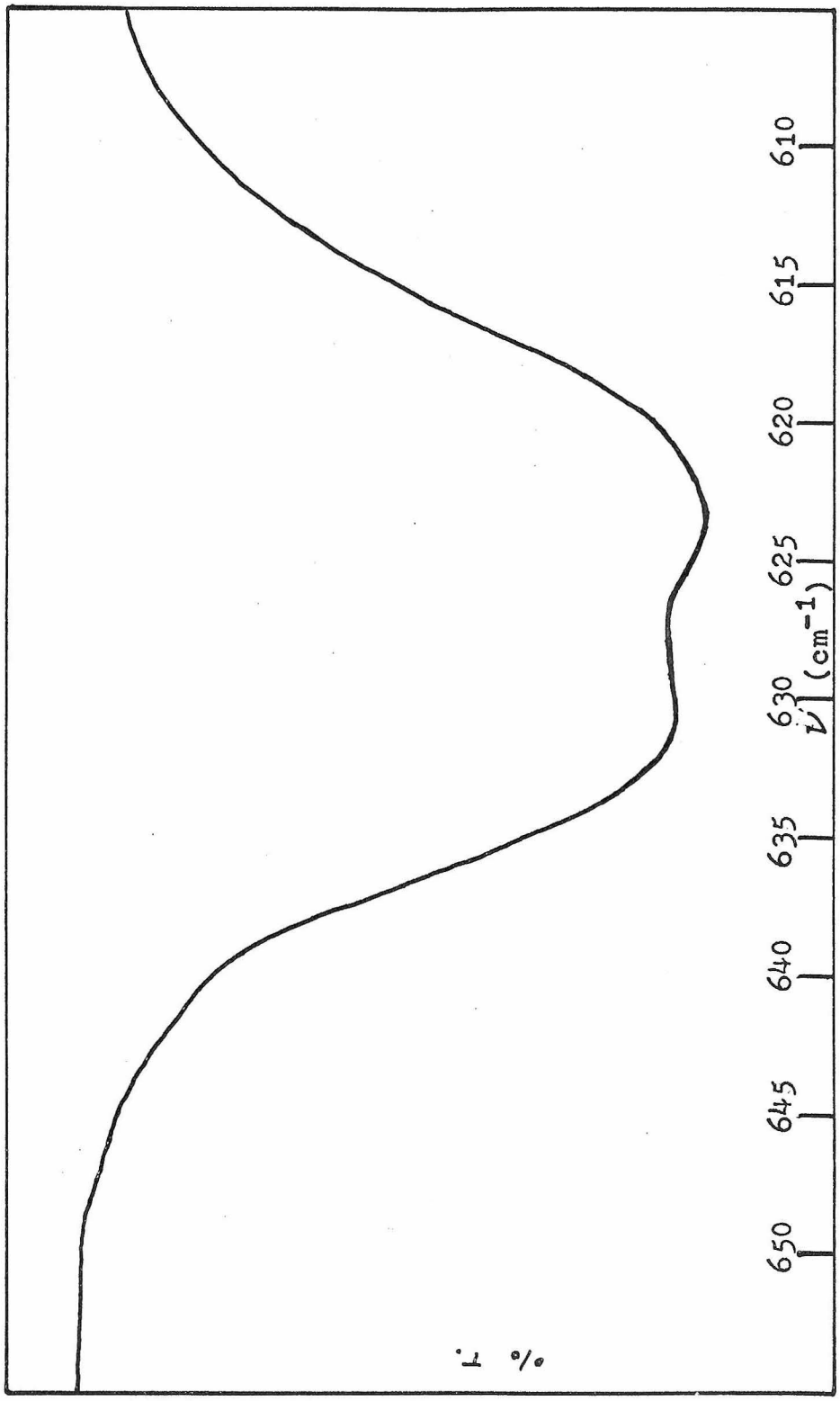

Figure 14. I.R. Spectrum of $Mn(^{13}C^{16}O)_5Br$ in CH_2Cl_2 Solution

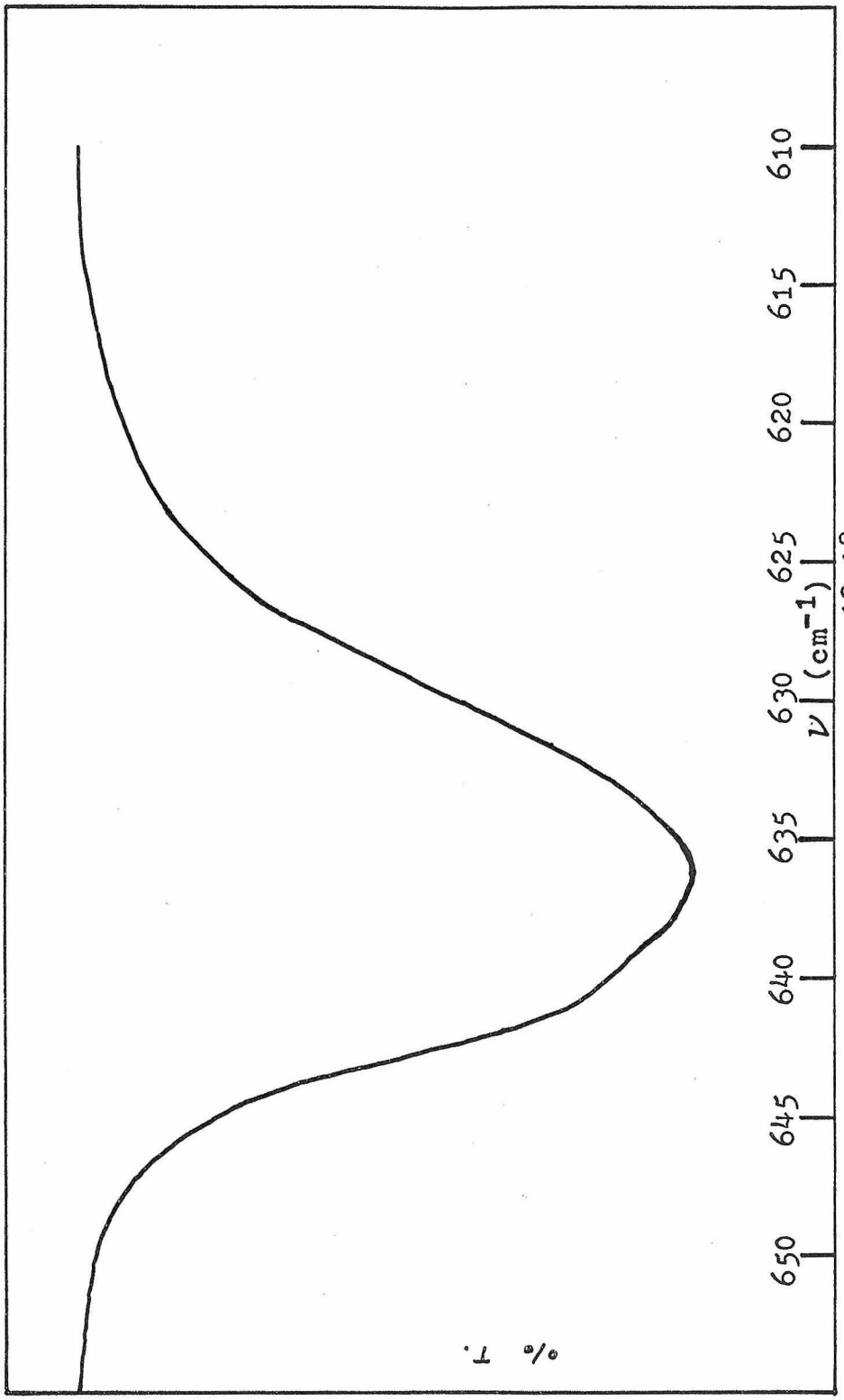

Figure 15. I.R. Spectrum of $Mn(^{12}C^{18}O)_5Br$ in CH_2Cl_2 Solution

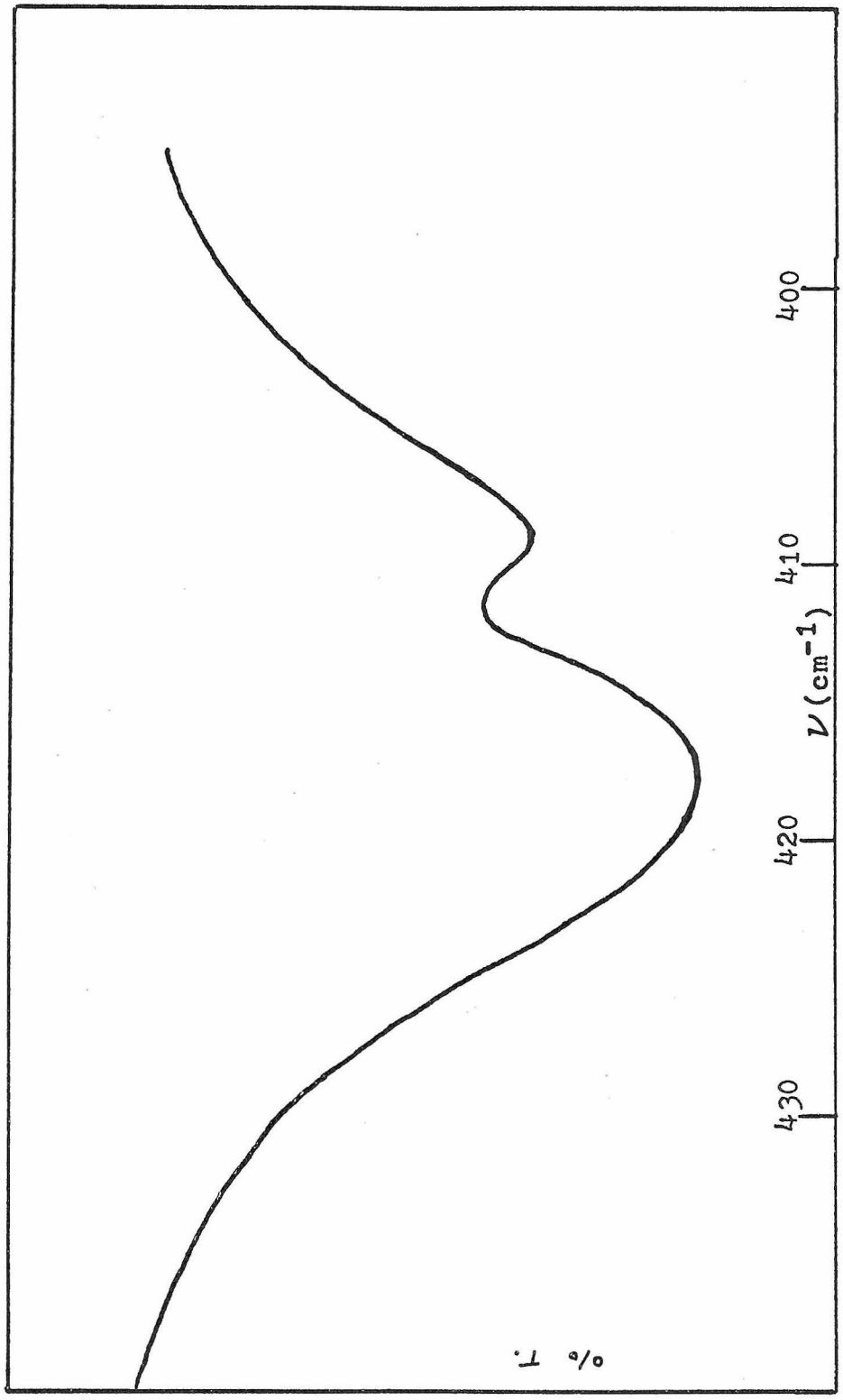

Figure 16. I.R. Spectrum of $Mn(CO)_5Br$ in CH_2Cl_2 Solution

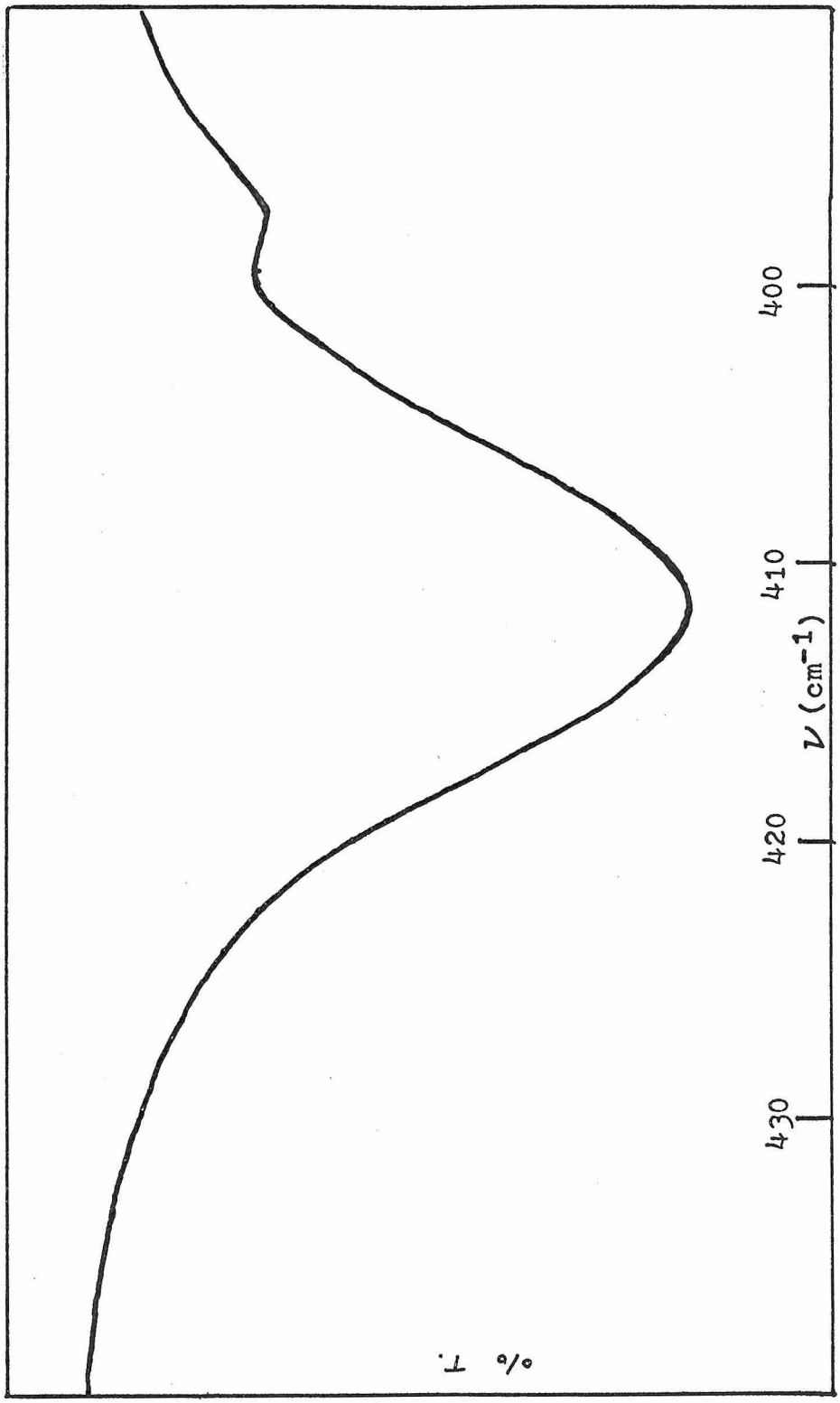

Figure 17. I.R. Spectrum of $Mn(C^{13}O)_5Br$ in CH_2Cl_2 Solution

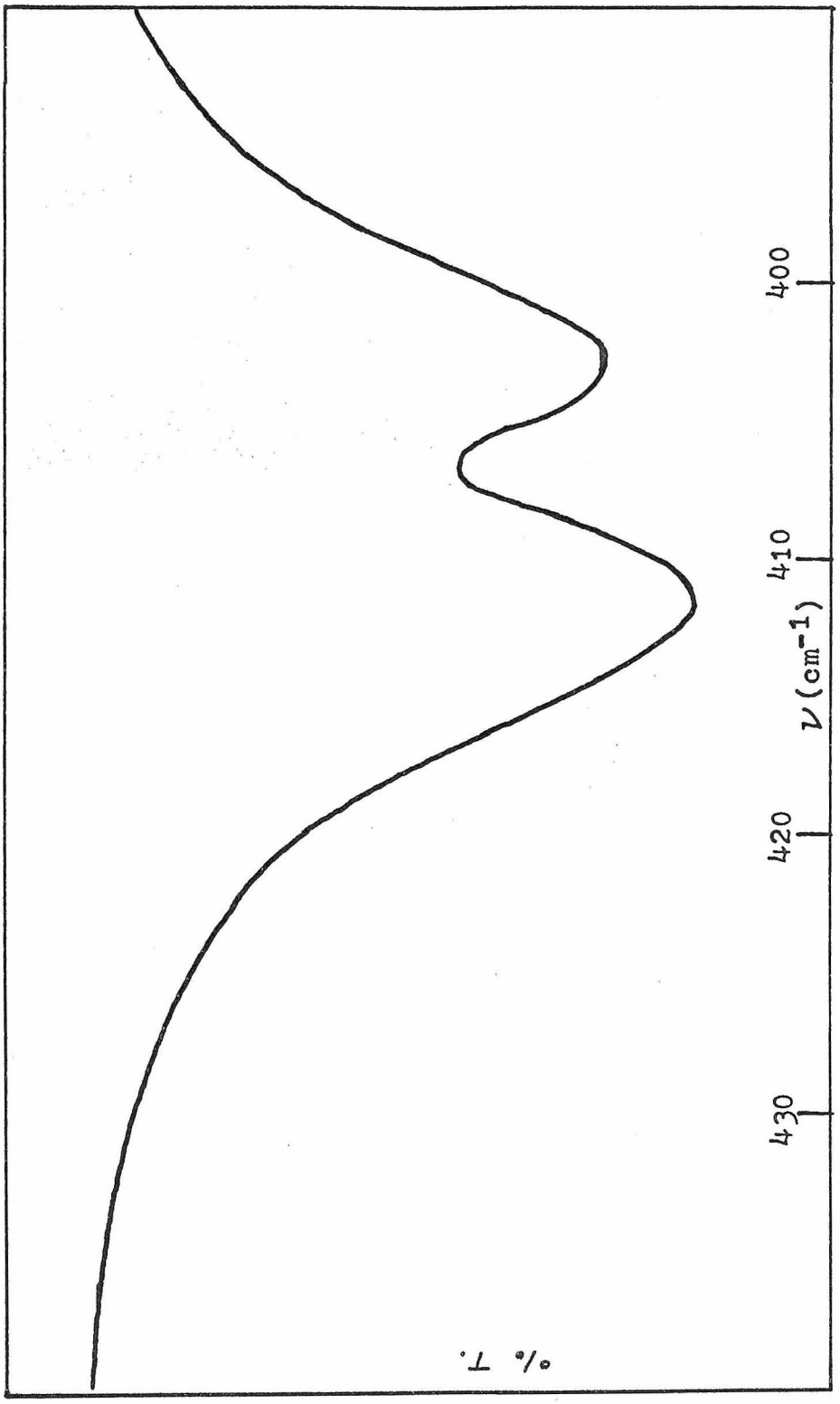

Figure 18. I.R. Spectrum of $Mn(CO^{18})_5Br$ in CH_2Cl_2 Solution

of the bands around 420cm^{-1} is also greatest for ^{13}CO substitution. As the band at higher energy, $(E)_{d_i}$ exhibits the greatest shift on $C^{18}O$ substitution, it is correspondingly assigned as an M--C stretch.

The band at lower energy shows the opposite behavior and it is tempting to assign it as an MCO bending fundamental.

However, unlike the pair of bands in figures 13, 14, and 15, the band at lower energy is seen to lose intensity drastically as the splitting increases. This is exactly the behavior expected of a combination band near a fundamental of the same symmetry. Ordinarily this band would be forbidden in the I. R. spectrum, but an increasing amount of mixing (Fermi resonance) may occur as it approaches the energy a fundamental of the same symmetry.

Thus we may explain this band as the combination $\nu_{13} - \nu_{20}$ (537cm^{-1} -133cm^{-1} = 407cm^{-1}). As the combination must be of E symmetry to interact with $(E)_{d_i}$, and as ν_{13} is of B_2 symmetry, we have that ν_{20} is necessarily of E symmetry (as only X = E holds for $B_2 \times X = E$) thus confirming the symmetry of the 133cm^{-1} band's assignment in Chapter 2.

Potential Field Calculations

Excluding the inactive A_2 mode we now have 21 x 3 = 63 observed frequencies. This will be adequate to determine at least fairly well the important constants in the General Quadratic Potential Field (GQPF). This potential field itself utilizes an approximation. The solution of the vibrational equation is in terms of a harmonic oscillator. Thus serious errors may be introduced into a solution if any anharmonicity effects are not taken into account.

In reference (23) it is shown by a comparison of the fundamental and combination bands that the C--O stretching vibrations of $Mn(CO)_5Br$ are fairly anharmonic. From the observed binary and tertiary combinations the true harmonic fundamentals may be approximated (22), and the results for $Mn(CO)_5Br$ in CCl_4 solution are:

ν	Observed	Harmonic
$(A_1)_{r_i}$	2137.9	2158.7
$(B_1)_{r_i}$	2085.4	2083.8
$(E)_{r_i}$	2052.2	2078.5
$(A_1)_{r_o}$	2001.3	2030.8

The I. R. combination spectra for the solid in the regions 2600 to 2400cm^{-1} and 1200 to 650cm^{-1} are presented in Table 4 along with their assigned combinations.

These assignments result from fundamentals whose combinations possess either the I. R. active A_1 or E symmetry. These calculated combinations are shown in Table 5.

These combination bands may be fitted, with one exception (the very weak peak at 2445cm^{-1}) to within 15cm^{-1} by combinations of observed fundamentals. The average fit is better than 5cm^{-1}, and only 6 bands are fit more poorly than this. This indicates that as long as at least one component of a combination band is not a C--O stretch, that band will exhibit good harmonic behavior. Therefore anharmonic corrections were made only for the C--O stretching frequencies. The corrections for the isotopically shifted frequencies were obtained from

$$X_{kl}^{(j)} = X_{kl}^{(i)} \left(\nu_k^{(j)} \nu_l^{(j)} / \nu_k^{(i)} \nu_l^{(i)}\right) \qquad (22)$$

where $\nu_k^{(i)}$ = frequency k for isotopic molecule i

where $X_{kl}^{(i)}$ = k-lth anharmonicity constant for isotopic molecule i

These observed frequencies are then fitted by a potential field of the General Quadratic form. Starting values for this field were obtained by the transfer of the most nearly equivalent element from the $M(CO)_6$ system (L.H. Jones, et al. (14) and L.H. Jones; private

TABLE 4

Observed Sum Combination Infra-red Spectrum: Solid $Mn(CO)_5Br$ in KBr Pellet

ν	Intensity	Combination(s); (Γ)
652	m	$\nu_{116} + \nu_{537} = 653$; (E)-- $\nu_{53} + \nu_{604} = 657$; ($A_1$)
764	vvw	$(\nu_{384})^2 = 768$; (A_1)-- $\nu_{219} + \nu_{546} = 765$; (E)-- $\nu_{133} + \nu_{627} = 760$; (E)-- $\nu_{129} + \nu_{638} = 767$; (E)-- $\nu_{116} + \nu_{645} = 761$; ($A_1$)
788	m	$\nu_{133} + \nu_{645} = 778$; (E)
798	m	$\nu_{384} + \nu_{414} = 798$; (E)
813	vw	$(\nu_{414})^2 = 828$; (A_1)-- $\nu_{219} + \nu_{604} = 823$; (E)
879	w	$\nu_{219} + \nu_{645} = 864$; ($A_1$)
899	m	$\nu_{414} + \nu_{473} = 887$; (E)
940	m	$(\nu_{473})^2 = 946$; (A_1)
1036	w(br)	$\nu_{414} + \nu_{627} = 1041$; (E)-- $\nu_{384} + \nu_{645} = 1029$; (E)
1055	w	$\nu_{414} + \nu_{638} = 1052$; (E)
1077	w	$(\nu_{537})^2 = 1074$; (A_1)

TABLE 4 continued

ν	Intensity	Combination(s); (Γ)
1168	w	$\nu_{546} + \nu_{627} = 1173$; (E)
1191	vw	$\nu_{546} + \nu_{645} = 1191$; (E)
2419	vvw	$\nu_{2000} + \nu_{414} = 2414$; (E)
2430	w	$\nu_{2050} + \nu_{384} = 2434$; (E)
2445	vvw	?
2468	w	$\nu_{2050} + \nu_{414} = 2469$; ($A_1$,E)-- $\nu_{1991} + \nu_{473} = 2464$; ($A_1$)
2488	vw	$\nu_{2074} + \nu_{414} = 2488$; ($A_1$,E)
2497	w	$\nu_{2086} + \nu_{414} = 2500$; ($A_1$,E)
2506	w	$\nu_{2088} + \nu_{414} = 2502$; ($A_1$,E)
2545	w	$\nu_{2000} + \nu_{546} = 2546$; (E)
2555	w	$\nu_{2137} + \nu_{414} = 2551$; (E)
2584	vvw	$\nu_{2050} + \nu_{537} = 2587$; (E)

TABLE 5

Calculated Sum Combination Infra-red Spectrum: Solid $Mn(CO)_5Br$ in KBr Pellet

	Γ	A_1	E, B_1	A_1	B_1	E	E	B_2	E	A_1
Γ	ν	384	414	473	537	546	604	627	638	645
E	53	437	467	526	590	599	657	680	691	698
A_1	99	483	513	572		645	703		737	744
E	116	500	530	589	654	662	720	743	754	761
B_1	121		535		658	667	725		759	
B_2	129		543			675	733	756	767	
E	133	517	547	606	667	679	737	760	771	778
A_1	219	603	633	692		765	823		857	864
A_1	384	768	798	857		930	988		1022	1029
E, B_1	414		828	887	951	960	1018	1041	1052	1059
A_1	473			946		1019	1077		1111	1118
B_1	537				1074	1083	1141		1175	
E	546					1092	1150	1173	1184	1191

TABLE 5 continued

Γ	ν	Γ	A_1	E, B_1	A_1	B_1	E	E	B_2	E	A_1
		ν	384	414	473	537	546	604	627	638	645
E	604							1208	1231	1242	1249
B_2	627								1254	1265	
E	638									1276	1283
A_1	645										1290
A_1	1986		2370	2400	2459		2532	2590		2624	2631
	1989		2373	2403	2462		2535	2593		2627	2634
	1991		2375	2405	2464		2537	2593		2629	2636
	2000		2384	2414	2473		2546	2604		2638	2645
E	2050		2434	2464	2523	2587	2596	2654	2677	2688	2695
B_1	2074			2488		2611	2620	2678		2712	
	2086			2500		2623	2632	2690		2724	
	2088			2502		2625	2634	2692		2726	
A_1	2137		2521	2551	2610		2683	2741		2775	2782

communication). Calculations were done by a least-squares fitting computer program originally written by Schachtschneider (24) and since modified by Jones and Ryan at LASL. The problem was then solved on the IBM 360/375 at Caltech and the CDC6600 machine at LASL.

The problem was formulated according to the FG method of Wilson, et al. (25). This method presents the vibrational problem in matrix form, and these series of equations are then solved numerically via high speed computer.

Two matrices, F and G, are responsible for the name of the method. Briefly, the F matrix contains the force constant for each symmetry coordinate (which were presented on pps. 25-30) along the diagonal and the interaction force constant between two symmetry coordinates in the appropriate off-diagonal element.

The G matrix is often referred to as the "inverse kinetic-energy" matrix. This is indeed the form of this array in a Cartesian coordinate system; however, with internal molecular vibrations a solution in terms of internal coordinates is much more desirable than one in terms of an externally imposed Cartesian system. We have this situation for the F matrix as the symmetry coordinates are simple combinations of the internal coordinates shown in figure 2. Thus the next step is

the unenviable transformation of the G matrix from its Cartesian formulation to symmetry coordinates. This is also accomplished by a computer program by Schachtschneider (24) and the result is symmetry blocks along the diagonal which correspond to the symmetrized F matrices.

The least-squares program forms the product FG which in turn is diagonalized and solved. The resulting eigenvalues are directly related to the frequencies of vibration; the observed frequencies are compared to the calculated frequencies and from the error encountered, a perturbation is induced in each unconstrained force constant and a new calculation is begun.

These cyclical calculations continue until a convergence limit selected by the user is reached (specifying either the size of errors in the calculated frequencies or in the size of the perturbations of the force constants for each cycle) or until the problem becomes divergent.

The calculations done for $Mn(CO)_5Br$, however, did not involve the above mentioned force constants.

The elements of the F matrix were replaced with compliance constants which are described in (26). The reason for this departure from the usual procedure in vibrational analyses is that compliance constants

are uniquely defined for a given molecule while the values of the force constants depend on the internal coordinate system chosen. This is clearly shown in comparison calculations for the H_2O and D_2O molecules in (27).

Furthermore, if redundant symmetry coordinates exist for the molecule in question, additional relationships may be obtained between the compliance constants involved. For example the values of C_α, $C'_{\alpha\alpha}$, $C''_{\alpha\alpha}$, $C'''_{\alpha\alpha}$, and $C''''_{\alpha\alpha}$ are uniquely determined for $M(CO)_6$ (L.H. Jones; private communication) while only the force constant combinations $F_\alpha - F''_{\alpha\alpha}$, $F_\alpha - F''''_{\alpha\alpha}$, and $F'_{\alpha\alpha} - F'''_{\alpha\alpha}$ may be calculated (14). As <u>starting</u> values for these calculations utilized either the C_{ij} or F_{ij} from the hexacarbonyl calculations, it was decided to solve the problem in terms of the more uniquely determined compliance constants.

The relation between the compliance and force constants is quite simply $\underline{C} = \underline{F}^{-1}$. Thus after a set of compliance constants was obtained as a solution for a given symmetry block, the C matrix was simply inverted to obtain the corresponding force constant solution.

The "kinetic-energy" matrix, $\underline{K}$, which corresponds to the G matrix is simply $\underline{K} = \underline{G}^{-1}$. Throughout the remainder of this thesis the units of all C_{ij} will be

angstroms/millidyne, and similarly the units of all F_{ij} are millidynes/angstrom.

A_1 Symmetry Block Calculations

This block contains 7 frequencies and 28 independent compliance constants. Isotopic data raised the number of observed frequencies to 21; however, the problem remained convergent only if the 15 constants (or less) in Table 6 shown with standard deviations were allowed to vary. Although the degree of convergence was rather low, the frequencies (also in Table 6) are seen to be fit quite well.

The potential energy distribution for each vibration among the various C_{ij} is shown in Table 7. These figures show the nature of the normal vibration coordinates. For instance, as was predicted on page 38, there is considerable mixing of the $(A_1)_\gamma$ and $(A_1)_{d_o}$ modes. The potential energy for ν_γ is seen to be 60% $C_{3,3}$ and 15% $C_{4,4}$ while the distribution for ν_{d_o} is 22% $C_{3,3}$ and 70% $C_{4,4}$.

The calculations also indicate that the only mixing of any consequence with the "Mn--Br" stretching mode is with the C--M--C deformation mode. It is therefore expected that this will also be the case for the "Mn--Mn" stretching mode in $Mn_2(CO)_{10}$ examined in Part

TABLE 6

Compliance Constant and Frequency Calculation for $Mn(CO)_5Br$: A_1 Symmetry Block (with ν_7 assigned to 115.8 cm^{-1})		
Calculated $C_{i,j}$ ± Standard Deviation	Calculated $C_{i,j}$ ± Standard Deviation	Calculated $C_{i,j}$ ± Standard Deviation
$C_{1,1} = .05532 \pm .00029$	$C_{1,5} = -.0066 \pm .0030$	$C_{3,5} = 0$
$C_{2,2} = .06057 \pm .00024$	$C_{1,6} = 0$	$C_{3,6} = -.157 \pm .68$
$C_{3,3} = 1.394 \pm .60$	$C_{1,7} = -.0107$	$C_{3,7} = -.045 \pm .53$
$C_{4,4} = .437 \pm .43$	$C_{2,3} = .0106$	$C_{4,5} = 0$
$C_{5,5} = .413 \pm .017$	$C_{2,4} = -.0186 \pm .0063$	$C_{4,6} = -.088 \pm .27$
$C_{6,6} = .843 \pm .23$	$C_{2,5} = .0044$	$C_{4,7} = -.233 \pm .88$
$C_{7,7} = 1.784 \pm .97$	$C_{2,6} = 0$	$C_{5,6} = 0$
$C_{1,2} = -.0016$	$C_{2,7} = .0107$	$C_{5,7} = .14$
$C_{1,3} = 0$	$C_{3,4} = .0775 \pm .42$	$C_{6,7} = -.241 \pm .23$
$C_{1,4} = .0044$		

TABLE 6 continued

$Mn(^{12}C^{16}O)_5Br$			$Mn(^{13}C^{16}O)_5Br$			$Mn(^{12}C^{18}O)_5Br$		
$\nu_{obsd.}$	$\nu_{calcd.}$	Δ	$\nu_{obsd.}$	$\nu_{calcd.}$	Δ	$\nu_{obsd.}$	$\nu_{calcd.}$	Δ
2158.7	2158.8	-.1	2108.2	2108.1	.1	2110.6	2110.6	0
2030.8	2031.1	-.3	1984.2	1984.0	.2	1985.0	1984.9	.1
645.0	645.9	-.9	632.0	631.7	.3	641.3	640.8	.5
470.4	470.5	-.1	462.3	462.2	.1	459.8	459.8	0
380.5	380.5	0	374.8	374.4	.4	366.5	366.9	-.4
222.4	222.5	-.1	221.6	221.5	.1	220.6	220.6	0
115.8	114.8	1.0	114.0	114.4	-.4	109.9	110.6	-.7

TABLE 7

Potential Energy Distribution
for A_1 Symmetry Block Calculation
(with ν_7 assigned to 115.8 cm^{-1})

Frequency (Approximate Description)	2159 (CO-rad.)	2031 (CO-ax.)	645 (MCO)	470 (MC-ax.	380 (MC-rad.)	222 (MX)	116 (CMC)
$C_{i,j}$							
$C_{1,1}$	.90	.07	0	0	.03	0	0
$C_{2,2}$	.06	.94	.01	.01	0	0	0
$C_{3,3}$	0	0	.60	.22	.01	0	.20
$C_{4,4}$	0	.05	.15	.70	.02	.03	.19
$C_{5,5}$	.04	0	0	0	.96	0	.02
$C_{6,6}$	0	0	.03	.04	0	.99	.06
$C_{7,7}$	0	0	.21	0	0	.15	.83
$C_{1,2}$	.01	-.01	0	0	0	0	0
$C_{1,3}$	0	0	0	0	0	0	0
$C_{1,4}$	0	0	0	0	0	0	0
$C_{1,5}$	0	0	0	0	.01	0	0
$C_{1,6}$	0	0	0	0	0	0	0
$C_{1,7}$	0	0	0	0	0	0	0
$C_{2,3}$	0	0	-.01	0	0	0	0
$C_{2,4}$	0	-.05	.01	.01	0	0	0
$C_{2,5}$	0	0	0	0	0	0	0
$C_{2,6}$	0	0	0	0	0	0	0
$C_{2,7}$	0	0	0	0	0	0	0

TABLE 7 continued

Frequency (Approximate Description)	2159 (CO-rad.)	2031 (CO-ax.)	645 (MCO)	470 (MC-ax.)	381 (MC-rad.)	222 (MX)	116 (CMC)
$C_{i,j}$							
$C_{3,4}$	0	0	-.04	.06	0	0	-.03
$C_{3,5}$	0	0	0	0	0	0	0
$C_{3,6}$	0	0	-.03	.03	0	0	-.03
$C_{3,7}$	0	0	.03	0	0	0	-.03
$C_{4,5}$	0	0	0	.01	-.02	0	.01
$C_{4,6}$	0	0	-.02	-.06	0	.07	-.04
$C_{4,7}$	0	0	.11	-.02	0	-.04	-.24
$C_{5,6}$	0	0	0	0	0	0	0
$C_{5,7}$	0	0	.01	0	-.02	0	-.05
$C_{6,7}$	0	0	-.04	0	0	-.19	.11

II as this frequency lies even closer to the C--M--C bending mode than the analagous Mn--Br stretch.

Finally, equivalent force constants obtained from $\underline{C}^{-1}$ are shown in Table 8.

A_2 Symmetry Block Calculation

As this frequency was not observed, only an estimate of $C_{8,8}$ in terms of interal coordinate compliance constants:

$$C_{8,8} = C_\beta + 2C^c_{\beta\beta} + C^t_{\beta\beta}$$

From the values in Table 20 this gives $C_{8,8} = 1.85$ ($F_{8,8} = 1/1.85 = .54$) yielding a calculated $\nu_8 = 449 cm^{-1}$ for $Mn(^{12}C^{16}O)_5Br$.

Bands of A_2 symmetry may combine with other A_2 bands or with E bands to give combinations of A_1 or E symmetry which are expected to have the greatest I. R. intensity. These combinations in the energy region covered in Table 5 are predicted to be: 863, 986, 995, 1053, 1076, 1087, 2499, 2523, 2535, and $2537 cm^{-1}$.

These frequencies either are not observed or do not fit an observed band uniquely. Thus the observed combination spectra neither confirms or denies this frequency prediction. Further experiments are necessary at low temperature in order to reveal some of the weaker combination bands. This assignment for ν_{A_2}

TABLE 8

Equivalent Force Constants for A_1 Block Calculation (ν_7 = 115.8 cm^{-1})

$F_{1,1}$ = 18.144	$F_{1,5}$ = .260	$F_{3,5}$ = 0
$F_{2,2}$ = 16.792	$F_{1,6}$ = 0	$F_{3,6}$ = .135
$F_{3,3}$ = .740	$F_{1,7}$ = .07	$F_{3,7}$ = .0260
$F_{4,4}$ = 2.622	$F_{2,3}$ = -.16	$F_{4,5}$ = -.14
$F_{5,5}$ = 2.504	$F_{2,4}$ = .758	$F_{4,6}$ = .369
$F_{6,6}$ = 1.318	$F_{2,5}$ = -.18	$F_{4,7}$ = .396
$F_{7,7}$ = .663	$F_{2,6}$ = .05	$F_{5,6}$ = -.08
$F_{1,2}$ = .408	$F_{2,7}$ = .02	$F_{5,7}$ = -.22
$F_{1,3}$ = 0	$F_{3,4}$ = -.0970	$F_{6,7}$ = .236
$F_{1,4}$ = -.13		

would be greatly substantiated by the presence of $(\nu_{A_2})^2$ around 998cm^{-1} as the next nearest predicted combination is 10cm^{-1} away.

B_1 Symmetry Block Calculation

Good convergence was obtained for this calculation and the calculated $C_{i,j}$ and frequencies are shown in Table 9.

Only five of the ten constants could be varied for the calculation to remain stable. $C_{10,12}$ was adjusted through a range of +.2 to -.8 in steps of .1, and the best fit was obtained for $C_{10,12} = -.5$.

The fit of ν_{10} is rather poor, the standard deviation being $\pm$ 2.7cm^{-1} for the three isotopic species. A calculation assigning this frequency to $(B_2)_\beta$ was fit equally poorly and the reason for this is not known.

This frequency is a moderately intense Raman band and its position was determined with good experimental precision ($\pm$ .2cm^{-1} from Table 2). The interaction constant between $(B_1)_\gamma$ and $(B_1)_{d_i}$ also had little effect on the quality of the frequency fitting. Better agreement may possibly be obtained by further very careful refinement of the potential field.

TABLE 9

Compliance Constant and Frequency Calculation for $Mn(CO)_5Br$: B_1 Symmetry Block

Calculated $C_{i,j}$ ± Standard Deviation	Calculated $C_{i,j}$ ± Standard Deviation	Calculated $C_{i,j}$ ± Standard Deviation
$C_{9,9} = .05758 \pm .00036$	$C_{9,10} = -.0053$	$C_{10,11} = 0$
$C_{10,10} = .945 \pm .0031$	$C_{9,11} = -.0198 \pm .0043$	$C_{10,12} = -.5$
$C_{11,11} = .361 \pm .0055$	$C_{9,12} = -.0053$	$C_{11,12} = .07$
$C_{12,12} = 2.153 \pm .093$		

$Mn(^{12}C^{16}O)_5Br$			$Mn(^{13}C^{16}O)_5Br$			$Mn(^{12}C^{18}O)_5Br$		
obsd.	calcd.		obsd.	calcd.		obsd.	calcd.	
2083.8	2084.3	-.5	2036.7	2036.3	.4	2036.5	2036.4	.1
626.8	630.2	-3.4	613.4	611.3	2.1	623.2	622.0	1.2
414.3	413.6	.7	407.7	406.7	1.0	397.2	399.1	-1.9
99.0	99.5	- .5	98.5	98.6	-.1	95.6	95.1	- .5

The other observed frequencies are fit quite well and the Potential Energy Distribution and Equivalent Force Constants are presented in Tables 10 and 12.

B_1 Symmetry Block Calculation

Amazingly enough a stable solution for this small block with 2 frequencies and only 3 compliance constants could be obtained only by constraining $C_{13,14}$. As in the case $C_{10,12}$ above, this constant was varied through the range +.5 to -.5 in steps of .1, and the best value was thus determined to be -.1.

A good fit of the frequencies was obtained, and this along with the calculated C_{ij} and the potential energy distribution are shown in Table 11. Equivalent F_{ij} are shown in Table 12.

E Symmetry Block Calculation

This was by far the most difficult and least satisfactory of the calculations. To start with, the three isotopic species give a maximum of 3 x 8 = 24 frequencies to determine the 36 independent constants.

Another major problem was that the three M--C--O bends lay within 100cm^{-1} of each other; the mixing of the internal symmetry coordinates shown in figure 2 is thus likely to be quite large and the perturbation

TABLE 10

Potential Energy Distribution for B_1 Symmetry Block Calculation				
Frequency (Approximate Description)	2084 CO-rad.	627 MCO	414 MC-rad.	100 CMC
$C_{i,j}$				
$C_{9,9}$	1.01	0	.01	0
$C_{10,10}$	0	1.13	0	.01
$C_{11,11}$	.05	0	.96	.01
$C_{12,12}$	0	.09	0	1.06
$C_{9,10}$	0	0	0	0
$C_{9,11}$	-.06	0	.03	0
$C_{9,12}$	0	0	0	0
$C_{10,11}$	0	0	0	0
$C_{10,12}$	0	-.22	0	-.06
$C_{11,12}$	0	0	0	-.02

TABLE 11

Compliance Constant and Frequency Calculation for $Mn(CO)_5Br$: B_2 Symmetry Block		
Calculated $C_{i,j} \pm$ Standard Deviation	Calculated $C_{i,j} \pm$ Standard Deviation	Calculated $C_{i,j} \pm$ Standard Deviation
$C_{13,13} = 1.692 \pm .032$	$C_{14,14} = 1.696 \pm .09$	$C_{13,14} = -.1$

$Mn(^{12}C^{16}O)_5Br$			$Mn(^{13}C^{16}O)_5Br$			$Mn(^{12}C^{18}O)_5Br$		
obsd.	calcd.		obsd.	calcd.		obsd.	calcd.	
537.2	537.4	.2	518.6	517.4	-1.2	533.7	534.7	1.0
130.4	129.6	-.8	(129.8)	129.6	-1.2	123.8	122.8	-1.0

TABLE 11 contd.

Frequency (Approximate Description)	537 MCO	130 CMC
$C_{i,j}$		
$C_{13,13}$	.75	.70
$C_{14,14}$	.31	.25
$C_{13,14}$	-.05	.05

TABLE 12

Equivalent Force Constants for B_1 Block Calculation

$F_{9,9} = 17.713$	$F_{9,10} = .12$	$F_{10,11} = -.05$
$F_{10,10} = 1.209$	$F_{9,11} = .964$	$F_{10,12} = .283$
$F_{11,11} = 2.846$	$F_{9,12} = .04$	$F_{11,12} = -.1$
$F_{12,12} = .533$		

Equivalent Force Constants for B_2 Block Calculation

$F_{13,13} = .593$	$F_{14,14} = .592$	$F_{13,14} = .035$

of one compliance constant therefore may be quite complex and poorly determined in its effects.

The geometry of symmetry coordinate S_{16} (corresponding to $(E)_\beta$) very closely resembles the form of the in-plane F_{1u} M--C--O bend for $M(CO)_6$ (14). For this reason and the fact that the observed frequencies are quite close together, ν_β is assigned with a high degree of certainty to the intense I.R. band at $638cm^{-1}$.

As was discussed in Chapter 2, the assignment of $(E)_\gamma$ and $(E)_\phi$ to the I.R. bands at 545 and $604cm^{-1}$ is considerably more uncertain and there should be considerable mixing between these modes.

Two series of calculations were done to ascertain the assignment of these modes. The first assigned $\nu_\beta \longrightarrow 638cm^{-1}$, $\nu_\phi \longrightarrow 604cm^{-1}$, and $\nu_\gamma \longrightarrow 545cm^{-1}$. This ordering gave almost no mixing between $(E)_\gamma$ and $(E)_\phi$, however, and a large amount of mixing of $(E)_\beta$ with $(E)_\phi$ both of which results were unexpected. Furthermore, the internal coordinate compliance constants $C^c_{\gamma\gamma}$ and $C^t_{\gamma\gamma}$ were very different from the analogous constants for the $M(CO)_6$ system (14).

The second assignment was $\nu_\beta \longrightarrow 638cm^{-1}$, $\nu_\gamma \longrightarrow 604cm^{-1}$, and $\nu_\phi \longrightarrow 545cm^{-1}$; it produced values for $C^c_{\gamma\gamma}$ and $C^t_{\gamma\gamma}$ which agree much more closely with their counterparts in the hexacarbonyls (.112 compared to .24 and -.02

TABLE 13

Compliance Constant and Frequency Calculation for E Symmetry Block		
Calculated $C_{i,j}$ ± Standard Deviation	Calculated $C_{i,j}$ ± Standard Deviation	Calculated $C_{i,j}$ ± Standard Deviation
$C_{15,15}$ = .05741 ± .00030	$C_{15,20}$ = 0	$C_{17,21}$ = -.46
$C_{16,16}$ = 2.234 ± .15	$C_{15,21}$ = 0	$C_{17,22}$ = 0
$C_{17,17}$ = 1.303 ± .081	$C_{15,22}$ = -.011	$C_{18,19}$ = -.11
$C_{18,18}$ = 2.299 ± .40	$C_{16,17}$ = 0	$C_{18,20}$ = -.18
$C_{19,19}$ = .584 ± .035	$C_{16,18}$ = -1.04 ± .23	$C_{18,21}$ = -.13
$C_{20,20}$ = 1.5	$C_{16,19}$ = .16	$C_{18,22}$ = -.06
$C_{21,21}$ = 5.2	$C_{16,20}$ = .06	$C_{19,20}$ = 0
$C_{22,22}$ = 3.2	$C_{16,21}$ = .06	$C_{19,21}$ = 0
$C_{15,16}$ = -.01	$C_{16,22}$ = .75	$C_{19,22}$ = .14
$C_{15,17}$ = 0	$C_{17,18}$ = -.1	$C_{20,21}$ = -.9
$C_{15,18}$ = .007	$C_{17,19}$ = .2	$C_{20,22}$ = -.62
$C_{15,19}$ = -.0284 ± .013	$C_{17,20}$ = .46	$C_{21,22}$ = -1.05

TABLE 13 continued

$Mn(^{12}C^{16}O)$ Br			$Mn(^{13}C^{16}O)$ Br			$Mn(^{12}C^{18}O)$ Br		
$\nu_{obsd.}$	$\nu_{calcd.}$	Δ	$\nu_{obsd.}$	$\nu_{calcd.}$	Δ	$\nu_{obsd.}$	$\nu_{calcd.}$	Δ
2078.5	2079.1	-.6	2032.8	2032.3	.5	2029.7	2029.6	.1
638.4	639.2	-.8	622.0	623.7	-1.7	636.2	634.3	1.9
604.2	605.7	-1.5	591.3	589.8	1.5	600.8	600.2	-.6
545.5	546.0	-.5	527.1	529.8	-2.7	542.8	539.9	2.9
417.2	418.8	-1.6	411.7	409.4	2.3	411.2	411.8	-.6
133.0	132.8	.2	-----	132.1	---	-----	126.7	---
87.0	87.3	-.3	-----	86.7	---	-----	84.0	---
52.9	52.8	.1	-----	52.4	---	51.0	51.1	-.1

TABLE 14

Potential Energy Distribution for
E Symmetry Block Calculation

Frequency (Approximate Description)	2079 (CO- rad.	638 (MCO β-)	604 (MCO γ-)	546 (MCO ϕ-)	417 (MC- rad.	133 (CMC ψ-)	87 (CMC α-)	53 (CMX δ-)
$C_{i,j}$								
$C_{15,15}$	1.02	0	0	0	0	0	0	0
$C_{16,16}$	0	.51	.01	.03	.14	.42	.26	.08
$C_{17,17}$	0	.01	.32	.59	.28	0	0	0
$C_{18,18}$	0	.02	.24	.30	.11	.62	.01	0
$C_{19,19}$	.04	.11	.16	.01	.69	.05	.06	0
$C_{20,20}$	0	0	.30	.02	.08	.66	.46	0
$C_{21,21}$	0	0	0	.02	.02	0	.40	.92
$C_{22,22}$	0	.11	0	.01	0	0	.57	.77
$C_{15,16}$	0	0	0	0	0	0	0	0
$C_{15,17}$	0	0	0	0	0	0	0	0
$C_{15,18}$	0	0	0	0	0	0	0	0

TABLE 14 continued

Frequency (Approximate Description)	2079 (CO- rad.)	638 (MCO β-)	604 (MCO γ-)	546 (MCO ϕ-)	417 (MC- rad.)	133 (CMC ψ-)	87 (CMC α-)	53 (CMX δ-)
$C_{i,j}$								
$C_{15,19}$	-.06	0	0	0	.01	0	0	0
$C_{15,20}$	0	0	0	0	0	0	0	0
$C_{15,21}$	0	0	0	0	0	0	0	0
$C_{15,22}$	0	0	0	0	0	0	0	0
$C_{16,17}$	0	-.01	.01	.02	-.03	.01	0	0
$C_{16,18}$	0	.08	.04	-.09	-.11	-.46	-.04	.01
$C_{16,19}$	0	-.04	.01	0	.06	-.03	-.02	0
$C_{16,20}$	0	.01	-.02	.01	.03	-.15	.10	0
$C_{16,21}$	0	0	0	.01	-.01	.01	-.08	.07
$C_{16,22}$	0	.16	0	.01	.01	-.03	-.26	-.16
$C_{17,18}$	0	0	.02	-.03	.01	-.01	0	0
$C_{17,19}$	0	.02	.11	-.03	-.21	-.01	0	0
$C_{17,20}$	0	0	-.19	.07	-.09	-.06	-.01	0

TABLE 14 continued

Frequency (Approximate Description)	2079 (CO- rad.)	638 (MCO β-)	604 (MCO γ-)	546 (MCO ϕ-)	417 (MC- rad.)	133 (CMC ψ-)	87 (CMC α-)	53 (CMX δ-)
$C_{i,j}$								
$C_{17,21}$	0	0	0	-.01	-.01	0	0	0
$C_{17,22}$	0	0	0	.01	0	0	0	0
$C_{18,19}$	0	0	-.01	0	.02	-.01	0	0
$C_{18,20}$	0	0	.03	.01	.01	-.06	0	0
$C_{18,21}$	0	0	0	0	0	0	0	0
$C_{18,22}$	0	.01	0	-.01	0	.01	.01	-.01
$C_{19,20}$	0	0	-.02	0	-.03	-.03	-.02	0
$C_{19,21}$	0	0	0	0	.01	0	-.01	0
$C_{19,22}$	0	.01	0	0	0	0	-.02	0
$C_{20,21}$	0	0	-.02	.02	-.03	-.03	-.34	.03
$C_{20,22}$	0	.01	.02	.01	.01	.05	-.44	-.03
$C_{21,22}$	0	.01	0	.01	-.01	0	.38	-.68

TABLE 15

Equivalent Force Constants for E Block Calculation

$F_{15,15} = 17.879$	$F_{15,20} = .07$	$F_{17,21} = .02$
$F_{16,16} = .649$	$F_{15,21} = 0$	$F_{17,22} = -.05$
$F_{17,17} = .930$	$F_{15,22} = .037$	$F_{18,19} = .031$
$F_{18,18} = .565$	$F_{16,17} = .06$	$F_{18,20} = .035$
$F_{19,19} = 1.913$	$F_{16,18} = .275$	$F_{18,21} = .011$
$F_{20,20} = 1.011$	$F_{16,19} = -.10$	$F_{18,22} = -.04$
$F_{21,21} = .260$	$F_{16,20} = -.12$	$F_{19,20} = .07$
$F_{22,22} = .459$	$F_{16,21} = -.05$	$F_{19,21} = -.02$
$F_{15,16} = -.006$	$F_{16,22} = -.18$	$F_{19,22} = -.05$
$F_{15,17} = -.16$	$F_{17,18} = .030$	$F_{20,21} = .210$
$F_{15,18} = -.014$	$F_{17,19} = -.325$	$F_{20,22} = .290$
$F_{15,19} = .914$	$F_{17,20} = -.291$	$F_{21,22} = .140$

compared to -.18). The potential energy distribution shown in Table 14 is much more physically reasonable. The in-plane $(E)_\beta$ mode is now relatively unmixed except with the $(E)_\alpha$ in-plane C--M--C deformation. $(E)_\gamma$ is now 32% $C_{17,17}$ and 24% $C_{18,18}$ while $(E)_\phi$ is 59% $C_{17,17}$ and 30% $C_{18,18}$. The modes are so highly mixed that a more accurate set of symmetry coordinates would be $(S_{17} + S_{18})/\sqrt{2}$ and $(S_{17} - S_{18})/\sqrt{2}$.

The next major difficulty encountered was with the fitting of the two C--M--C bending modes and the C--M--Br bending mode all of which lie within 80cm^{-1} of each other. These modes are even more highly mixed than the M--C--O bending modes and it was necessary to constrain all compliance constants involving them for the calculation to remain stable. Constants $C_{20,20}$, $C_{21,21}$, $C_{22,22}$, $C_{20,21}$, $C_{20,22}$, $C_{21,22}$, and $C_{16,22}$ were adjusted first individually to determine their effect on the frequency fitting and potential energy distribution and finally "en masse" to give the set which best fit the observed frequencies.

Naturally this procedure was extremely tedious and time consuming (not to mention being frustrating and expensive), and the "best values" of the compliance constants finally obtained represent only one possible solution.

If time had permitted, a more reasonable approach in the long run would have been to form combinations of the original E block symmetry coordinates which would more closely approximate the normal coordinates of vibration. After the calculation of a new G matrix, the compliance constant calculation might be considerably more stable as the different C_{ij} would be less correlated with each other. The unscrambling of these values into internal coordinate constants then would be only slightly more difficult than it was in the present system.

The calculated values for C_{ij} and the frequencies are shown in Table 13. The fit obtained for the seven constants allowed to vary is only moderately good and it is felt that the adoption of the above procedure would significantly improve this calculation. Nevertheless the present values are felt to be accurate enough to proceed with the calculation of the internal coordinate compliance constants. The equivalent symmetry force constants are shown in Table 15.

Internal Coordinate Compliance and Force Constants

The calculated values of the symmetry potential constants may now be transformed to internal coordinate potential constants by means of the formulas presented

in Tables 16, 17, and 18. These formulas are arrived at by standard group theoretical methods (22 and 25) for a GQPF. The internal coordinate interaction constants are in the form C_{ij} where i and j now refer to the respective internal (rather than symmetry) coordinates involved. Thus C_{ij} is the change in the compliance of coordinate j when coordinate i is forced through one positive unit displacement.

The calculated internal coordinate compliance and force constants are presented in Tables 19, 20, and 21; along with these values are the nearest equivalent elements of the GQPF for $M(CO)_6$ with their calculated values (14). Where the value of a given element for $Cr(CO)_6$ was substantially different from the mean value of $Cr(CO)_6$, $Mo(CO)_6$, and $W(CO)_6$, this individual value was used in the starting calculations and this is indicated in the tables by a double asterisk.

Stretch-Stretch Constants

The σ- and π- synergic bonding model is again used to interpret changes in potential constants between $M(0)(CO)_6$ and $Mn^{(+1)}(CO)_5Br^{(-1)}$. Lower case c_{ij} and f_{ij} will be used when the hexacarbonyls are under discussion to distinguish between the C_{ij} and F_{ij} for the Mn compound.

TABLE 16

SYMMETRY AND INTERNAL COMPLIANCE CONSTANTS: STRETCH--STRETCH TERMS

$$C_{1,1} = C_{r_i} + 2C^c_{r_i,r_i} + C^t_{r_i,r_i}$$
$$C_{9,9} = C_{r_i} - 2C^c_{r_i,r_i} + C^t_{r_i,r_i}$$
$$C_{15,15} = C_{r_i} - C^t_{r_i,r_i}$$

$$C_{2,2} = C_{r_o}$$

$$C_{4,4} = C_{d_o}$$

$$C_{5,5} = C_{d_i} + 2C^c_{d_i,d_i} + C^t_{d_i,d_i}$$
$$C_{11,11} = C_{d_i} - 2C^c_{d_i,d_i} + C^t_{d_i,d_i}$$
$$C_{19,19} = C_{d_i} - C^t_{d_i,d_i}$$

$$C_{6,6} = C_{\Delta}$$

$$C_{1,2} = 2C^c_{r_i,r_o}$$
$$C_{1,4} = 2C^c_{r_i,d_o}$$
$$C_{1,5} = C_{r_i,d_i} + 2C^c_{r_i,d_i} + C^t_{r_i,d_i}$$
$$C_{1,6} = 2C_{r_i,\Delta}$$
$$C_{2,4} = C_{r_o,d_o}$$
$$C_{2,5} = C_{1,4}$$
$$C_{2,6} = C_{r_o,\Delta}$$
$$C_{4,5} = 2C^c_{d_o,d_i}$$
$$C_{4,6} = C_{d_o,\Delta}$$
$$C_{5,6} = 2C_{d_i,\Delta}$$

$$C_{9,11} = C_{r_i,d_i} - 2C^c_{r_i,d_i} + C^t_{r_i,d_i}$$

$$C_{15,19} = C_{r_i,d_i} - C^t_{r_i,d_i}$$

TABLE 17

SYMMETRY AND INTERNAL COMPLIANCE CONSTANTS: BEND--BEND TERMS

$$C_{3,3} = C_\gamma + 2C^c_{\gamma,\gamma} + C^t_{\gamma,\gamma}$$
$$C_{10,10} = C_\gamma - 2C^c_{\gamma,\gamma} + C^t_{\gamma,\gamma}$$
$$C_{17,17} = C_\gamma - C^t_{\gamma,\gamma}$$

$$C_{8,8} = C_\beta + 2C^c_{\beta,\beta} + C^t_{\beta,\beta}$$
$$C_{13,13} = C_\beta - 2C^c_{\beta,\beta} + C^t_{\beta,\beta}$$
$$C_{16,16} = C_\beta - C^t_{\beta,\beta}$$

$$C_{18,18} = C_\phi - C^t_{\phi,\phi} = C'_\phi$$

$$C_{7,7} = C_\psi + 2C^c_{\psi,\psi} + C^t_{\psi,\psi} - C_{\psi,\delta} - 2C^c_{\psi,\delta} - C^t_{\psi,\delta}$$
$$C_{12,12} = C_\psi - 2C^c_{\psi,\psi} + C^t_{\psi,\psi} - C_{\psi,\delta} + 2C^c_{\psi,\delta} - C^t_{\psi,\delta}$$
$$C_{20,20} = C_\psi - C^t_{\psi,\psi}$$
$$C_{21,21} = C_\delta - C^t_{\delta,\delta}$$

$$C_{14,14} = C_\alpha - 2C^c_{\alpha,\alpha} + C^t_{\alpha,\alpha}$$
$$C_{22,22} = C_\alpha - C^t_{\alpha,\alpha}$$

$$C_{3,7} = (1/\sqrt{2})(C_{\gamma,\psi} + 2C^c_{\gamma,\psi} + C^t_{\gamma,\psi} - C_{\gamma,\delta} - 2C^c_{\gamma,\delta} - C^t_{\gamma,\delta})$$
$$C_{10,12} = (1/\sqrt{2})(C_{\gamma,\psi} - 2C^c_{\gamma,\psi} + C^t_{\gamma,\psi} - C_{\gamma,\delta} + 2C^c_{\gamma,\delta} - C^t_{\gamma,\delta})$$

$$C_{13,14} = C_{\alpha,\beta} - 2C^c_{\alpha,\beta} + C^t_{\alpha,\beta}$$

$$C_{16,17} = C_{\beta,\gamma} - C^t_{\beta,\gamma}$$
$$C_{16,18} = \sqrt{2}\, C_{\beta,\phi}$$

TABLE 17 continued

$$C_{16,20} = 2C_{\beta,\psi}$$

$$C_{16,21} = 2C_{\beta,\delta}$$

$$C_{16,22} = \sqrt{2}\,(C_{\alpha,\beta} - C^{t}_{\alpha,\beta})$$

$$C_{17,18} = \sqrt{2}\,C_{\gamma,\phi}$$

$$C_{17,20} = C_{\gamma,\psi} - C^{t}_{\gamma,\psi}$$

$$C_{17,21} = C_{\gamma,\delta} - C^{t}_{\gamma,\delta}$$

$$C_{17,22} = \sqrt{2}\,(C_{\gamma,\alpha} - C^{t}_{\gamma,\alpha}) = \sqrt{2}\,C'_{\gamma,\alpha}$$

$$C_{18,20} = \sqrt{2}\,C_{\phi,\psi}$$

$$C_{18,21} = \sqrt{2}\,C_{\phi,\delta}$$

$$C_{18,22} = 2C_{\phi\alpha}$$

$$C_{20,21} = C_{\psi,\delta} - C^{t}_{\psi,\delta}$$

$$C_{20,22} = \sqrt{2}\,(C_{\psi,\alpha} - C^{t}_{\psi,\alpha}) = \sqrt{2}\,C'_{\psi,\alpha}$$

$$C_{21,22} = \sqrt{2}\,(C_{\delta,\alpha} - C^{t}_{\delta,\alpha}) = \sqrt{2}\,C'_{\delta,\alpha}$$

TABLE 18

SYMMETRY AND INTERNAL COMPLIANCE CONSTANTS: STRETCH--BEND TERMS

$$C_{1,3} = C_{r_i,\gamma} + 2C^c_{r_i,\gamma} + C^t_{r_i,\gamma}$$

$$C_{1,7} = (1/\sqrt{2})(C_{r_i,\psi} + 2C^c_{r_i,\psi} + C^t_{r_i,\psi} - C_{r_i,\delta} - 2C^c_{r_i,\delta} - C^t_{r_i,\delta})$$

$$= (1/\sqrt{2})(C'_{r_i,\psi} + 2C^{c\prime}_{r_i,\psi} + C^{t\prime}_{r_i,\psi})$$

$$C_{2,3} = 2C_{r_o,\gamma}$$

$$C_{2,7} = \sqrt{2}(C_{r_o,\psi} - C_{r_o,\delta}) = \sqrt{2}C_{r_o,\psi-\delta}$$

$$C_{3,4} = 2C_{d_o,\gamma}$$

$$C_{3,5} = C_{d_i,\gamma} + 2C^c_{d_i,\gamma} + C^t_{d_i,\gamma}$$

$$C_{3,6} = 2C_{\Delta,\gamma}$$

$$C_{4,7} = \sqrt{2}(C_{d_o,\psi} - C_{d_o,\delta}) = \sqrt{2}C_{d_o,\psi-\delta}$$

$$C_{5,7} = (1/\sqrt{2})(C_{d_i,\psi} + 2C^c_{d_i,\psi} + C^t_{d_i,\psi} - C_{d_i,\delta} - 2C^c_{d_i,\delta} - C^t_{d_i,\delta})$$

$$= (1/\sqrt{2})(C'_{d_i,\psi} + 2C^{c\prime}_{d_i,\psi} + C^{t\prime}_{d_i,\psi})$$

$$C_{6,7} = \sqrt{2}(C_{\Delta,\psi} - C_{\Delta,\delta}) = \sqrt{2}C_{\Delta,\psi-\delta}$$

$$C_{9,10} = C_{r_i,\gamma} - 2C^c_{r_i,\gamma} + C^t_{r_i,\gamma}$$

$$C_{9,12} = (1/\sqrt{2})(C'_{r_i,\psi} - 2C^{c\prime}_{r_i,\psi} + C^{t\prime}_{r_i,\psi})$$

$$C_{10,11} = C_{d_i,\gamma} - 2C^c_{d_i,\gamma} + C^t_{d_i,\gamma}$$

$$C_{11,12} = (1/\sqrt{2})(C'_{d_i,\psi} - 2C^{c\prime}_{d_i,\psi} + C^{t\prime}_{d_i,\psi})$$

$$C_{15,16} = C_{r_i,\beta} + 2C^c_{r_i,\beta} + C^t_{r_i,\beta}$$

$$C_{15,17} = C_{r_i,\gamma} - C^t_{r_i,\gamma}$$

$$C_{15,18} = \sqrt{2}C_{r_i,\phi}$$

TABLE 18 continued

$$C_{15,20} = C_{r_i,\psi} - C^t_{r_i,\psi}$$

$$C_{15,21} = C_{r_i,\delta} - C^t_{r_i,\delta}$$

$$C_{15,22} = \sqrt{2}(C_{r_i,\alpha} - C^c_{r_i,\alpha})$$

$$C_{16,19} = C_{d_i,\beta} + 2C^c_{d_i,\beta} + C^t_{d_i,\beta}$$

$$C_{17,19} = C_{d_i,\gamma} - C^t_{d_i,\gamma}$$

$$C_{18,19} = \sqrt{2}C_{d_i,\phi}$$

$$C_{19,20} = C_{d_i,\psi} - C^t_{d_i,\psi}$$

$$C_{19,21} = C_{d_i,\delta} - C^t_{d_i,\delta}$$

$$C_{19,22} = \sqrt{2}(C_{d_i,\alpha} - C^c_{d_i,\alpha})$$

TABLE 19

INTERNAL COORDINATE STRETCH--STRETCH COMPLIANCE AND FORCE CONSTANTS[a]

$C_{i,j}$	Calcd. for $Mn(CO)_5Br$	Approx. Equiv. for $M(CO)_6$	Ave. Value Calcd. for $M(CO)_6$[b]
C_{r_i}	.05693(17.904)	C_{CO}	.05905 **(17.04)**
C_{r_o}	.06057(16.792)	C_{CO}	.05905 **(17.04)**
C_{d_i}	.499(2.294)	C_{MC}	.509 **(2.10)**
C_{d_o}	.437(2.622)	C_{MC}	.509 **(2.10)**
C_{Δ}	.843(1.318)	No	Equivalent
$C^c_{r_i,r_i}$	-.00057(.108)	$C^c_{CO,C'O'}$	-.00077(.175)
$C^t_{r_i,r_i}$	-.00048(.025)	$C^t_{CO,C'O'}$	-.00025(.039)
$C^c_{r_i,r_o}$	-.0008*(.204)	$C^c_{CO,C'O'}$	-.00077(.175)
$C^c_{d_i,d_i}$	.013(-.086)	$C^c_{MC,MC'}$	.0023**(-.02)**
$C^t_{d_i,d_i}$	-.112(.381)	$C^t_{MC,MC'}$	-.114**(.47)**
$C^c_{d_i,d_o}$	0*(0)	$C^c_{MC,MC'}$	.0023**(-.02)**
C_{r_i,d_i}	-.0193(.763)	$C_{CO,MC}$	-.0238(.758)
$C^c_{r_i,d_i}$	.0033(-.176)	$C^c_{CO,MC'}$	.0022(-.088)
$C^t_{r_i,d_i}$	.0091(-.141)	$C^t_{CO,MC'}$	.0097(-.112)
$C^c_{r_i,d_o}$	.0022*(-.065)	$C^c_{CO,MC'}$	.0022(-.088)
C_{r_o,d_i}	is set =	C_{r_i,d_o}	
C_{r_o,d_o}	-.0186(.758)	$C_{MC,CO}$	-.0238(.758)

[a] * denotes values held constant in calculations; values in parentheses are equivalent force constants.

[b] ** denotes values for $Cr(CO)_6$; other values are averages for $Cr(CO)_6$, $Mo(CO)_6$, and $W(CO)_6$. Ref. (14).

TABLE 19 continued

$C_{r_i,\Delta}$	0*(0)	No	Equivalent
$C_{r_o,\Delta}$	0*(0)	No	Equivalent
$C_{d_i,\Delta}$	0*(0)	No	Equivalent
$C_{d_o,\Delta}$	-.088(.363)	No	Equivalent

TABLE 20

INTERNAL COORDINATE BEND--BEND COMPLIANCE AND FORCE CONSTANTS[a]

$C_{i,j}$	Calcd. for $Mn(CO)_5Br$	Approx. Equiv. for $M(CO)_6$	Ave. Value Calcd. for $M(CO)_6$[b]
C_β	1.970(.598)	C_β	1.919**(.48)**
C_γ	1.287(.953)	C_β	1.919**(.48)**
C'_ϕ	2.299(.565)	C_β	1.919**(.48)**
$C_\psi - C_{\psi\delta}$	2.149(.61)	$C_\alpha - C''''_{\alpha\alpha}$	2.62 **(.56)**
$C_\psi - C^t_{\psi\psi}$	1.5(1.011)	$C_\alpha - C''''_{\alpha\alpha}$	2.62 **(.56)**
$C_\delta - C^t_{\delta\delta}$	5.2 (.26)	No Equivalent	
C_α	2.67 (.53)	C_α	1.92 (.518)
$C^c_{\beta\beta}$	.07*(-.023)	$-C''_{\beta\beta}$	.07(-.023)
$C^t_{\beta\beta}$	-.264(-.051)	$C'_{\beta\beta}$	-.25(.068)
$C^c_{\gamma\gamma}$	.112(-.117)	$C'''_{\beta\beta}$	.24(-.029)
$C^t_{\gamma\gamma}$	-.017(.022)	$C'_{\beta\beta}$	-.25(.068)
$C^t_{\psi\psi} - C^t_{\psi\delta}$	-.18*(.01)	$C''''_{\alpha\alpha} - C''_{\alpha\alpha}$	-.18(.01)
$C^c_{\psi\psi} - C^c_{\psi\delta}$	-.093(.04)	$C'_{\alpha\alpha} - C'''_{\alpha\alpha}$	-.44(.13)
$C^c_{\alpha\alpha}$	.22*	$C''''_{\alpha\alpha}$	.22
$C^t_{\alpha\alpha}$	-.53	$C''_{\alpha\alpha}$	-.52
$C_{\beta\gamma} = C^c_{\beta\gamma} = C^t_{\beta\gamma} = 0$	No Equivalent		

[a] * denotes values held constant in calculations; values in parenthesees are equivalent force constants.

[b] ** denotes values for $Cr(CO)_6$; other values are average values for $Cr(CO)_6$, $Mo(CO)_6$, and $W(CO)_6$. Ref. (14).

TABLE 20 continued

$C_{\beta\phi}$	-.37(.134)	$-C''''_{\beta\beta}$	-.25(.029)
$C_{\gamma\phi} - C^{t}_{\gamma\phi}$	-.07*(.021)	$C''_{\beta\beta}$	-.07(.023)
$C_{\psi\delta} - C^{t}_{\psi\delta}$	-.9(.210)	$C''''_{\alpha\alpha} - C''_{\alpha\alpha}$	-.18**(.01)**
$C'_{\psi\alpha}$	-.22*(.11)	$C'_{\alpha\alpha}$	-.22(.14)
$C'_{\delta\alpha}$	-.25(.07)	$C'_{\alpha\alpha}$	-.22(.14)
$C_{\beta\psi}$	.03*(-.06)	$C''''_{\alpha\beta}$	.03(-.03)
$C_{\beta\delta}$	.03*(-.03)	$C''''_{\alpha\beta}$	.03(-.03)
$C_{\beta\alpha}$	.21(-.05)	$C'_{\alpha\beta}$	.55(-.11)
$C^{c}_{\beta\alpha}$	-.26(.06)	$-C''_{\alpha\beta}$	-.09(.04)
$C_{\gamma,\psi-\delta} + C^{t}_{\gamma,\psi-\delta}$	-.20(.11)	$C'_{\alpha\beta} + C''_{\alpha\beta}$	.64(-.152)
$C^{c}_{\gamma\psi}$	.08(.05)	$C''''_{\alpha\beta}$	.03(-.015)
$C_{\gamma\psi} - C^{t}_{\gamma\psi}$	.46*(-.291)	$C'_{\alpha\beta} - C''_{\alpha\beta}$	.46(-.068)
$C_{\gamma\delta} - C^{t}_{\gamma\delta}$	-.46*(.02)	$-C'_{\alpha\beta} + C''_{\alpha\beta}$	-.46(.068)
$C'_{\gamma\alpha}$	0*(0)	No	Equivalent
$C_{\phi\psi}$	-.13*(.03)	$-C'_{\alpha\beta}$	-.55(.11)
$C_{\phi\delta}$	-.09*(.008)	$-C''_{\alpha\beta}$	-.09(.042)
$C_{\phi\alpha}$	-.03*(-.02)	$-C''''_{\alpha\beta}$	-.03(.015)

TABLE 21

INTERNAL COORDINATE STRETCH--BEND COMPLIANCE AND FORCE CONSTANTS[a]

$C_{i,j}$	Calcd. for $Mn(CO)_5Br$	Approx. Equiv. for $M(CO)_6$	Ave. Value Calcd. for $M(CO)_6$[b]
$C_{r_i,\beta}+2C^c_{r_i,\beta}+C^t_{r_i,\beta}$	0*(0)	No	Equivalent
$C_{r_i,\gamma}=C^c_{r_i,\gamma}=C^t_{r_i,\gamma}$	= 0*(0)	No	Equivalent
$C_{r_i,\phi}$	.005*(0)	$-C'_{CO,\beta}$	.0053(0)
$C'_{r_i,\psi}+C^{t\prime}_{r_i,\psi}$	0*(0)	$C'_{CO,\alpha}-C'_{CO,\alpha}$	0(0)
$C^{c\prime}_{r_i,\psi}$	0*(0)	No	Equivalent
$C_{r_i,\psi}-C^t_{r_i,\psi}$	0*(0)	$C'_{CO,\alpha}-C''_{CO,\alpha}$	-.0076(0)
$C_{r_i,\delta}-C^t_{r_i,\delta}$	0*(0)	$C'_{CO,\alpha}-C''_{CO,\alpha}$	-.0076(0)
$C_{r_i,\alpha}$	-.004*(.037)	$C'_{CO,\alpha}$	-.0038
$C_{r_o,\gamma}$	.0053*(-.08)	$C''_{CO,\beta}$	.0053(0)
$C_{r_o,\psi-\delta}$	.0038*(.02)	$-C'_{CO,\alpha}$	.0038(0)
$C_{d_i,\beta}+2C^c_{d_i,\beta}+C^t_{d_i,\beta}$	.16*(-.05)	$2C'_{MC,\beta}$	.16(-.102)
$C_{d_i,\gamma}=C^c_{d_i,\gamma}=C^t_{d_i,\gamma}$	= 0*(0)	No	Equivalent
$C_{d_i,\phi}$	-.08*(.011)	$-C'_{MC,\beta}$	-.08(.05)
$C_{d_i,\psi}-C_{d_i,\delta}$	.10*	$2C'_{MC,\alpha}$	.10
$C_{d_i,\psi}-C^t_{d_i,\delta}$	-.10*	$-2C'_{MC,\alpha}$	-.10

[a] * denotes values held constant in calculations; values in parentheses are equivalent force constants.

[b] ** denotes values for $Cr(CO)_6$; other values are averages for $Cr(CO)_6$, $Mo(CO)_6$, and $W(CO)_6$. Ref. (14).

TABLE 21 continued

$C^{c}_{d_i,\psi} - C^{c}_{d_i,\delta}$	.10*	$2C^{\bullet}_{MC,\alpha}$	.10
$C_{d_i,\alpha} - C^{c}_{d_i,\alpha}$	.10*(-.05)	$C^{\bullet}_{MC,\alpha} - C^{\bullet\bullet}_{MC,\alpha}$	.10(-.20)
$C_{d_o,\gamma}$	.0388(-.049)	$C^{\bullet}_{MC,\beta}$	.08(-.051)
$C_{d_o,\psi-\delta}$	-.12(.20)	$-C^{\bullet}_{MC,\alpha}$	-.05(.10)
$C_{\Delta,\gamma}$	-.078(.068)	No	Equivalent
$C_{\Delta,\psi-\delta}$	-.09(.09)	No	Equivalent

It is immediately obvious that $C_{r_i} < C_{r_o}$ (i.e. $F_{r_i} > F_{r_o}$) and $C_{d_i} > C_{d_o}$ ($F_{d_i} < F_{d_o}$). This is due to the effect of greater $d\pi - \pi^*$ bonding from Mn to the axial-CO ligand relative to the radial-CO ligands.

This is also obvious in the difference of C_{d_o} for Mn(I) and c_{MC} for M(0)($C_{d_o} = .437$ and $c_{MC} = .509$). The radial M--C constants are about the same ($C_{d_i} = .449$ and $c_{MC} = .509$) indicating little net change has occurred in these bonds.

This is somewhat deceptive, however, as the radial-CO stretching constant is a good deal lower for $Mn^{(+1)}$ than c_{CO} ($C_{r_i} = .05693$ and $c_{CO} = .05905$) while the axial-CO stretching constant is approximately the same as c_{CO} ($C_{r_o} = .06057$ and $c_{CO} = .05905$). Thus sigma-bonding changes and their consequent effect on the pi-bonding system must not be ignored in these systems as is tacitly done in the majority of "approximate" force fields for C--O stretching only (1, 5, 15). The presence of a larger positive charge on the Mn atom relative to the neutral hexacarbonyl system shrinks the occupied $d\pi$- orbitals sufficiently so that the population of the axial-CO π^* level is roughly the same as in $M(CO)_6$ (as $C_{r_o} \cong c_{CO}$). This increase in C--O bond order is clear in the case of

the radial-CO groups where $C_{r_i} < c_{CO}$ where there is less compensating effect due to the substituted ligand's much lower π-electron accepting capability.

The greater positive charge on the Mn atom is also partly responsible for the greater Mn--C bonding as both C_{d_i} and C_{d_o} are $< c_{MC}$. The importance of sigma-bonding (30) in the interpretation of bonding changes will be discussed further in connection with the $Mn(CO)_5X$ and $Cr(CO)_5X^-$ systems in Part III.

Another approximation inherent in many simplified potential field calculations (1,5,8,15,18) is that the magnitude of the various CO, C'O' interaction constants is determined primarily by the amount of π-bonding d-orbitals common to CO and C'O'. As force constants were used in that formulation, this discussion will also be in terms of force constants.

The approximation that $F^t_{r_i,r_i} = 2F^c_{r_i,r_i}$ (1) is shown to be in fortuitous agreement with the approximate calculations of reference (18) by the fact that $F^t_{r_i,r_i} \cong .25F^c_{r_i,r_i}$ in the present calculation. As was illustrated by comparison calculations in (14), this error is introduced primarily by the neglect of the anharmonic nature of the C--O stretching modes and the neglect of mixing primarily with the appropriate M--C stretching modes.

It might also be expected that the interaction of radial-MC with radial-CO would be <u>smaller</u> than the interaction of axial-MC with axial-CO due to the larger relative amount of $d\pi \rightarrow$ axial-CO π^* bonding. This is definitely not the case as $F_{r_i,d_i} = .763$ and $F_{r_o,d_o} = .758$. It is even more interesting that $f_{CO,MC} = .758$ for $M(CO)_6$ supporting the suggestion in (14) that these interactions may be due to induction effects of the changing CO dipole moments rather than changes in the pi-bonding system.

Little can be said of C_Δ. The observed M--X stretching frequency for $Cr(CO)_5Br^-$ is $188cm^{-1}$, and by a crude approximation:

$$C_\Delta(Cr) = C_\Delta(Mn) \frac{(\nu\ Mn\text{--}Br)^2}{(\nu\ Cr\text{--}Br)^2}$$

$$= .843\ (222/188)^2 = .995$$

with a corresponding decrease in F_Δ from 1.32 to 1.12; the higher bond order of Mn--Br compared to Cr--Br correlates well with the higher positive charge on Mn than Cr.

The greatest interaction of Δ with another stretching coordinate is $C_{\Delta,d_o} = -.088$; the standard error is $\pm$ .27, however, and thus this calculated value is judged to be not very significantly different from zero.

The implications of a slightly negative interaction compliance constant with d_o (and thus a slightly positive interaction force constant) may be interpreted in terms of a dominant sigma-bonding effect. When d_o is increased (stretching the axial-MC bond), the population of electrons in that sigma bond decreases creating an increased positive charge on the Mn atom. This in turn strengthens the Mn--Br bond; hence the sign of C_{Δ,d_o} and F_{Δ,d_o}.

Bend-Bend Constants

The most striking difference between the M--C--O bending constants for $Mn(CO)_5Br$ and $M(CO)_6$ is for C_γ and c_β (C_γ = 1.287 and c_β = 1.919).

This was more or less assumed to be the case earlier when $(E)_\gamma$ was assigned to the higher of the observed I. R. bands at 604 and 545cm^{-1} and it should be emphasized again that the choice of this assignment is supported by the reasonable potential energy distribution obtained and the far better agreement of $C^c_{\gamma,\gamma}$ and $C^t_{\gamma,\gamma}$ with values transferred from the $M(CO)_6$ system (see pages 75 and 76).

It is also apparent that the magnitudes of $C^c_{\gamma,\gamma}$ and $C^t_{\gamma,\gamma}$ are considerably less than their hexacarbonyl equivalent. Although the assignment of this mode has

been successful through the argument that the vibration would involve distortion of the strongest $d\pi \rightarrow \pi^*$ bonds, the interaction constants are less than those for a system with presumably weaker equivalent $d\pi \rightarrow \pi^*$ bonds.

Although it is a more tenuous argument than that advanced above for the more precisely determined stretch-stretch interactions, it seems that the M--C--O bend-bend interactions may also arise primarily through electrostatic effects rather than changes in the pi-bonding system. This is further supported in that $C^c_{\gamma,\gamma} \gg C^t_{\gamma,\gamma}$ as would be expected for a through-space electrostatic interaction.

The compliance constant C_β for the in-plane MCO bending coordinate is found to be quite near the value determined for $Cr(CO)_6$. The order $C_\beta > C_\gamma$ was predicted above due to changes in π-bonding between the $M(CO)_6$ and $Mn(CO)_5Br$ molecules and the calculated value of C_β agrees with this prediction. This similarity in the in-plane compliance constants for the systems is also reflected in the interaction constant $C^t_{\beta,\beta} = -.264$ while $c^\circ_{\beta\beta} = -.25$. Due to the fact that the A_2 frequency $(A_2)_\beta$ was not observed, insufficient information was available for the calculation of both $C^c_{\beta,\beta}$ and $C^t_{\beta,\beta}$, hence $C^c_{\beta,\beta}$ was held fixed at .07.

According to the π-bonding model we should expect that the bending of the axial M--C--O angle would show the least compliance (or greatest restoring force) of all the MCO bending coordinates. However, the calculated value of C'_{ϕ} is slightly more than the in-plane constant, C_{β}. One possible solution for this dilemma is the reversal of the assignments for $(E)_{\gamma}$ and $(E)_{\phi}$. As was mentioned above, this leads to an extremely undesirable potential energy distribution and solutions for C_{γ}, $C^{c}_{\gamma,\gamma}$, and $C^{t}_{\gamma,\gamma}$. Furthermore, the value of C'_{ϕ} only drops from 2.30 to 1.96 for this reversed assignment.

We may be more certain of the values calculated for C_{γ} and C_{β} because of the additional equations for these coordinates obtained in the accurately assigned and determined A_1, B_1, and B_2 blocks. The ϕ MCO bending coordinate, however, is involved only in the E symmetry block, and thus significant errors in C'_{ϕ} may have resulted from the imprecision in the present calculation for this symmetry block. Hopefully further calculations for this block will refine the value presented here for C'_{ϕ}.

Another mechanism which might account for the differences among the MCO compliance constants is the electrostatic repulsion between the moving carbon atom and the bromine atom; this is larger for the out-of-plane

γ coordinate than the β and ϕ coordinates and possibly could account for the ordering $C'_{\phi} \cong C_{\beta} > C_{\gamma}$. Corroborative evidence for this mechanism is found in that $(E_1)_{\gamma}$ for $Mn_2(CO)_{10}$, which is analogous to $(E)_{\gamma}$ for $Mn(CO)_5Br$, has shifted to a position within $10cm^{-1}$ of $(E_1)_{\phi}$ (see figure 24 in Part II). This implies a smaller electrostatic interaction for the out-of-plane bending coordinate which seems consistent with the much more covalent nature of the binuclear species.

The I.R. spectrum of $Mn(CO)_5H$ and its deuterium analogue have recently been reported (13) with a brief vibrational analysis; unfortunately the locations of ν_{β}, ν_{γ}, and ν_{ϕ} for this compound are quite obscured by the large amount of mixing of the C--Mn--H bending mode (also of E symmetry) with the Mn--C--O bending modes. A normal coordinate calculation for this molecule would be most interesting for the purpose of determining the importance of the electrostatic interaction mechanism for Mn--C--O bending modes. Recent neutron diffraction studies (28) have shown the Mn--H bond distance is 1.601 A. which is in good agreement with the covalent radii of Mn and H. However, the axial Mn--C is not foreshortened relative to the equatorial Mn--C distances. This is not expected on the basis of π-bonding considerations alone, and thus a fair amount of positive

charge on the central Mn atom must be hypothesized to account for this situation.

Considerable electrostatic interactions of the MCO bending and the polarized H ligand are therefore expected, and if this interaction is the dominant one in the determination of C_β, C_γ, and C'_ϕ, it is predicted that these values for $Mn(CO)_5H$ will more closely resemble those of $Mn(CO)_5Br$ than $Mn_2(CO)_{10}$.

Very little may be said about the calculated compliance constants for the C--Mn--C bending coordinates ψ and α, and the C--Mn--Br bending coordinate δ. The values for C_α, $C_\psi - C_{\psi\delta}$, and $C_\psi - C^t_{\psi,\psi}$ lie fairly close to their counterparts for the $M(CO)_6$ calculations. That the constants involving the out-of-plane coordinate $\psi - \delta$ generally exhibit <u>less</u> compliance than their hexacarbonyl analogues may be related to the behavior noted above for the MCO bending coordinates.

This self-consistency is a good indication that at least the frequency assignments for this low energy region are correct. Further refined calculations will be necessary, however, before a more definite relationship between MCO and CMC bending constants can be established.

The values calculated for $C^c_{\psi,\psi} - C^c_{\psi,\delta}$ and $C^c_{\alpha,\alpha}$ are seen to be in fair and good agreement, respectively, with their $M(CO)_6$ counterparts.

There remain to be discussed only those interactions between different symmetry coordinates. $C_{\beta,\gamma}$, $C^c_{\beta,\gamma}$, and $C^t_{\beta,\gamma}$ had no equivalents among the c_{ij} for $M(CO)_6$ and were all constrained equal to zero. $C_{\beta,\phi}$ was calculated = -.37 in fairly good agreement with the transferred value of -.25.

The CMC and MCO coordinates α and β are highly mechanically coupled and proved to be very sensitive to the values of the off-diagonal constants coupling them. The values for $C_{\beta,\alpha}$ and $C^c_{\beta,\alpha}$ are in fair agreement with transferred hexacarbonyl estimates.

The out-of-plane coordinates ψ-δ and ψ were also very sensitive to their off-diagonal coupling constants and it is seen that the value for $C_{\gamma,\psi\text{-}\delta} + C^t_{\gamma,\psi\text{-}\delta}$ is quite different from the hexacarbonyl equivalent. This is yet another indication that the major distinction among the bending coordinates of the two systems is between the out-of-plane modes.

The remainder of the bend-bend constants were judged to be of less physical significance than those above (indeed most of these were held constant during

the calculations) and no attempt will be made to discuss them at this point.

Stretch-Bend Interactions

All constants involving r_i and r_o were held at constant values in the calculations. These values proved to be quite small and poorly determined in the calculations for $M(CO)_6$ (14) so that the above approach was deemed most reasonable for the more complex $Mn(CO)_5Br$ system. A similar procedure was adopted with regard to constants involving d_i.

Values for $C_{d_o,\gamma}$ and $C_{d_o,\psi-\delta}$ are in fair agreement with values transferred from $M(CO)_6$. The remaining constants, $C_{\Delta,\gamma}$ and $C_{\Delta,\psi-\delta}$ are both negative and their interpretation is essentially the same as that for $C_{d_o,\Delta}$ (which was found = -.088); that is, the sign of these interactions is best explained by changes in the electron density of the appropriate metal-ligand bond due to the change in the charge of the central Mn atom; this in turn is caused by the stretching of the Mn--Br bond through a unit displacement.

The negative sign of these compliance constants can not be explained on the basis of changes in π-bonding. An increasing amount of positive charge on the Mn atom due to stretching the Mn--Br bond would be expected

to shrink the metal d-orbitals causing weaker Mn--C π-bonds; this mechanism would thus predict a more compliant C--Mn--C bending coordinate and positive values for $C_{\Delta,\gamma}$ and $C_{\Delta,\psi-\delta}$. This is contradictory with calculated values for these constants.

Conclusions

The following will summarize briefly the conclusions on the chemical bonding within the $Mn(CO)_5Br$ system on the basis of the vibration analysis presented in this chapter.

1. Changes in C--O bond order from $M(CO)_6$ to $Mn(CO)_5Br$ are seen primarily in the radial ligands which are approximately 5% less compliant than the C--O bonds in $M(CO)_6$. The compliance of the axial-CO bond is very nearly the same as that of a CO group in $M(CO)_6$.

2. These changes in C--O bond order are produced by two effects: a selectively increasing population of the CO π^* orbital in the axial-CO ligand due to the decreased pi-acceptor capability of the Br^- ligand; and by a concurrent decreasing population of both radial- and axial-CO π^* orbitals due to the shrinkage of the filled metal d-orbitals which is caused by the

relatively higher positive charge on the Mn atom compared to the M(O) atom in $M(CO)_6$.

3. The pi-effect described above is responsible for making the axial-MnC bond less compliant than the radial-MnC bonds; however, both axial- and radial-MnC bonds are less compliant than the M--C bonds in $M(CO)_6$ due to the greater amount of Mn--CO sigma bonding present.

4. Stretch-stretch interaction constants were found not to agree with values predicted from only simple π-bonding effects (1, 18). At least some contribution to these interactions must arise from electrostatic effects (or "oscillating dipoles") described in (8, 14, 29).

5. Changes in π-bonding did not fully explain the ordering of the primary MCO bending constants although it is correctly predicted that the compliance of the out-of-plane bend is less than the compliance of the in-plane bend.

An alternative mechanism was proposed to explain the anomalously high compliance of the axial-MCO bending coordinate. This mechanism is based on electrostatic interactions and successfully predicts the order $C_\gamma < C_\beta \cong C_\phi$.

6. CMC bending constants are rather poorly determined but seem to reflect the dependence of the MCO modes on electrostatic interactions.

7. Bend-bend interactions also are found not to change noticeably between the different π-bonding situations in $Mn(CO)_5Br$ and $M(CO)_6$ except for those interactions involving out-of-plane bending. This further supports the electrostatic interaction mechanism above.

8. Changes in the amount of charge on the central metal atom due to the difference in σ-bonding between $Mn(CO)_5Br$ and $M(CO)_6$ are necessary to explain the signs of the interaction constants between Mn--Br stretching and γ-MnCO bending, d_o-MnC stretching, and $(\gamma-\delta)$-CMnC bending, respectively, all of which constants are negative.

II.

VIBRATIONAL ANALYSIS OF DIMANGANESE DECACARBONYL

CHAPTER 1

VIBRATIONAL SPECTRUM OF DIMANGANESE DECACARBONYL

Preparation and Instrumentation

Normal $Mn_2(CO)_{10}$ was furnished by the Pressure Chemical Company and the $Mn_2(^{13}CO)_{10}$ used in this study was prepared by Mr. Maxwell Goldblatt at LASL by the reaction of $Mn(C_2H_3O_2)_2$ with ^{13}CO under pressure. Both compounds were quite impure on arrival and were sublimed in vacuo at 60° C. to obtain the pure, bright yellow $Mn_2(CO)_{10}$.

The purity of the resultant product was checked by comparison with the reported I. R. spectrum in the 1900 to 2100 cm^{-1} region (3) and this criterion was used in all subsequent investigations.

Although the solid is stable in air over a period of weeks, solutions in CH_2Cl_2 were found to decompose rapidly within the course of a day. Therefore fresh solutions were prepared for each spectroscopic determination.

The instruments used were the same as those mentioned in Part I with the exception that far I. R. measurements with the Beckmann IR-11 were not made. Instead this portion of the spectrum is taken from Reference (20).

C--O Stretching Vibrations

The internal coordinates for $Mn_2(CO)_{10}$ are shown in figure 19 and the symmetry coordinates for the C--O stretching modes are shown in figure 20. For the A_1 and B_2, A_2 and B_1, and E_1 and E_3 modes the internal coordinates will be similar to A_1, A_2 and E modes, respectively, of $Mn(CO)_5Br$.

Each of the modes for the monomeric compound will have split into a pair of modes in the dimeric system. These modes will differ only in their symmetry with respect to those operations which interchange the two halves of the molecule and they correlate as follows:

		$Mn_2(CO)_{10}$		
$Mn(CO)_5Br$		In Phase		Out of Phase
A_1	$\longrightarrow$	A_1	+	B_2
A_2	$\longrightarrow$	A_2	+	B_1
E	$\longrightarrow$	E_1	+	E_3

The components of the degenerate E_2 mode are restricted to the separate halves of the molecule and resemble exactly their B_1 and B_2 analogues in the $Mn(CO)_5Br$ system.

Of these modes the A_1, E_2, and E_3 types are Raman active only, the B_2 and E_1 types are I. R. active only, while the A_2 and B_1 types are totally inactive.

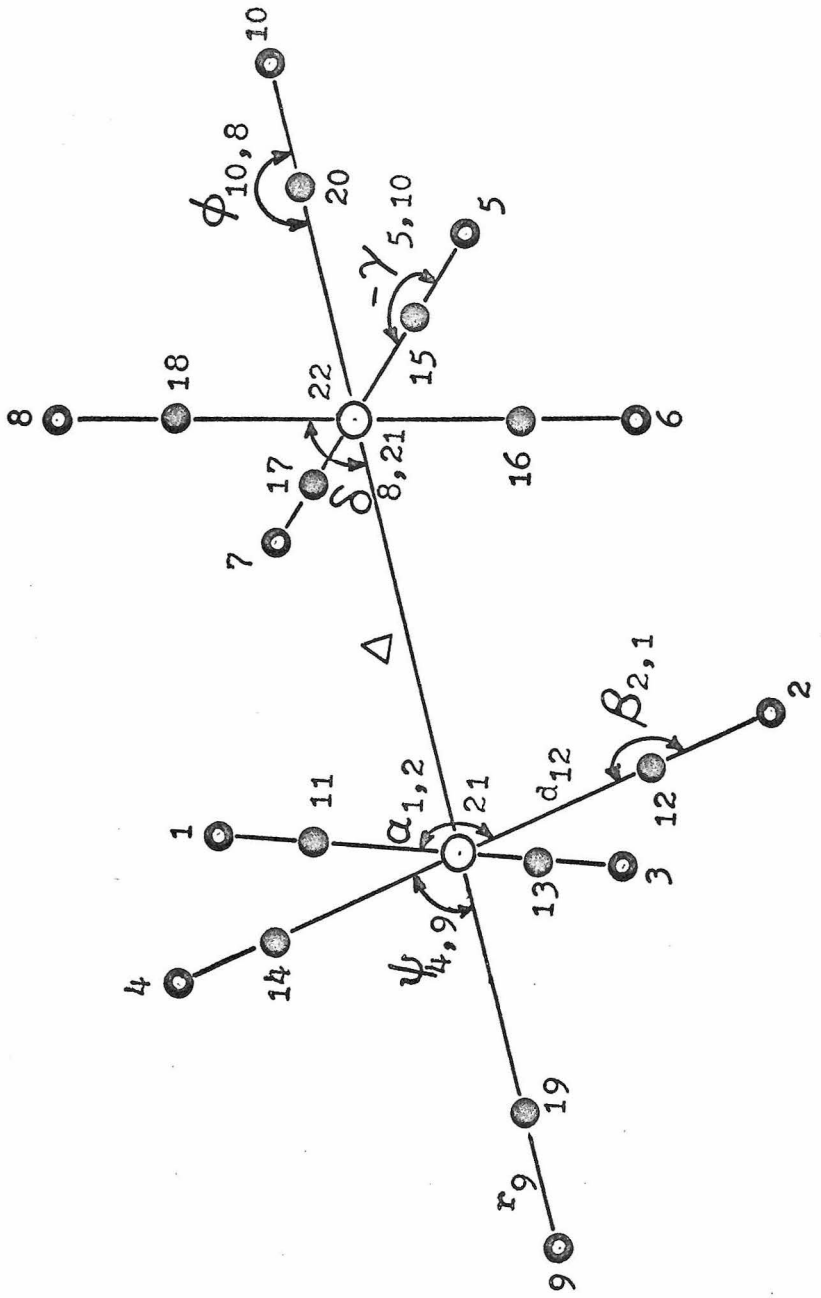

Figure 19. Internal Coordinates for $Mn_2(CO)_{10}$

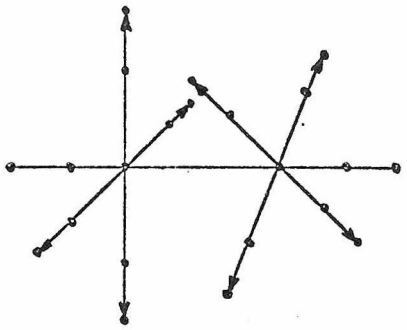

$\nu_{2114} \longrightarrow (A_1)_{r_i}$

$S_1 = 1/2\sqrt{2}(r_1+r_2+r_3+r_4+r_5+r_6+r_7+r_8)$

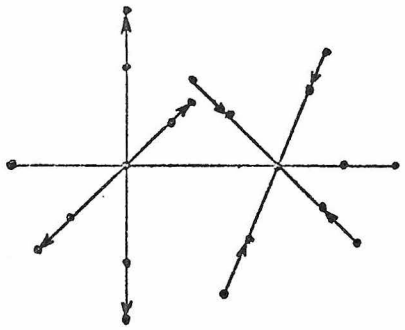

$\nu_{2067} \longrightarrow (B_2)_{r_i}$

$S_{11} = 1/2\sqrt{2}(r_1+r_2+r_3+r_4-r_5-r_6-r_7-r_8)$

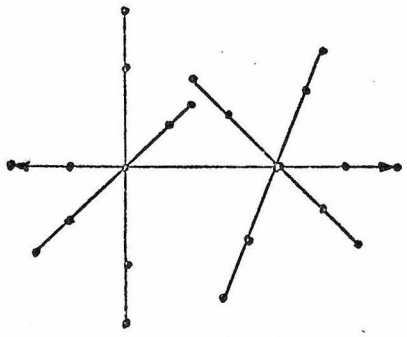

$\nu_{1992} \longrightarrow (A_1)_{r_o}$

$S_2 = 1/\sqrt{2}(r_9+r_{10})$

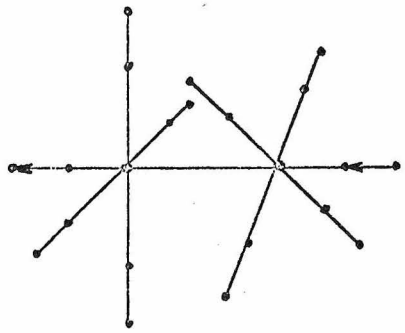

$\nu_{1979} \longrightarrow (B_2)_{r_o}$

$S_{12} = 1/\sqrt{2}(r_9-r_{10})$

Figure 20. Internal Symmetry Coordinates and Frequency Assignments for C--O Stretching Modes

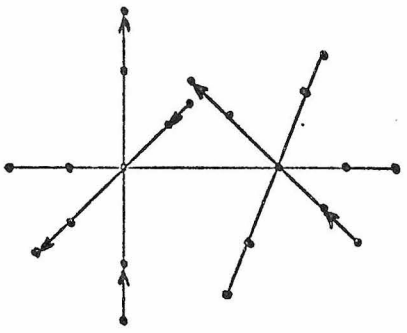

$\nu_{2012} \longrightarrow (E_1)_{r_i}$

$S_{17} = 1/2\sqrt{2}(r_1+r_2-r_3-r_4+\sqrt{2}r_5-\sqrt{2}r_7)$

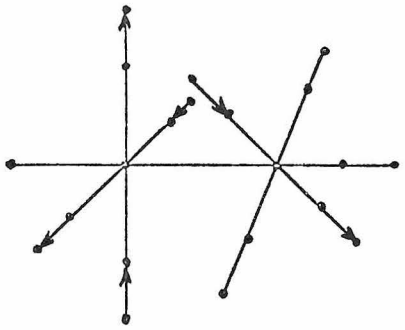

$\nu_{1978} \longrightarrow (E_3)_{r_i}$

$S_{31} = 1/2\sqrt{2}(r_1+r_2-r_3-r_4-\sqrt{2}r_5+\sqrt{2}r_7)$

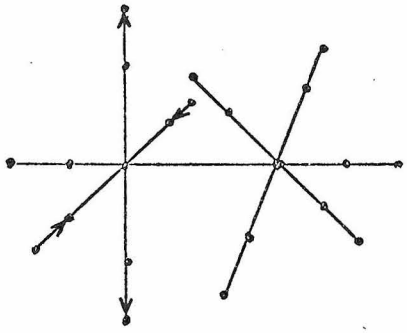

$\nu_{2020} \longrightarrow (E_2)_{r_i}$

$S_{25} = 1/2(r_1-r_2+r_3-r_4)$

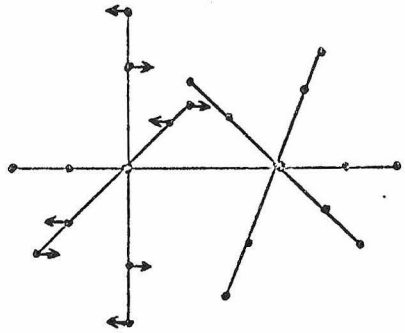

$\nu_{(673?)} \longrightarrow (E_2)_{\gamma}$

$S_{26} = 1/2(\gamma_1-\gamma_2+\gamma_3-\gamma_4)$

Figure 20. Internal Symmetry Coordinates and Frequency Assignments for C--O Stretching Modes and M--C--O Bending Mode

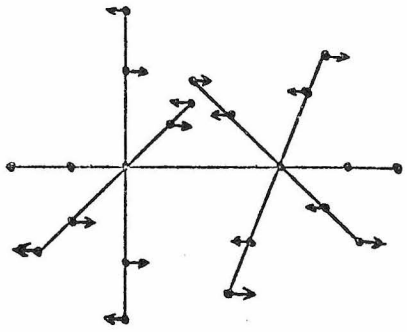

$\nu_{673} \longrightarrow (A_1)_\gamma$

$S_3 = 1/2\sqrt{2}(\gamma_1+\gamma_2+\gamma_3+\gamma_4+\gamma_5+\gamma_6+\gamma_7+\gamma_8)$

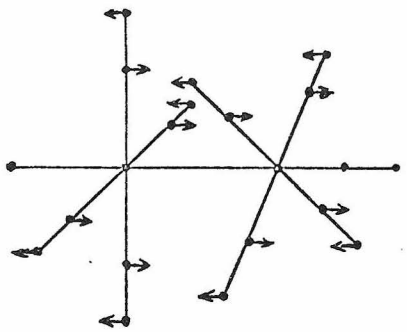

$\nu_{645} \longrightarrow (B_2)_\gamma$

$S_{13} = 1/2\sqrt{2}(\gamma_1+\gamma_2+\gamma_3+\gamma_4-\gamma_5-\gamma_6-\gamma_7-\gamma_8)$

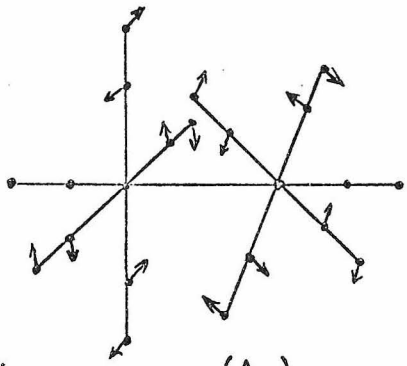

$\nu_? \longrightarrow (A_2)_\beta$

$S_8 = 1/2\sqrt{2}(\beta_1+\beta_2+\beta_3+\beta_4+\beta_5+\beta_6+\beta_7+\beta_8)$

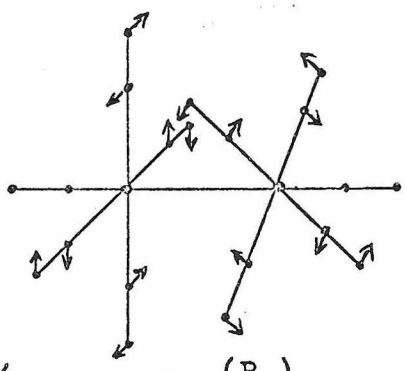

$\nu_? \longrightarrow (B_1)_\beta$

$S_9 = 1/2\sqrt{2}(\beta_1+\beta_2+\beta_3+\beta_4-\beta_5-\beta_6-\beta_7-\beta_8)$

Figure 20. Internal Symmetry Coordinates and Frequency Assignments for M--C--O Bending Modes

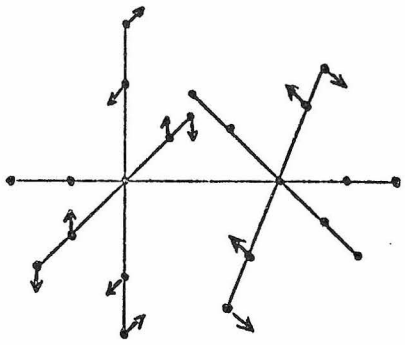

$\nu_{649} \longrightarrow (E_1)_\beta$

$S_{18} = 1/2\sqrt{2}(\beta_1-\beta_2-\beta_3+\beta_4 - \sqrt{2}\beta_6+\sqrt{2}\beta_8)$

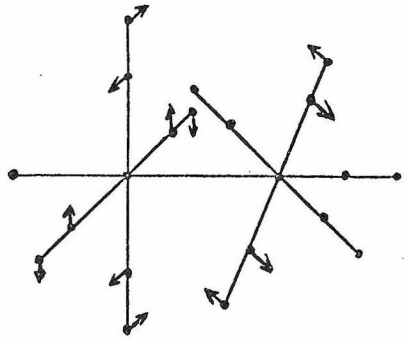

$\nu_{?} \longrightarrow (E_3)_\beta$

$S_{32} = 1/2\sqrt{2}(\beta_1-\beta_2-\beta_3+\beta_4 + \sqrt{2}\beta_6-\sqrt{2}\beta_8)$

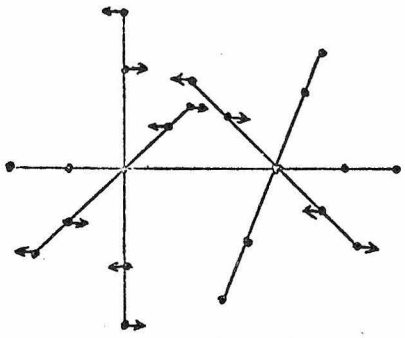

$\nu_{558} \longrightarrow (E_1)_\gamma$

$S_{19} = 1/2\sqrt{2}(\gamma_1+\gamma_2-\gamma_3-\gamma_4 + \sqrt{2}\gamma_5+\sqrt{2}\gamma_7)$

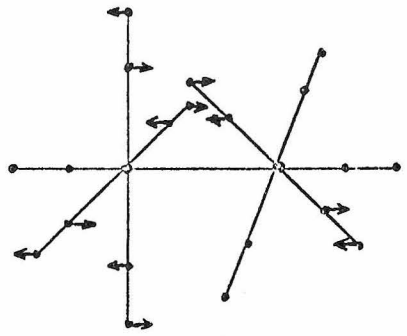

$\nu_{555} \longrightarrow (E_3)_\gamma$

$S_{33} = 1/2\sqrt{2}(\gamma_1+\gamma_2-\gamma_3-\gamma_4 + \sqrt{2}\gamma_5-\sqrt{2}\gamma_7)$

Figure 20. Internal Symmetry Coordinates and Frequency Assignments for M--C--O Bending Modes

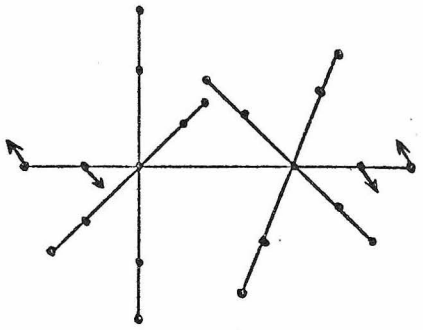

$\nu_{547} \longrightarrow (E_1)_\phi$

$S_{20} = 1/2(-\phi_1-\phi_2+\sqrt{2}\phi_7)$

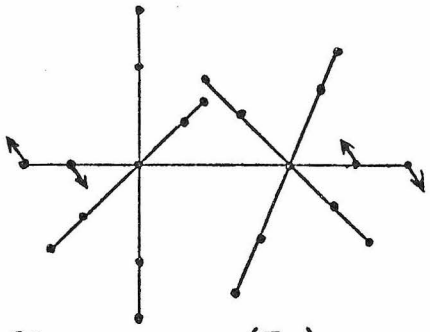

$\nu_{541} \longrightarrow (E_3)_\phi$

$S_{34} = 1/2(-\phi_1-\phi_2-\sqrt{2}\phi_7)$

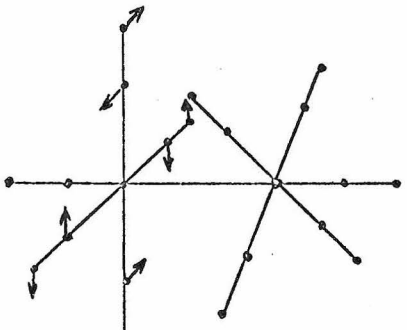

$\nu_{480} \longrightarrow (E_2)_\beta$

$S_{27} = 1/2(\beta_1-\beta_2+\beta_3-\beta_4)$

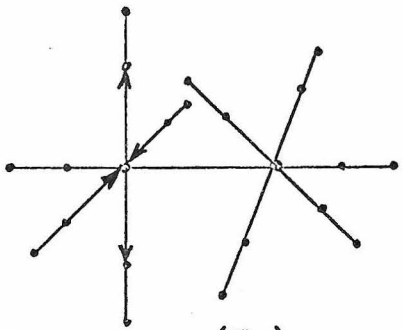

$\nu_{421} \longrightarrow (E_2)_{d_i}$

$S_{28} = 1/2(d_1-d_2+d_3-d_4)$

Figure 20. Internal Symmetry Coordinates and Frequency Assignments for M--C--O Bending Modes and M--C Stretching Mode

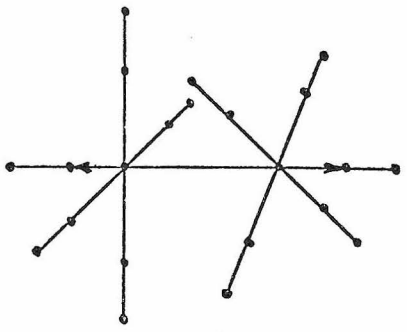

$\nu_{482} \longrightarrow (A_1)_{d_o}$

$S_4 = 1/\sqrt{2}(d_9+d_{10})$

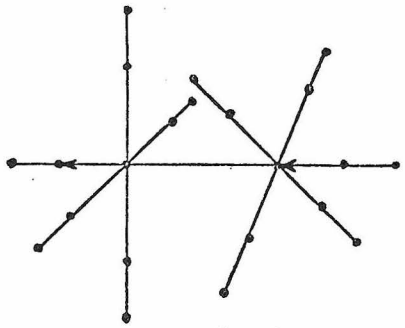

$\nu_{468} \longrightarrow (B_2)_{d_o}$

$S_{14} = 1/\sqrt{2}(d_9-d_{10})$

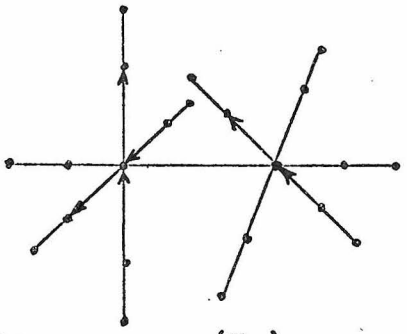

$\nu_{468} \longrightarrow (E_1)_{d_i}$

$S_{21} = 1/2\sqrt{2}(d_1+d_2-d_3-d_4 +\sqrt{2}d_5-\sqrt{2}d_7)$

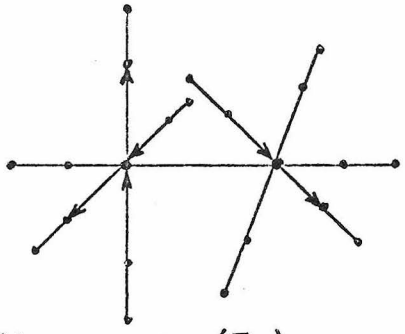

$\nu_{465} \longrightarrow (E_3)_{d_i}$

$S_{35} = 1/2\sqrt{2}(d_1+d_2-d_3-d_4 -\sqrt{2}d_5+\sqrt{2}d_7)$

Figure 20. Internal Symmetry Coordinates and Frequency Assignments for M--C Stretching Modes

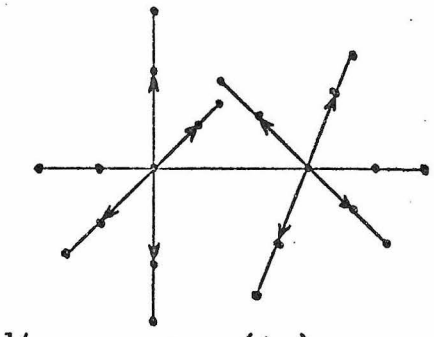

$\nu_{411} \longrightarrow (A_1)_{d_i}$

$S_5 = 1/2\sqrt{2}(d_1+d_2+d_3+d_4+d_5+d_6+d_7+d_8)$

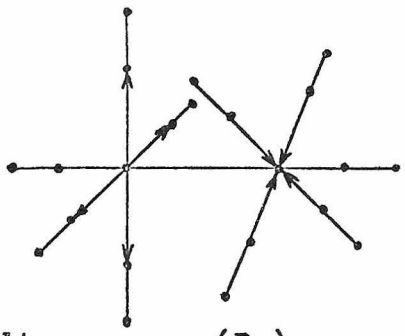

$\nu_{399} \longrightarrow (B_2)_{d_i}$

$S_{15} = 1/2\sqrt{2}(d_1+d_2+d_3+d_4-d_5-d_6-d_7-d_8)$

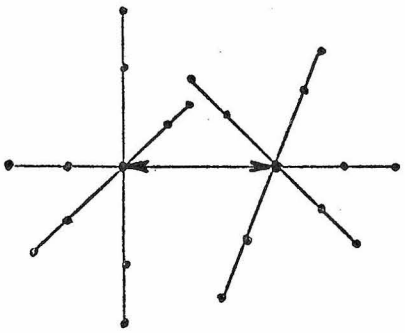

$\nu_{160} \longrightarrow (A_1)_{\Delta}$

$S_6 = \Delta$

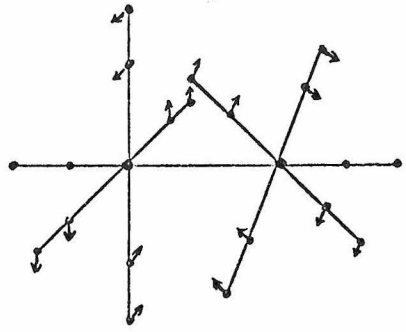

$\nu_{?} \longrightarrow (B_1)_{\tau}$

$S_{10} = 1/2(\tau_1+\tau_2+\tau_3+\tau_4)$

Figure 20. Internal Symmetry Coordinates and Frequency Assignments for M--C Stretching Modes, C--M--M--C Torsional Mode

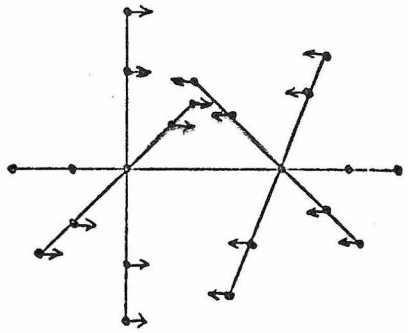

$\nu_{113} \longrightarrow (A_1)_{\psi-\delta}$

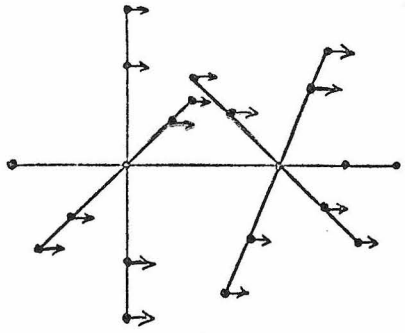

$\nu_{\sim 113} \longrightarrow (B_2)_{\psi-\delta}$

$$S_7 = 1/4(\psi_1+\psi_2+\psi_3+\psi_4+\psi_5+\psi_6+\psi_7+\psi_8-\delta_1-\delta_2-\delta_3-\delta_4-\delta_5-\delta_6-\delta_7-\delta_8)$$

$$S_{17} = 1/4(\psi_1+\psi_2+\psi_3+\psi_4-\psi_5-\psi_6-\psi_7-\psi_8-\delta_1-\delta_2-\delta_3-\delta_4+\delta_5+\delta_6+\delta_7+\delta_8)$$

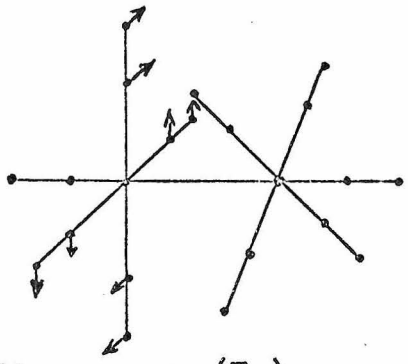

$\nu_{140} \longrightarrow (E_2)_{\alpha}$

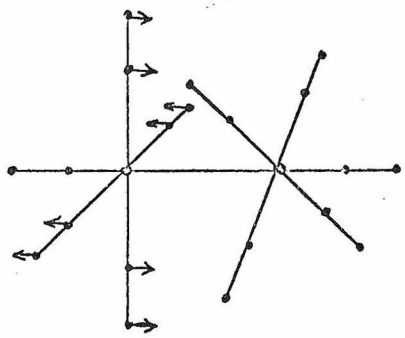

$\nu_{95} \longrightarrow (E_2)_{\psi-\delta}$

$$S_{29} = 1/2(\alpha_{1,2}-\alpha_{2,3}+\alpha_{3,4}-\alpha_{4,1})$$

$$S_{30} = 1/2\sqrt{2}(\psi_1-\psi_2+\psi_3-\psi_4-\delta_1+\delta_2-\delta_3+\delta_4)$$

Figure 20. Internal Symmetry Coordinates and Frequency Assignments for C--M--C Bending Modes

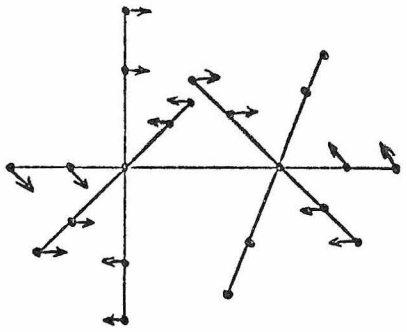

$\nu_{130} \longrightarrow (E_1)_\psi$

$S_{22} = 1/2\sqrt{2}(\psi_1+\psi_2-\psi_3-\psi_4 - \sqrt{2}\psi_5+\sqrt{2}\psi_7)$

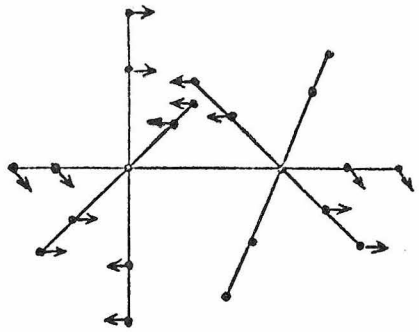

$\nu_{131} \longrightarrow (E_3)_\psi$

$S_{36} = 1/2\sqrt{2}(\psi_1+\psi_2-\psi_3-\psi_4 + \sqrt{2}\psi_5-\sqrt{2}\psi_7)$

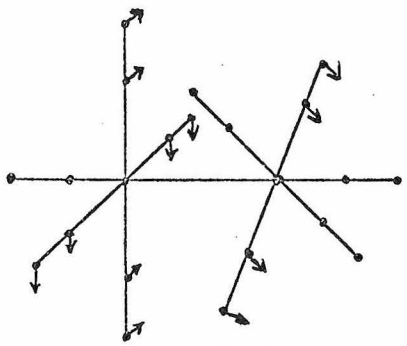

$\nu_{107?} \longrightarrow (E_1)_\alpha$

$S_{23} = 1/2\sqrt{2}(\sqrt{2}\alpha_{1,2}-\sqrt{2}\alpha_{3,4} + \alpha_{5,6}-\alpha_{6,7}-\alpha_{7,8}+\alpha_{8,5})$

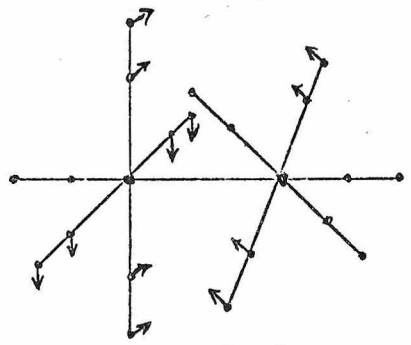

$\nu_{75} \longrightarrow (E_3)_\alpha$

$S_{37} = 1/2\sqrt{2}(\sqrt{2}\alpha_{1,2}-\sqrt{2}\alpha_{3,4} - \alpha_{5,6}+\alpha_{6,7} + \alpha_{7,8}-\alpha_{8,5})$

Figure 20. Internal Symmetry Coordinates and Frequency Assignments for C--M--C Bending Modes

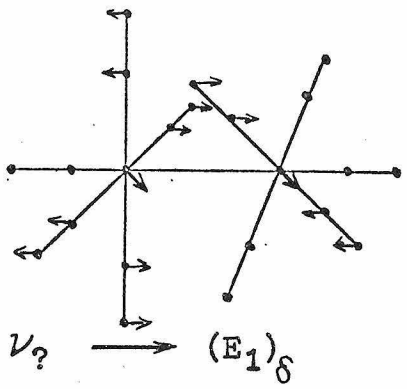

$$S_{24} = 1/2\sqrt{2}(\delta_1+\delta_2-\delta_3-\delta_4 -\sqrt{2}\delta_5+\sqrt{2}\delta_7)$$

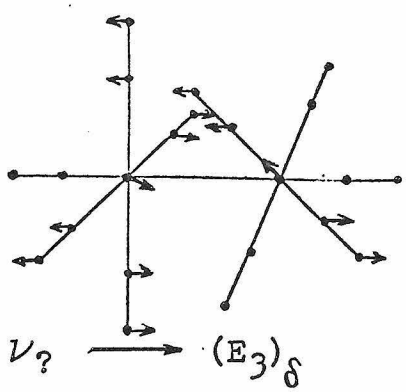

$$S_{38} = 1/2\sqrt{2}(\delta_1+\delta_2-\delta_3-\delta_4 +\sqrt{2}\delta_5-\sqrt{2}\delta_7)$$

Figure 20. Internal Symmetry Coordinates and Frequency Assignments for C--M--M Bending Modes

The three intense I. R. modes in the 1900 to 2100 cm^{-1} region have been reported and assigned a number of times (3, 5, 31, 32, 33, 34, 35). These assignments are $\nu_{2046} \longrightarrow (B_2)_{r_i}$, $\nu_{2012} \longrightarrow (E_1)_{r_i}$, and $\nu_{1979} \longrightarrow (B_2)_{r_o}$.

The Raman spectrum exhibits four bands and is shown in figure 22. The two at higher energy correlate with the $(A_1)_{r_i}$ and $(B_1)_{r_i}$ modes of $Mn(CO)_5Br$ and are thus assigned as $\nu_{2114} \longrightarrow (A_1)_{r_i}$ and $\nu_{2020} \longrightarrow (E_2)_{r_i}$. The assignment of the two bands at lower energy has been quite controversial among the various Raman studies of $Mn_2(CO)_{10}$. The assignment $\nu_{1978} \longrightarrow (A_1)_{r_o}$ and $\nu_{1992} \longrightarrow (E_3)_{r_i}$ has been argued for in (5) on the basis of positive CO-C'O' interaction force constants across the metal-metal bond. The authors in (31) and (34) favor the reverse assignment on the basis of the observed binary combination I. R. spectrum.

The present investigation has shown that the band at 1992 cm^{-1} in solution is very slightly polarized indicating that this is indeed the $(A_1)_{r_o}$ mode and thus the second assignment above is the preferred one.

M--C--O Bending Modes

The Raman and I. R. spectra of $Mn_2(CO)_{10}$ from 700 to 500 cm^{-1} are shown in figures 23 and 24. The

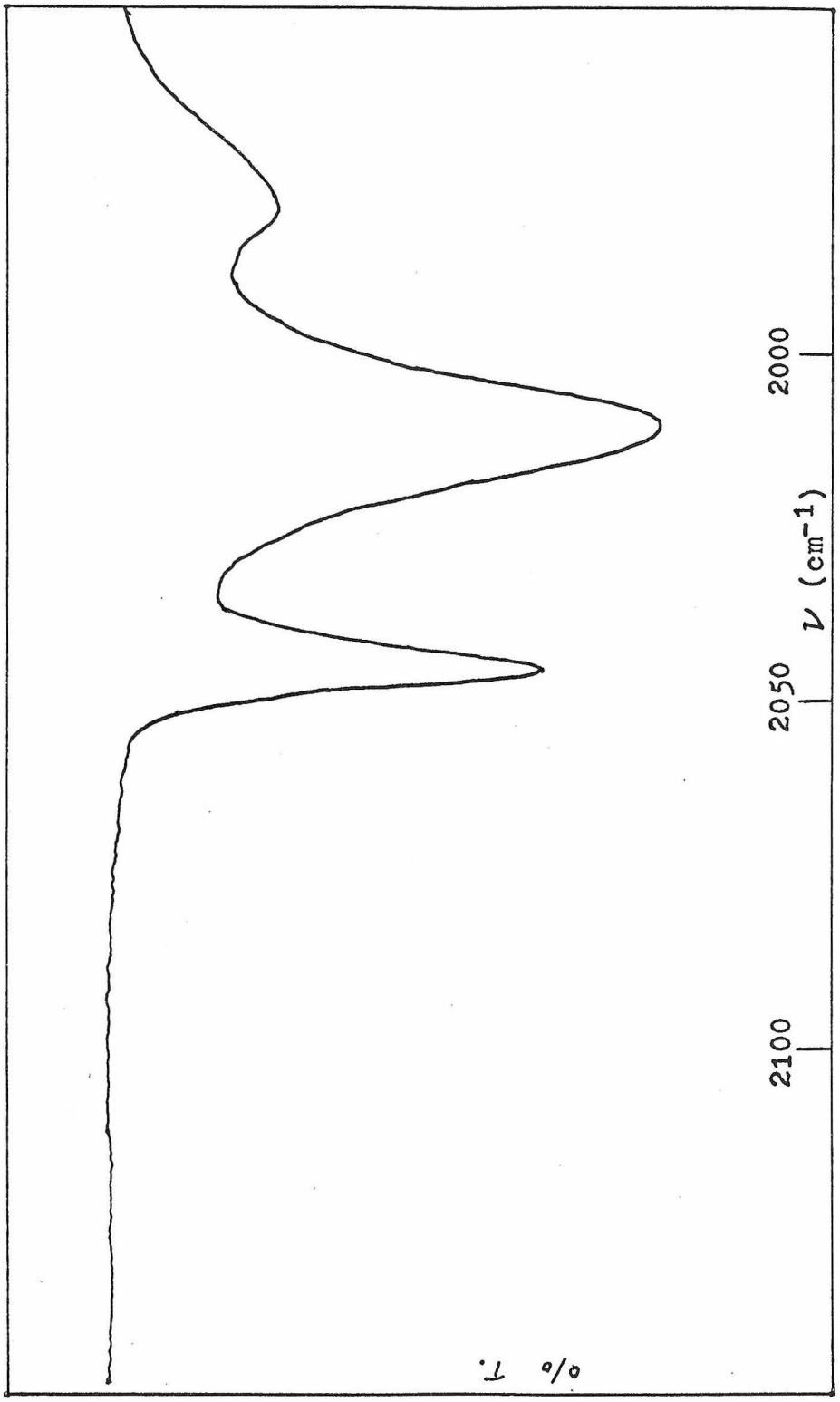

Figure 21 . I. R. Spectrum of $Mn_2(CO)_{10}$ in CH_2Cl_2 Solution.

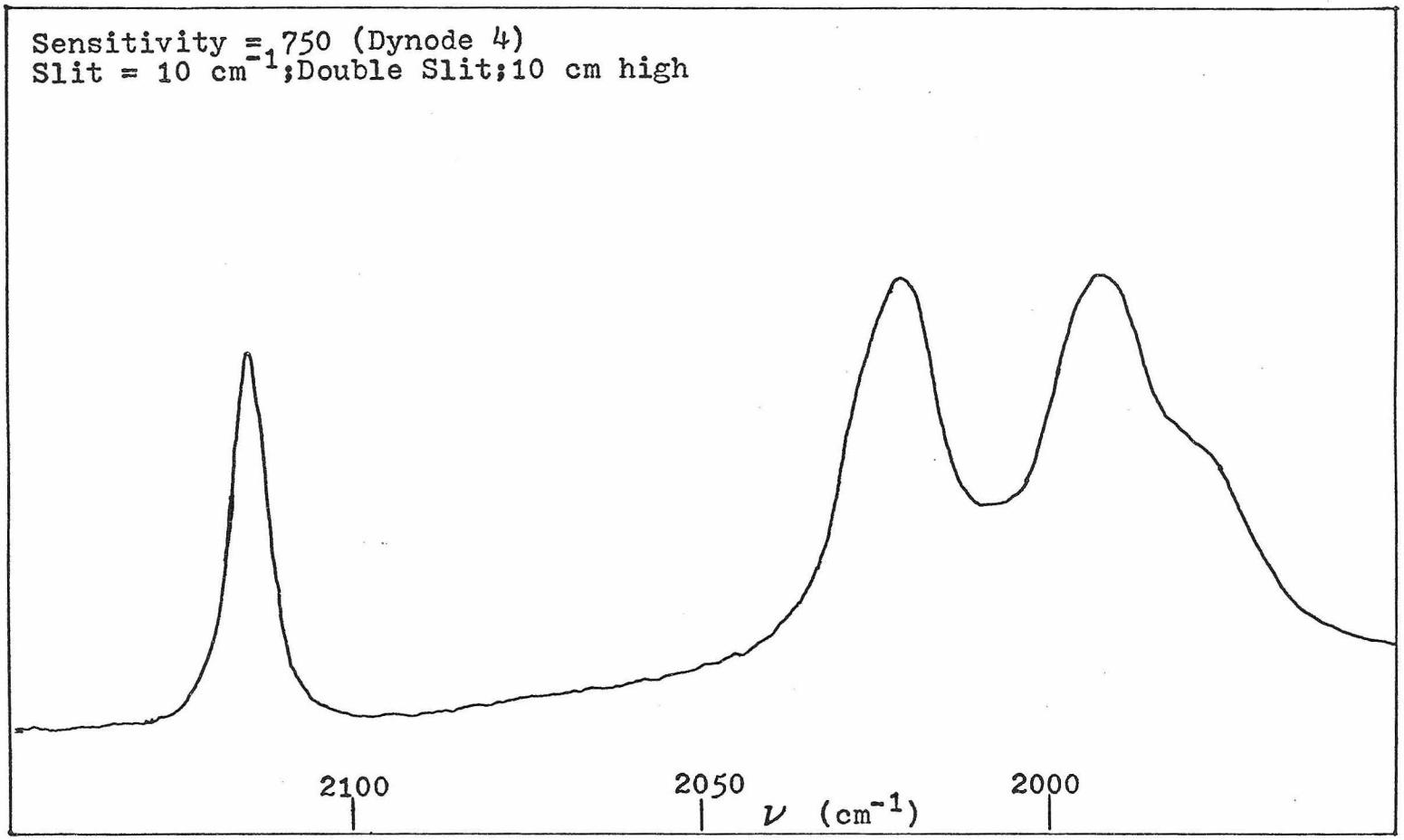

Figure 22. Raman Spectrum of $Mn_2(CO)_{10}$ in CH_2Cl_2 Solution.

three Raman bands around 625cm^{-1} for $Mn(CO)_5Br$ have apparently been replaced by the single peak at 672cm^{-1} for $Mn_2(CO)_{10}$. Depolarization measurements indicate that this is the $(A_1)_\gamma$ out-of-plane mode. As three modes are expected in this region it may be that either or both $(E_2)_\gamma$ and $(E_3)_\beta$ are accidentally degenerate with this mode. Further experiments with a more powerful exciting source than the 100 mw. He-Ne laser used in this study and low temperature apparatus will be necessary to establish the presence of weaker lines in the vicinity of 625cm^{-1}.

I. R. bands in this region consist of two strong peaks at 649 and 642cm^{-1}. Preliminary experiments by R. Levenson (36) reveal that the assignment of these bands should be $\nu_{649} \longrightarrow (B_2)_\gamma$ and $\nu_{642} \longrightarrow (E_1)_\beta$. This ordering was obtained from polarized I. R. spectra of $Mn_2(CO)_{10}$ in a nematic liquid crystal as described in (35).

Two pairs of Raman-I. R. splittings are observed at 555 and 558cm^{-1} and at 541 and 547cm^{-1}. One of these pairs is analogous to the $(E)_\phi$ mode of $Mn(CO)_5Br$ at 545cm^{-1} and thus we assign $\nu_{547} \longrightarrow (E_1)_\phi$ and $\nu_{541} \longrightarrow (E_3)_\phi$.

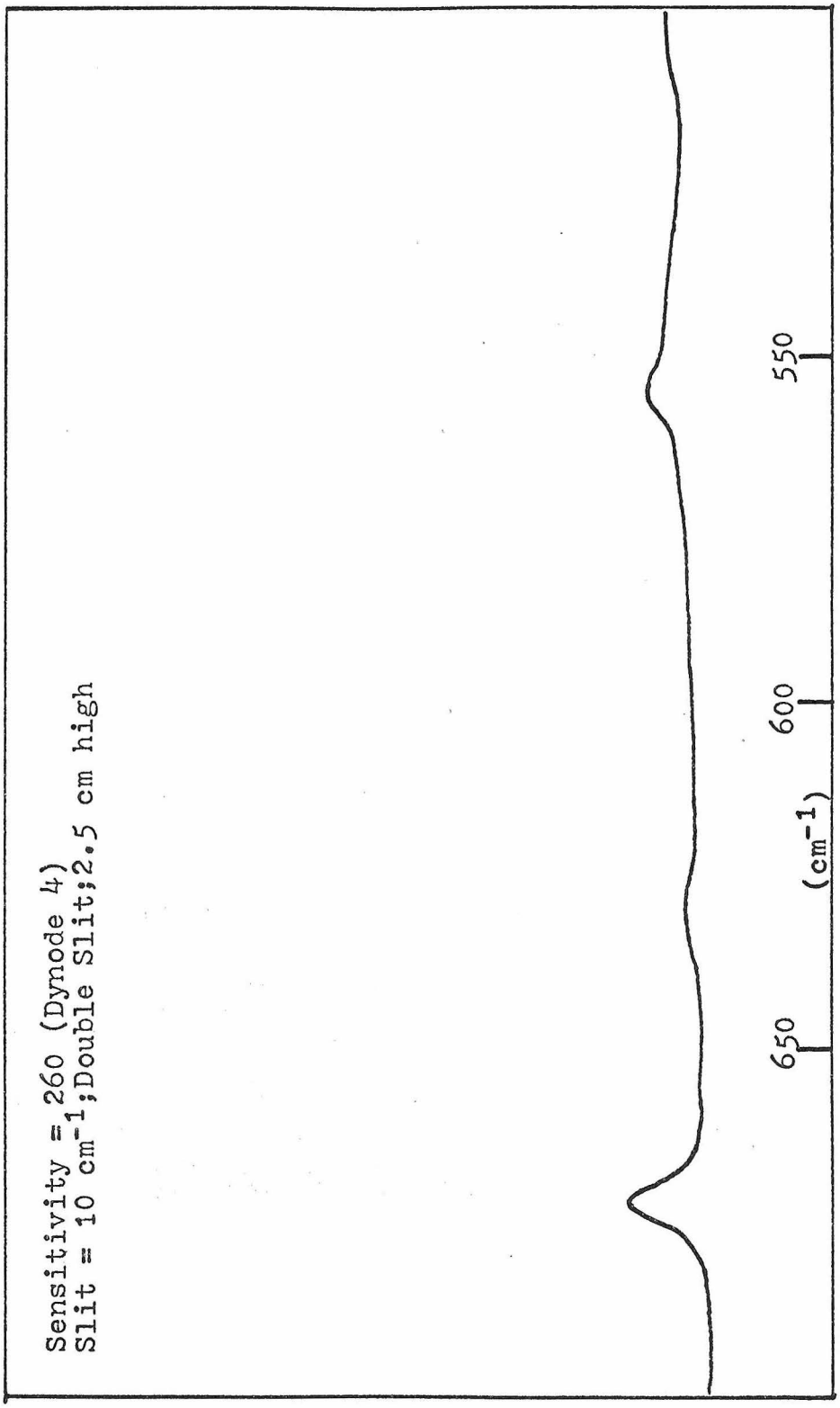

Figure 23. Raman Spectrum of Solid $Mn_2(CO)_{10}$

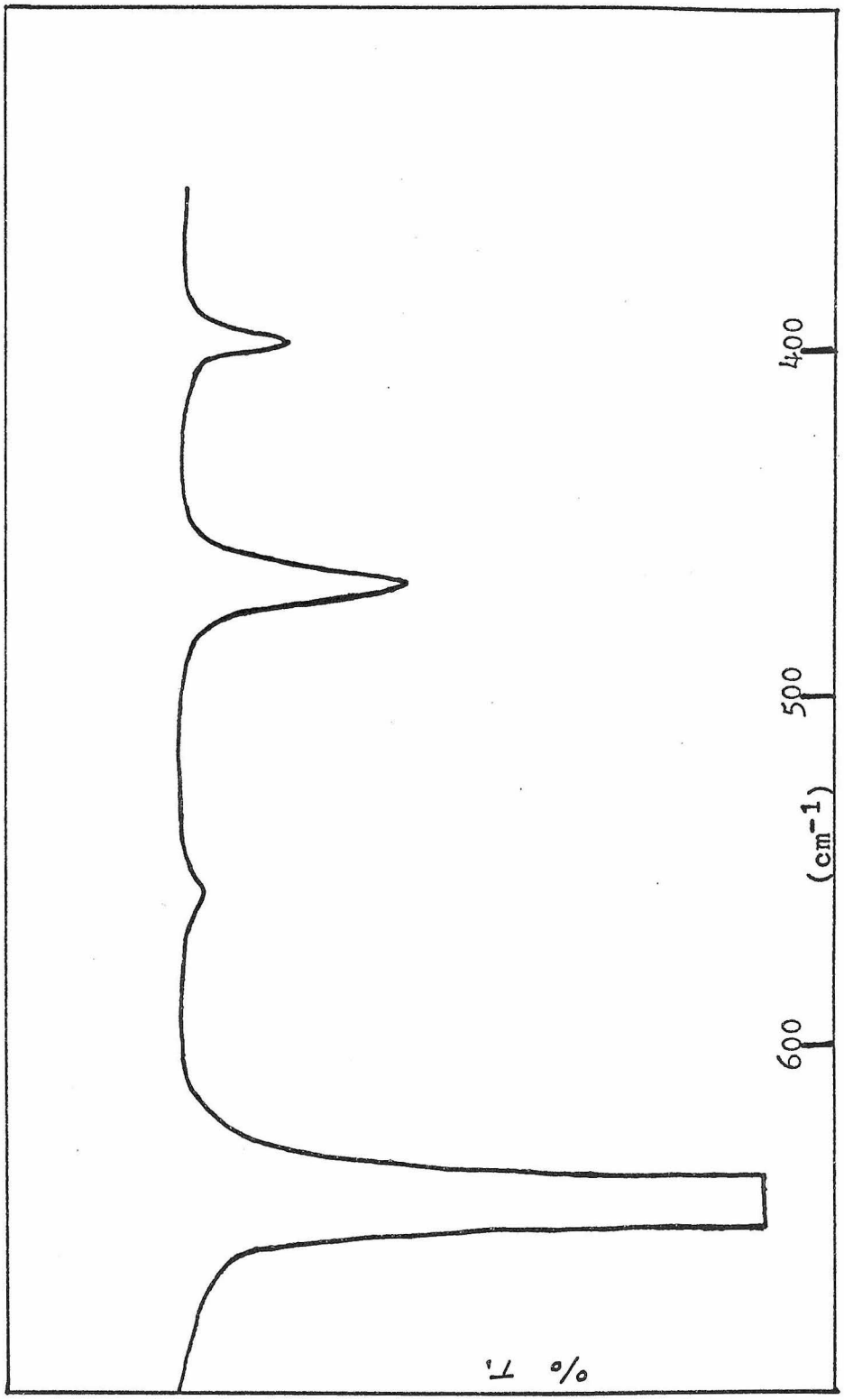

Figure 24. I.R. Spectrum of $Mn_2(CO)_{10}$ in a CCl_4 Solution

As there are no bands around 604cm^{-1} corresponding to the $(E)_\gamma$ mode in $Mn(CO)_5Br$ we assign the remaining pair as $\nu_{558} \longrightarrow (E_1)_\gamma$ and $\nu_{555} \longrightarrow (E_3)_\gamma$.

Upon ^{13}CO substitution a weak band appears between the two moderately strong Raman peaks at 473 and 453cm^{-1}. This is shown in figure 25 and the position of the weak band is indicated by an arrow.

In the normal compound, however, only two peaks are observed in this region. It is noted that the peak at higher energy is considerably more intense than its counterpart in $Mn_2(^{13}CO)_{10}$. This is due to the accidental degeneracy of the weakest bands which are clearly resolved in the spectrum of the ^{13}CO substituted molecule. Both of the stronger peaks may be assigned as Mn--C stretching modes as is discussed below. It was seen in (10), (14), and Part I that MCO bending modes shift further upon ^{13}CO substitution than MC stretching modes, thus the weakest band is assigned as $(E_2)_\beta$ analogous to $\nu_{535} \longrightarrow (B_2)_\beta$ for $Mn(CO)_5Br$.

The $(A_2)_\beta$ and $(B_1)_\beta$ modes are I. R. and Raman inactive and were not observed. Their positions were calculated with transferred potential constants from $Mn(CO)_5Br$ as is discussed below.

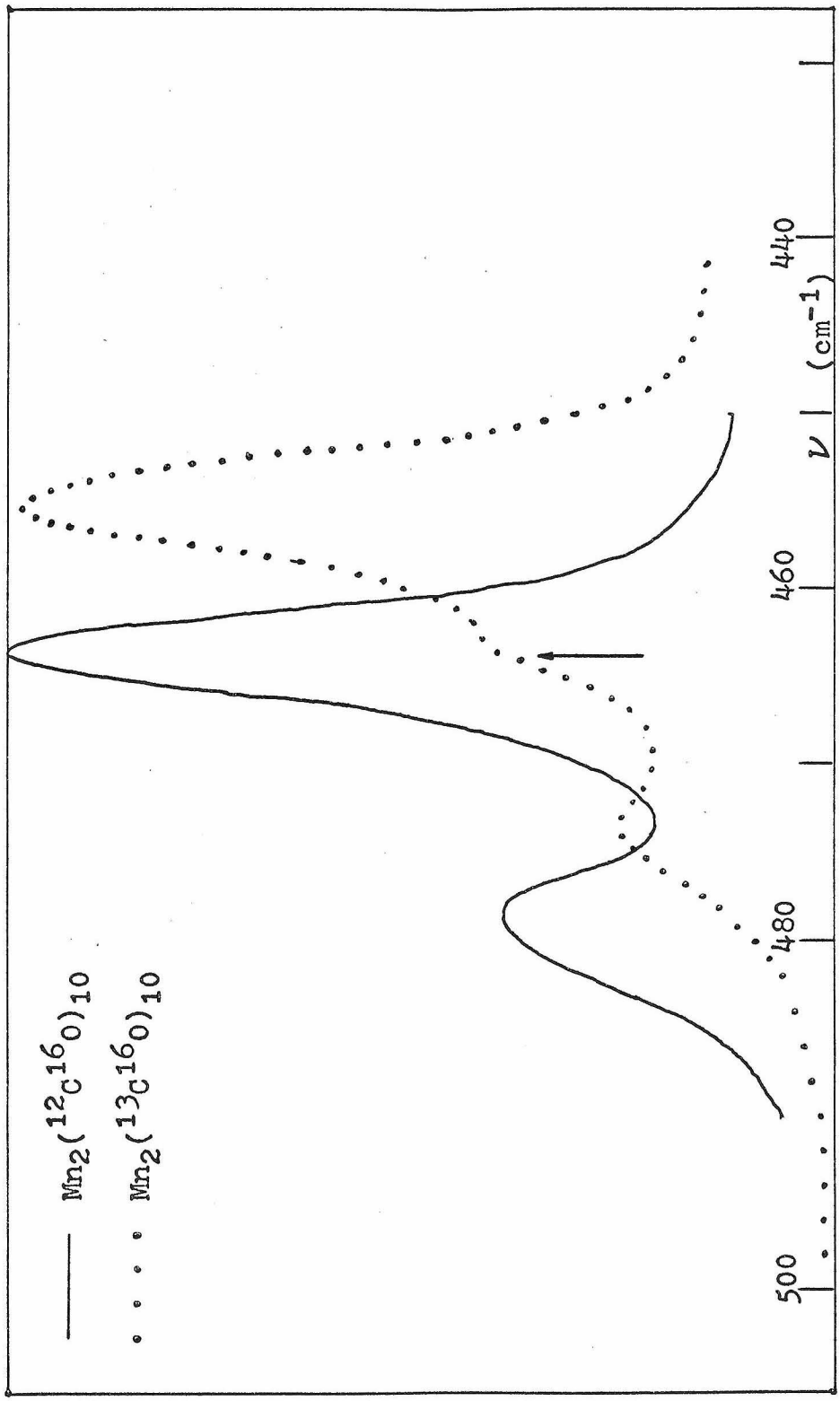

Figure 25. Raman Spectrum of Isotopically Substituted Solid $Mn_2(CO)_{10}$.

M--C Stretching Modes

The Raman and I. R. spectra for this region are shown in figures 26 and 24. Only two I. R. bands are observed in this region and they are assigned as $\nu_{468} \longrightarrow (E_1)_{d_i}$ and $\nu_{399} \longrightarrow (B_2)_{d_i}$ on the basis of similarity with the I. R. bands of $Mn(CO)_5Br$ regarding both position and intensity.

Four Raman bands were observed in solution two of which were quite polarized. These two polarized bands are thus assigned as the A_1 modes $\nu_{482} \longrightarrow (A_1)_{d_o}$ and $\nu_{408} \longrightarrow (A_1)_{d_i}$.

If there were no interactions across the Mn--Mn bond, $(E_1)_{d_i}$ and $(E_3)_{d_i}$ would be expected to occur at the same frequency; hence we assign $\nu_{465} \longrightarrow (E_3)_{d_i}$ leaving $\nu_{419} \longrightarrow (E_2)_{d_i}$.

Using this same argument we might reasonably expect the $(B_2)_{d_o}$ mode to occur in the vicinity of its Raman active A_1 counterpart at $482cm^{-1}$. This leads to the conclusion that either this mode has very little intensity in the infra-red or that it is accidentally degenerate with $(E_1)_{d_i}$ at $465cm^{-1}$. The latter interpretation is preferred in spite of the fact that this band is observed to be quite symmetrical in a variety of solvents. As B_2 modes develop intensity in the

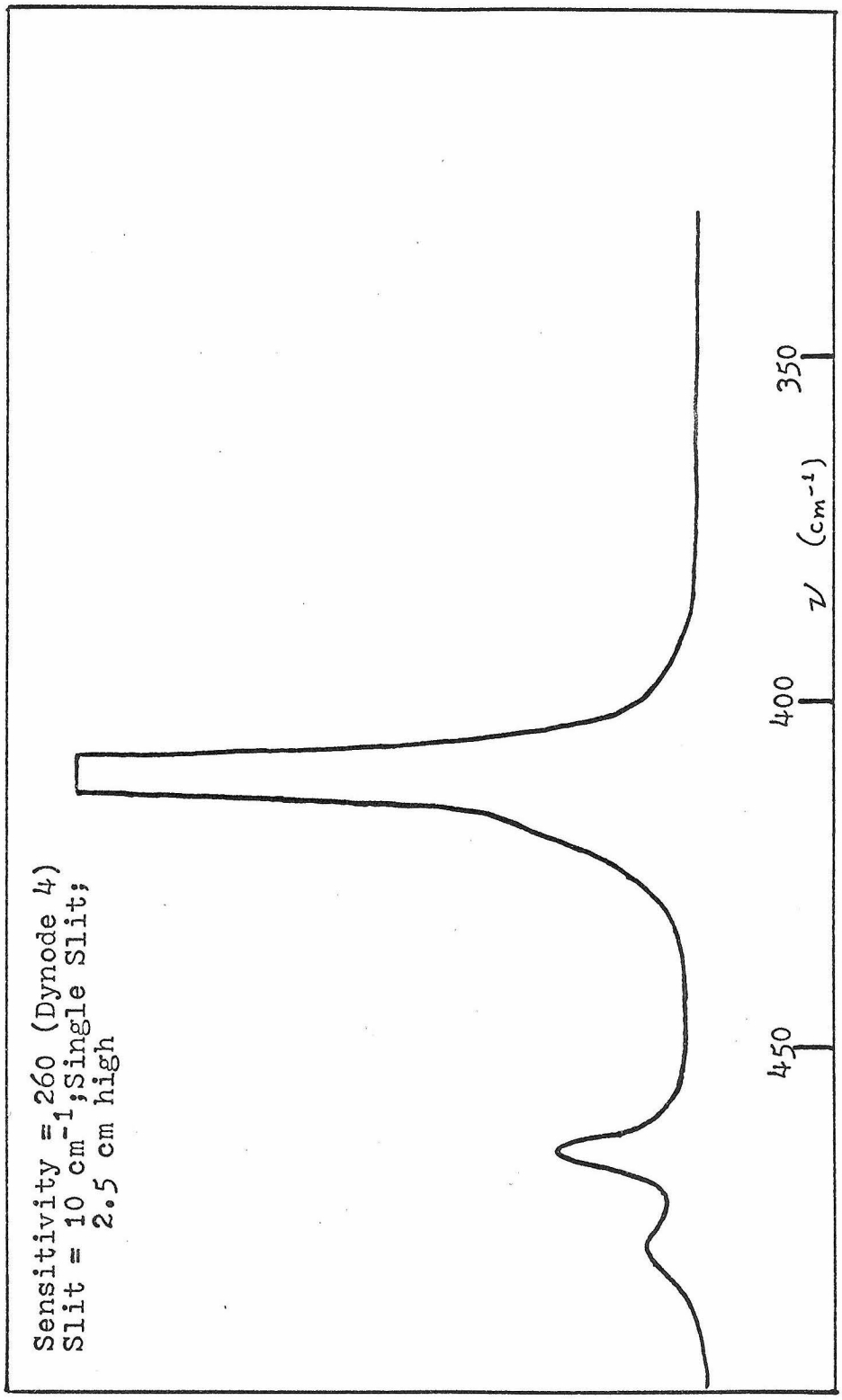

Figure 26. Raman Spectrum of Solid $Mn_2(CO)_{10}$

infra-red along the Z-axis (i.e. the Mn--Mn bond direction), it is expected that the axial-MC mode should be more intense than the radial-MC mode (as is the case for $Mn(CO)_5Br$). Confirmation of this hypothesis may perhaps be obtained by resolution of the two bands at liquid nitrogen temperature or a shift in band position and shape in polarized single crystal experiments.

M--M Stretch and C--M--C Bending Modes

The Raman spectrum from 200 to 50 cm^{-1} is presented in figure 27. This region is quite complex and no complete assignment will be attempted here in view of the uncertainties regarding this region in the simpler $Mn(CO)_5Br$ molecule.

Fortunately $Mn_2(CO)_{10}$ is a good deal more soluble in CH_2Cl_2 than the simpler pentacarbonyl halides and excellent polarization results were obtained. These are shown in figure 28 and clearly indicate that the bands at 160 and 113cm^{-1} are of A_1 symmetry. This is of considerable importance as one of the more fundamental questions to be answered by vibrational analyses of metal-metal bonded systems is how much mixing occurs between the pure metal-metal stretching coordinate and ligand-metal-ligand deformation coordinates of the same

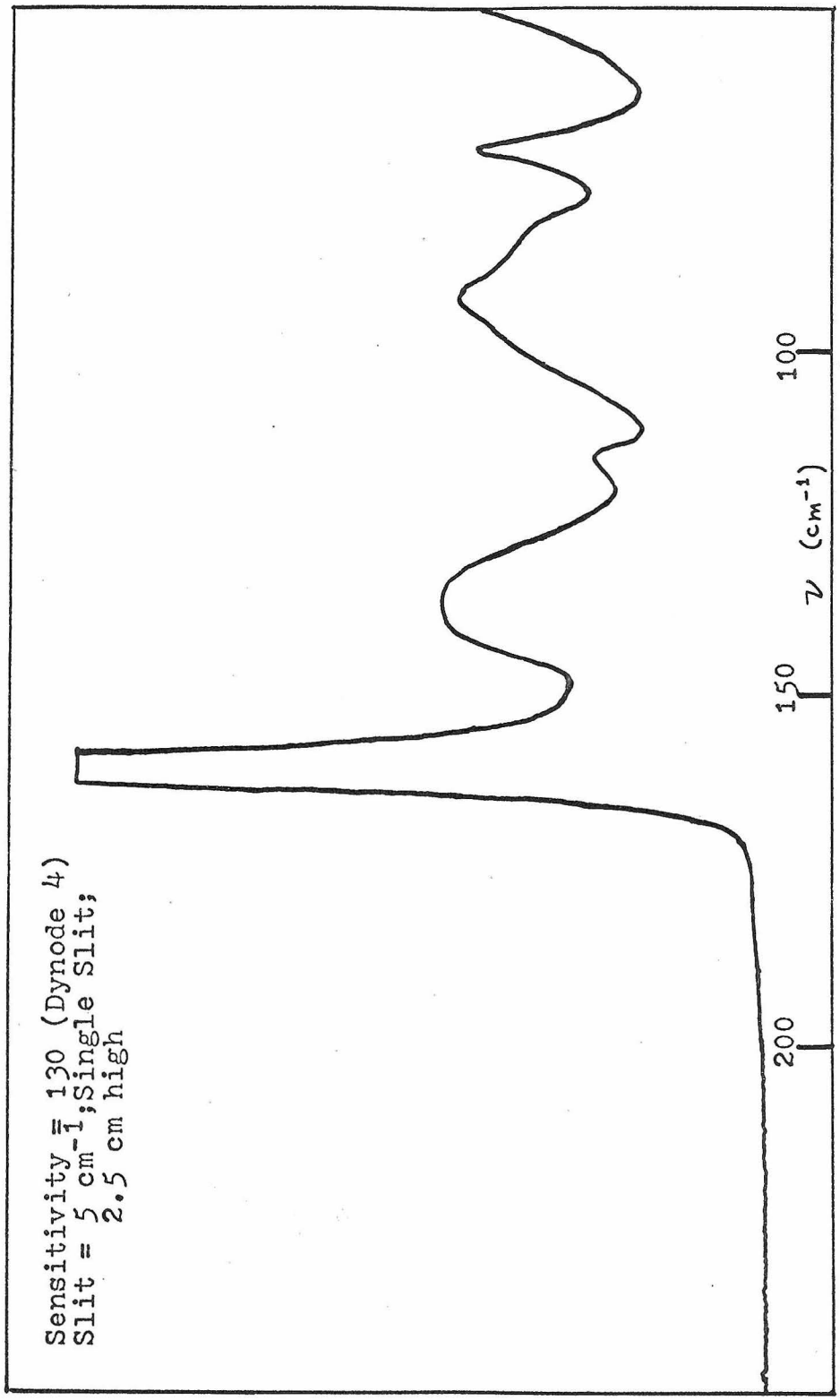

Figure 27. Raman Spectrum of Solid $Mn_2(CO)_{10}$

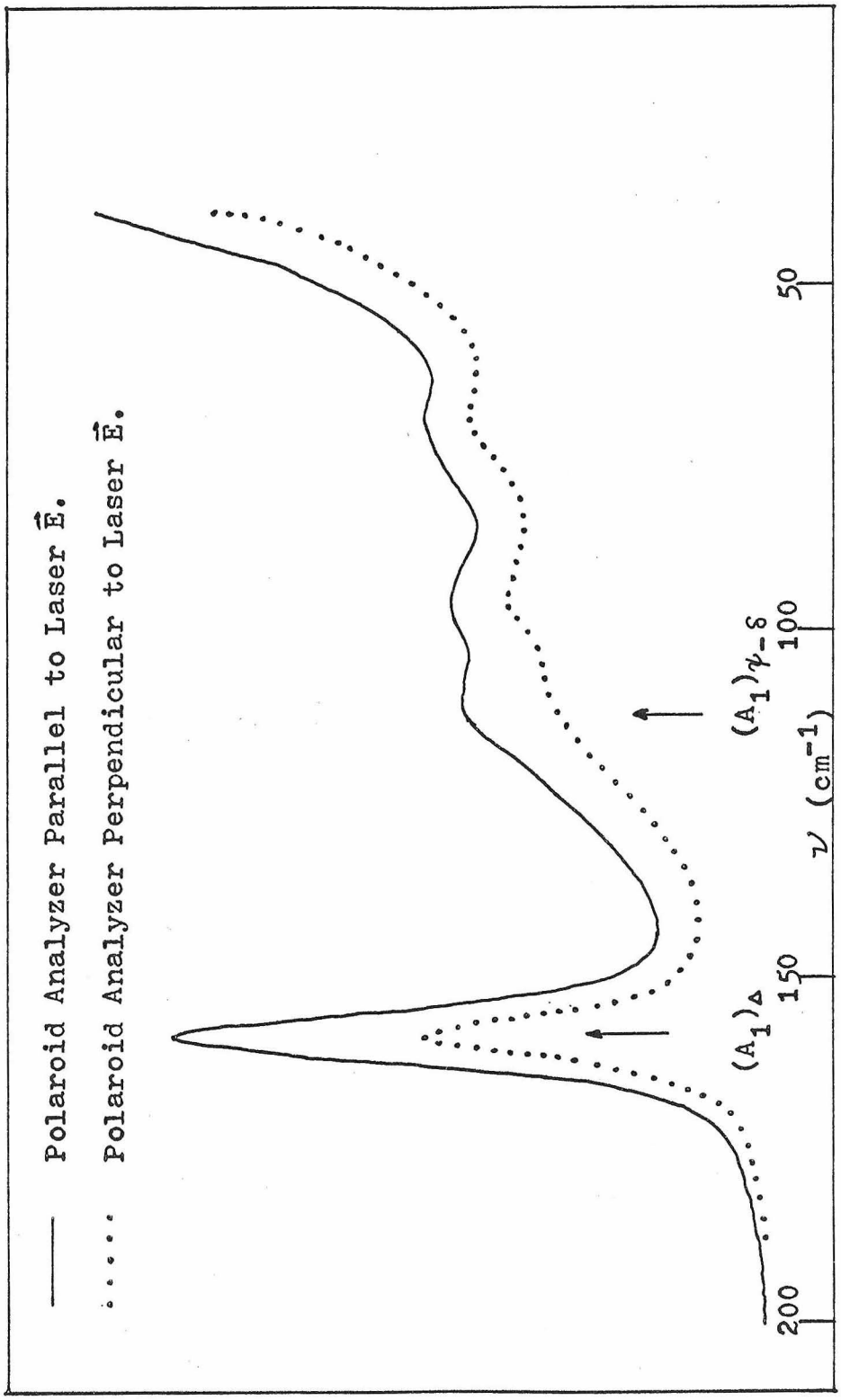

Figure 28. Polarized Raman Spectrum of $Mn_2(CO)_{10}$ in CH_2Cl_2 Solution.

symmetry. Obviously nothing too definite can be said in this regard if these frequencies are not accurately assigned.

For the purposes of potential constant calculations the remaining frequencies were assigned as similarly as possible to the assignments for $Mn(CO)_5Br$ from an energy standpoint. Thus we assign $\nu_{140} \longrightarrow (E_3)_\psi$, $\nu_{131} \longrightarrow (E_2)_\alpha$, $\nu_{95} \longrightarrow (E_2)_{\psi-\delta}$, and $\nu_{75} \longrightarrow (E_3)_\alpha$. ν_{160} and ν_{113} are assigned as above to $(A_1)_\Delta$ and $(A_1)_{\psi-\delta}$. The ordering of these A_1 modes is quite certain as the polarizability change with the change in the normal coordinate of vibration (which determines the Raman intensity of a given mode (22,25)) should be considerably greater for the stretching of the bond between two diffuse heavy atoms than for the ligand-metal-ligand deformation mode. The importance of this concept in the interpretation of Raman spectra of metal-metal bonded systems in this region is discussed further in (37).

The C--M--M deformation (similar to $(E)_\delta$ for $Mn(CO)_5Br$) is expected to occur at an energy lower than $53cm^{-1}$. That no band was observed in this immediate area gives additional support to the assignment for the monomeric system. The torsional mode $(B_1)_\tau$ is expected to lie well below $50cm^{-1}$ and is also both I. R. and Raman inactive.

CHAPTER 2

POTENTIAL CONSTANT CALCULATION FOR DIMANGANESE DECACARBONYL

Isotopic Substitution

The observed Raman and infra-red bands for $Mn_2(CO)_{10}$ and $Mn_2(^{13}CO)_{10}$ in both CH_2Cl_2 solution and polycrystalline phases are presented in Tables 22, 23, and 24.

Unfortunately time limitations did not permit the recording of spectra for $Mn_2(C^{18}O)_{10}$ (also prepared by Mr. M. Goldblatt of LASL). Due to the approximate nature of the calculations below the lack of these data is not too serious a detriment; however, more detailed future calculations should definitely include this information for the most accurate fitting of the M--C stretching and C--M--C bending modes which are particularly sensitive to $C^{18}O$ substitution.

Anharmonic Corrections

The binary combination region of CO stretching bands in the I. R. spectrum of $Mn_2(CO)_{10}$ has been reported and assigned a number of times (5, 34, 38). Unfortunately reasonably correct harmonic frequencies can not be calculated until data for the ternary and

TABLE 22

Observed Intense Raman and Infra-red Bands for $Mn_2(CO)_{10}$ in CH_2Cl_2 Solutions			
$Mn_2(^{12}C^{16}O)_{10}$		$Mn_2(^{13}C^{16}O)_{10}$	
Raman	Infra-red	Raman	Infra-red
74.6 ± .5		74.2 ± .4	
95.2 ± .2		93.7 ± .7	
113.4 ± .6		112.5 ± .6	
160.3 ± .1		158.9 ± .1	
	398.7 ± .3		392.4 ± .1
407.7 ± .2		401.6 ± .1	
419.0 ± .8		413.0 ± .6	
464.6 ± .2		456.3 ± .5	
	467.9 ± .1		460.5 ± .1
481.8 ± .2		476.1 ± .4	
	546.5 ± 2.0		not msrd.
	558.0 ± 2.0		not msrd.
	642.8 ± 1.0		not msrd.
	649.0 ± 1.0		not msrd.
672.7 ± .1		658.3 ± .1	
1978.2 ± 1.0		1933.1 ± 1.0	
	1978.7 ± .1		1933.6 ± .3
1991.8 ± .3		1947.2 ± .3	

TABLE 22 continued

$Mn_2(^{12}C^{16}O)_{10}$		$Mn_2(^{13}C^{16}O)_{10}$	
Raman	Infra-red	Raman	Infra-red
	2011.5 ± .1		1966.9 ± .1
2020.3 ± .3		1975.7 ± .3	
	2045.9 ± .1		1999.0 ± .1
2113.5 ± .2		2066.6 ± .2	

TABLE 23

Observed Intense Raman Bands for Solid $Mn_2(CO)_{10}$[a]	
$Mn_2(^{12}C^{16}O)_{10}$	$Mn_2(^{13}C^{16}O)_{10}$
70.7 ± .2	70.3 ± .1
not resolved by hand	81.7 ± 1.5*
	91.6 ± 1.5*
	98.5 ± 1.5*
115.5 ± .1	114.8 ± .1
not resolved by hand	129.8 ± 1.0*
	138.5 ± 1.0*
160.0 ± .1	158.8 ± .1
411.0 ± .3	405.3 ± .2
421.1 ± .3	414.5 ± .7
465.1 ± .2	456.8 ± .3
not obsvd.	464.5 ± .7
480.1 ± .5	474.1 ± .4
540.7 ± .4	522.3 ± .4
554.8 ± .6	535.7 ± .2
672.6 ± .2	657.9 ± .2

[a] * denotes bands lying close together which were resolved by hand.

TABLE 24

Observed Intense Infra-red Bands for Solid $Mn_2(CO)_{10}$[a]

Reference (20a)		Reference (20b)	
130	s	129	sh
121	s	118	sh
115	vs		
107	s	109	m

[a] Frequencies given are for $Mn_2(^{12}C^{16}O)_{10}$ only and are taken exclusively from References (20a) and (20b) as noted above.

quaternary CO stretching combinations are obtained.

As a first approximation the harmonic corrections for the observed C--O stretching frequencies of $Mn(CO)_5Br$ will be applied to the observed frequencies for $Mn_2(CO)_{10}$ using the symmetry correlations for $C_{4v} \longrightarrow D_{4d}$ given in Chapter 1. Thus we obtain:

ν	Observed	Harmonic
$(A_1)_{r_i}$	2113.5	2134.3
$(B_2)_{r_i}$	2045.9	2066.7
$(E_2)_{r_i}$	2020.3	2018.7
$(E_1)_{r_i}$	2011.5	2037.8
$(E_3)_{r_i}$	1978.2	2007.2
$(A_1)_{r_o}$	1991.8	2012.6
$(B_2)_{r_o}$	1978.7	2002.2

Admittedly this is a dubious procedure but these corrections will probably be correct to a first approximation; as these calculations themselves are a first full approximation, the transfer of anharmonic corrections from $Mn(CO)_5Br$ to $Mn_2(CO)_{10}$ is justified on the basis that a more accurate harmonic potential field would result than if only the observed frequencies of $Mn_2(CO)_{10}$ were used.

As was done for $Mn(CO)_5Br$, only observed frequencies for modes other than CO stretching were used in potential constant calculations.

Potential Constant Calculations

The calculations for $Mn_2(CO)_{10}$ followed the same procedures outlined in Part I. A new G matrix was calculated using data from the crystal structure determination of Dahl and Rundle (39). The formulation of the symmetry coordinates was carried out in a manner which would most facilitate the direct transfer of symmetry potential constants from $Mn(CO)_5Br$ to $Mn_2(CO)_{10}$.

It was hoped that the values of the transferred off-diagonal constants in $\underline{C}$ would be accurate enough that a satisfactory fit of the frequency data could be obtained by perturbing only the diagonal constants.

A_1 and B_2 Symmetry Blocks

As in the case of the monomeric pentacarbonyl bromide, these are by far the most accurately assigned frequencies. A splitting diagram in figure 29 shows the steps in the calculation. First, the frequencies are calculated from a direct transfer of compliance constants from $\underline{C}_{A_1}$ of $Mn(CO)_5Br$. Second, the C_{ij} are adjusted for the best fit of the data for $Mn_2(CO)_{10}$ still with no splitting between pairs of A_1 and B_2 modes. Finally the split A_1 and B_2 frequencies are

compared with the observed values.

Convergence for the six frequencies of the B_2 block was obtained rapidly and with excellent fitting of the data by adjusting only the diagonal C_{ii}. A considerable amount of difficulty was encountered with this procedure in the A_1 block. As can be seen in the direct transfer calculation (figure 29) $(A_1)_\Delta$ was too high and $(A_1)_{\psi-\delta}$ was too low. Calculations by Spiro (37) have also shown this behavior. There a "reasonable amount" (to be specified in a later more detailed publication) of mixing between these two coordinates is assumed and the $(A_1)_\Delta$ mode is fitted to a frequency of $160cm^{-1}$. This yields a calculated value for $(A_1)_{\psi-\delta}$ of $57cm^{-1}$ which is a factor of two lower than the observed value of $113cm^{-1}$.

It was found in the present study that a satisfactory fit of these two frequencies could not be obtained with the value of $C_{6,7}$ transferred. The problem was complicated by the fact that $(A_1)_\gamma$ and $(A_1)_{\psi-\delta}$ are very highly mechanically coupled. Thus the large changes required in $C_{7,7}$ to fit $(A_1)_{\psi-\delta}$ had a most undesirable effect on the fit of $(A_1)_\gamma$.

The final adjusted C_{ij} are presented in Table 25. Symmetry coordinate compliance and force constants are presented in Table 26 while the internal coordinate

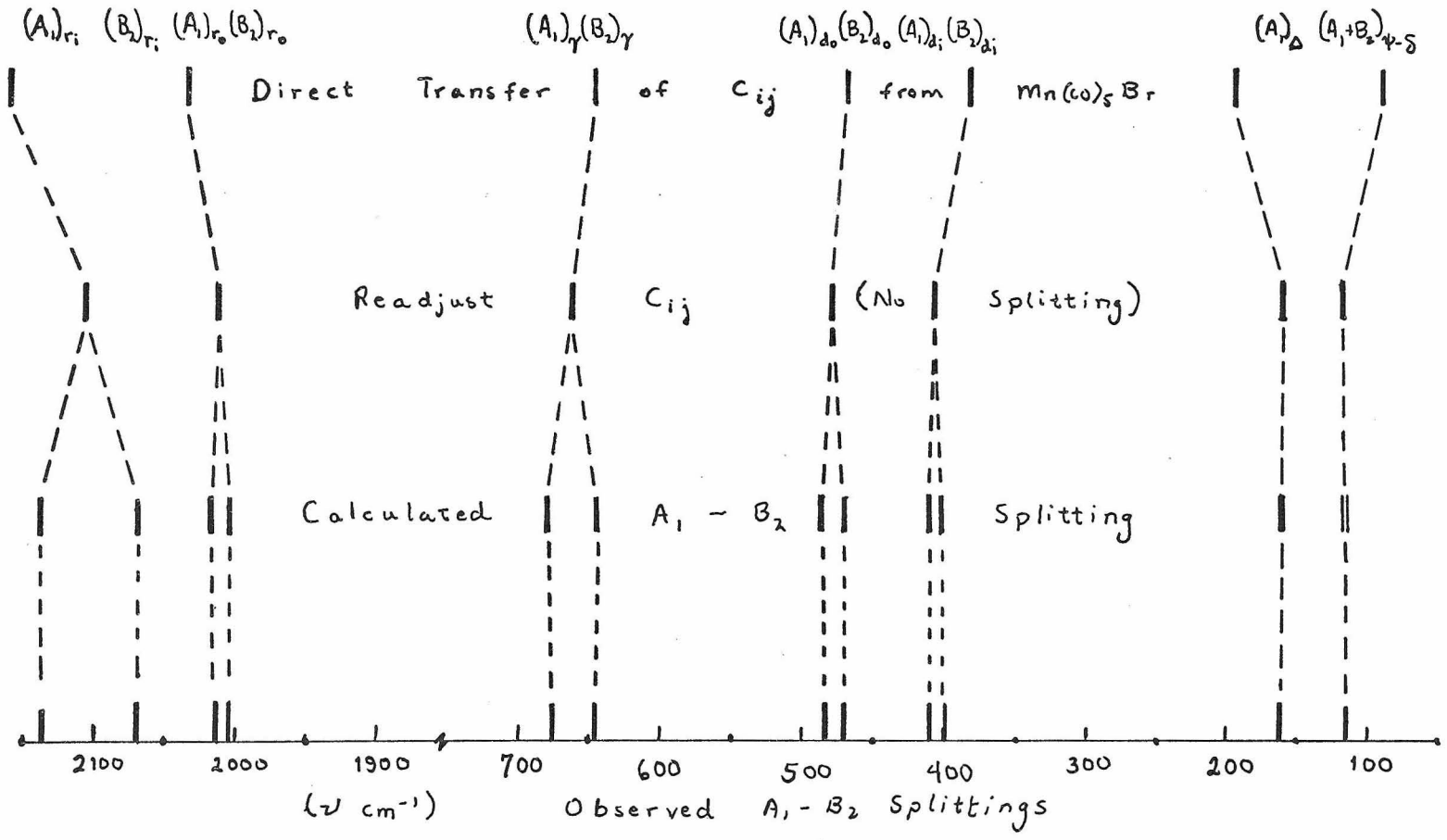

Figure 29. A_1 and B_2 Vibrational Calculations for $Mn_2(CO)_{10}$.

TABLE 25

Compliance and Force Constant[a] Calculation for A_1 Symmetry Block	
$C_{1,1} = .0569$	$F_{1,1} = 17.64$
$C_{2,2} = .0621$	$F_{2,2} = 16.38$
$C_{3,3} = 1.311$	$F_{3,3} = .794$
$C_{4,4} = .435$	$F_{4,4} = 3.16$
$C_{5,5} = .359$	$F_{5,5} = 2.99$
$C_{6,6} = 1.594$	$F_{6,6} = 1.26$
$C_{7,7} = 1.7$	$F_{7,7} = 1.29$
$C_{6,7} = -1.0$	$F_{6,7} = .88$

[a] Force constants were derived from elements of $\underline{C^{-1}}$.

TABLE 25 continued

Frequency Calculation for A_1 Symmetry Block								
$Mn_2(^{12}C^{16}O)_{10}$			$Mn_2(^{13}C^{16}O)_{10}$			$Mn_2(^{12}C^{18}O)_{10}$		
$\nu_{obsd.}$	$\nu_{calcd.}$	Δ	$\nu_{obsd.}$	$\nu_{calcd.}$	Δ	$\nu_{obsd.}$	$\nu_{calcd.}$	Δ
2134.3	2136.0	-1.7	2086.6	2085.1	1.5	----	2089.2	---
2012.6	2014.7	-2.1	1967.5	1967.3	.2	----	1970.1	---
672.7	677.5	-4.8	658.3	662.9	-4.6	---	671.1	---
481.8	483.6	-1.8	476.1	474.2	1.9	---	471.9	---
407.7	407.9	-.2	401.6	401.5	.1	---	393.4	---
160.3	158.4	1.9	158.9	157.2	1.7	---	156.1	---
113.4	116.3	-2.9	112.5	115.5	-3.0	---	111.0	---

TABLE 25 continued

Compliance and Force Constant[a] Calculation for B_2 Symmetry Block	
$C_{11,11} = .0617$	$F_{11,11} = 16.26$
$C_{12,12} = .0612$	$F_{12,12} = 16.60$
$C_{13,13} = 1.138$	$F_{13,13} = .891$
$C_{14,14} = .451$	$F_{14,14} = 2.39$
$C_{15,15} = .371$	$F_{15,15} = 2.76$
$C_{16,16} = 2.59$	$F_{16,16} = .41$

[a] Force constants were derived from elements of $\underline{C^{-1}}$.

TABLE 25 continued

Frequency Calculation for B_2 Symmetry Block								
$Mn_2(^{12}C^{16}O)_{10}$			$Mn_2(^{13}C^{16}O)_{10}$			$Mn_2(^{12}C^{18}O)_{10}$		
$\nu_{obsd.}$	$\nu_{calcd.}$	Δ	$\nu_{obsd.}$	$\nu_{calcd.}$	Δ	$\nu_{obsd.}$	$\nu_{calcd.}$	Δ
2066.7	2067.2	-.5	2019.0	2018.4	.6	----	2021.5	---
2002.2	2002.4	-.2	1956.0	1955.9	.1	----	1957.0	---
642.8	643.5	-.7	628.4	627.6	.8	---	638.2	---
467.9	467.6	.3	460.5	460.8	-.3	---	456.2	---
398.7	398.7	0	392.4	392.4	0	---	384.3	---
113.4(?)	113.2	.2	---	112.7	---	---	109.1	---

TABLE 26

Symmetry Coordinate Splitting Constants

Internal Coord.	ΔC_{ii}	ΔF_{ii}
A_1-B_2 Blocks		
r_i	.0569 - .0617 = -.0048	17.64 - 16.26 = +1.38
r_o	.0621 - .0612 = +.0009	16.38 - 16.60 = -.22
γ	1.311 - 1.138 = +.17	.794 - .891 = -.10
d_o	.435 - .451 = -.02	3.16 - 2.39 = +.77
d_i	.359 - .371 = -.01	2.99 - 2.76 = +.23
E_1-E_3 Blocks		
r_i	.0596 - .0616 = -.0020	17.21 - 16.67 = +.54

TABLE 27

Internal Coordinate Splitting Constants

A_1-B_2 Blocks

$$\Delta C_{r_i} = 4(C_{r_i,45} + C_{r_i,135}) \qquad \Delta F_{r_i} = 4(F_{r_i,45} + F_{r_i,135})$$
$$\Delta C_{r_o} = 2(C_{r_o,j}) \qquad \Delta F_{r_o} = 2(F_{r_o,j})$$
$$\Delta C_{\gamma} = 4(C_{\gamma,45} + C_{\gamma,135}) \qquad \Delta F_{\gamma} = 4(F_{\gamma,45} + F_{\gamma,135})$$
$$\Delta C_{d_o} = 2(C_{d_o,j}) \qquad \Delta F_{d_o} = 2(F_{d_o,j})$$
$$\Delta C_{d_i} = 4(C_{d_i,45} + C_{d_i,135}) \qquad \Delta F_{d_i} = 4(F_{d_i,45} + F_{d_i,135})$$

E_1-E_3 Blocks

$$\Delta C_{r_i} = 2\sqrt{2}(C_{r_i,45} - C_{r_i,135}) \qquad \Delta F_{r_i} = 2\sqrt{2}(F_{r_i,45} - F_{r_i,135})$$

$C_{i,j}$	This Work	$F_{i,j}$	This Work	(5)	(31)
$C_{r_i,45}$	-.0010	$F_{r_i,45}$	.27	.33	.22
$C_{r_i,135}$	-.0002	$F_{r_i,135}$	.08	0	.03
$C_{r_o,j}$	.0004	$F_{r_o,j}$	-.11	-.12	.20
$C_{\gamma,45} + C_{\gamma,135}$	.04	$F_{\gamma,45} + F_{\gamma,135}$	-.03	not calcd.	
$C_{d_o,j}$	-.01	$F_{d_o,j}$	.77	"	"
$C_{d_i,45} + C_{d_i,135}$	-.003	$F_{d_i,45} + F_{d_i,135}$	.06	"	"

constants are shown in Table 27.

The value of $C_{7,7}$ should be compared with that for $C_{16,16}$ in the B_2 block calculation shown in Table 25. The compliance of the A_1 C--M--C bending mode is much less than its B_2 counterpart and this suggests that perhaps a higher frequency should be assigned to $(B_2)_{\psi-\delta}$.

The "metal-metal" stretching <u>force</u> constant is determined to be 1.26 and the mixing constant with the C--M--C bending mode is 0.88. This very large value for $F_{\Delta,\psi-\delta}$ indicates a considerable interaction of the Δ and $\psi-\delta$ coordinates as predicted in Part I. This is at variance with conclusions drawn earlier (37, 40, 41) and the present results are compared with some previous approximate calculations:

F_{ij}	This Work	Ref. (37)	Ref. (40)	Ref. (41)
F_Δ	1.26	.59	1.4	1.45
$F_{\Delta,\psi-\delta}$	.88	?	?	?
$F_{\psi-\delta}$	1.7	?	?	?
ν_i				
ν_Δ	160	160	157	159
$\nu_{\psi-\delta}$	113	cald. 57	?	?

The calculations from (40) and (41) were done on a diatomic approximation with the mass of each "particle"

equal to the mass of a $Mn(CO)_5$ unit. These two results are much more accurate than the normal coordinate calculation in (37), but this agreement is seen to be purely fortuitous as neither the off-diagonal force constant nor the mechanical coupling is explicitly taken into consideration.

Values for F_Δ were also calculated in (37) for $Tc_2(CO)_{10}$, $Re_2(CO)_{10}$, and $Re(CO)_5Mn(CO)_5$, and the trend in the force constants obtained was discussed. However, in (41) an entirely different trend was obtained by use of the "diatomic" approximation. Thus by the incorrect assignment of $(A_1)_{\psi-\delta}$, not only are the <u>absolute</u> values of F_Δ incorrect for the $M_2(CO)_{10}$ series in (37), but the <u>relative</u> values may also be incorrect for these F_Δ and this renders somewhat premature any conclusions drawn from these results.

From the general agreement of these F_Δ with conclusions drawn from electron impact measurements (42) it is expected that the trends in metal-metal bonding observed by Spiro (37) will be borne out; however, a <u>complete</u> normal coordinate analysis on $Re_2(CO)_{10}$ based on calculations for isotopically

substituted $Re(CO)_5X$ systems should be a minimum requirement to establish the nature of the F_Δ for the $M_2(CO)_{10}$ system.

Calculated values for the C_{ij} which were adjusted are presented in Table 25. For both Mn--C and C--O stretching modes the A_1 frequency for a given coordinate is at higher energy than its B_2 counterpart. This is reflected in the larger F_{ii} and smaller C_{ii} for the A_1 modes compared to the corresponding B_2 modes except for $(A_1)_{r_o}$ and $(B_2)_{r_o}$. These results give rise to positive interaction force constants across the metal-metal bond. These constants are $C_{r_i,45}$ ($+r_1$ with $+r_5$ or $+r_8$), $C_{r_i,135}$ ($+r_1$ with $+r_6$ or $+r_7$), and $C_{r_o,j}$($+r_9$ with $+r_{10}$). The nomenclature is similar for d_i and d_o coordinates.

In these calculations interactions between axial coordinates on one Mn atom and radial coordinates on the other Mn atom were assumed to be equal to zero.

If these interactions are assumed to arise through a conjugated π-electronic system involving the filled metal d-orbitals, valence bond theory (32) would predict that the stretching of a given CO bond (or MnC bond) on one Mn atom would produce <u>weaker</u> CO bonds (or MnC bonds) in the other $Mn(CO)_5$ group.

This predicts negative interaction force constants across the Mn--Mn bond which is in disagreement with this study and three previous works (5, 31, 34).

An attractive mechanism proposed by Cotton (5) predicts correctly the signs of these interaction constants by assuming the major effects involved are changes in repulsion between the various metal d-π orbitals. Stretching of a radial-CO bond would increase the associated d-Mn$\longrightarrow\pi^*$CO back-bonding and lower the electron density in this metal d-orbital. The interaction across the Mn--Mn bond would then be a stabilization in the appropriate d-orbitals of the other Mn atom causing a <u>decrease</u> in d-Mn$\longrightarrow\pi^*$CO bonding and a consequent strengthening of those CO bonds.

Through-space electrostatic interactions as proposed in (14) and Part I of this work form a satisfactory alternative mechanism. Electrostatic effects in this molecule are shown to be significant by the large asymmetry parameter in the electric field gradient about each Mn atom as found by an investigation of the pure quadrupole resonance spectrum of polycrystalline $^{55}Mn_2(CO)_{10}$ (43). This asymmetry presumably arises from distortions of the charged radial-CO ligands from D_{4d} symmetry as revealed

by the crystal structure determination of $Mn_2(CO)_{10}$ (39).

This X-ray diffraction study also revealed that the radial-CO groups on one Mn atom were bent an average of 4 degrees out of an MnC_4 plane toward the other $Mn(CO)_5$ group. This electronic repulsion between the axial-CO group and the radial-CO groups may be expected to have its counterpart in interactions across the metal-metal bond. This would predict that the largest A_1-B_2 splitting due to electrostatic effects would occur for the radial-CO mode.

This is seen to be the case from the splitting diagram in figure 29. Thus electrostatic interaction between nearby CO groups must be of considerable importance for the correct interpretation of spectra and potential field calculations.

The nature of these interactions may be thought of as follows. The change in dipole moment along r_1 by stretching this coordinate will oppose the oscillating dipoles in r_8 and r_5 during in-phase (A_1 and E_1) modes and result in the lowest energy during the out-of-phase B_2 and E_3 modes. The net repulsion or attraction

of these dipoles satisfactorily explains the signs of the splitting constants $C_{r_i,45}$ and $F_{r_i,45}$ in Table 27.

This mechanism predicts values for $C_{r_o,j}$ and $F_{r_o,j}$ of nearly zero (or very slightly negative) due to the large distance and number of atoms separating the axial coordinates r_9 and r_{10}. This is indeed the case in this work where $C_{r_o,j} = +.0004$ and $F_{r_o,j} = -.11$.

The value of $F_{r_o,j}$ can not be compared to the value of -.12 obtained in (5) due to the uncertainties in the input frequency $(A_1)_{r_o}$ in that work.

Recently Bor (31) has calculated a value of +.20 for $F_{r_o,j}$. The large disagreement between that value and the value in this work must arise principally from differences in the value of $F^{c}_{r_o,r_i}$ used. This constant determines the mixing of the axial A_1 and B_2 modes with the respective radial A_1 and B_2 modes; due to the large differences in "symmetry" splittings of the two A_1 modes and the two B_2 modes, the value used for $F^{c}_{r_o,r_i}$ will be very important in determining the value of $F_{r_o,j}$.

That the values of $F_{r_{o,j}}$ and $F_{r_{i,135}}$ are much smaller than the value of +.35 for $F_{r_{i,45}}$ is taken as good evidence that the dominant mechanism of CO-C'O' interaction across the Mn--Mn bond involves primarily the oscillating dipole moments in the CO ligands themselves rather than the more internal mutual repulsion of metal d-orbitals. These considerations also offer an explanation for the very large anharmonicity corrections and solvent shifts found for the CO stretching modes when compared to the other internal vibrational modes.

The signs of the interaction constants for d_i and d_o coordinates are predicted by either of the two mechanisms discussed above. However, the larger magnitudes of $C_{d_{o,j}}$ and $F_{d_{o,j}}$ compared to $C_{d_{i,45}}$ and $F_{d_{i,45}}$ would indicate that electrostatic interactions play a very small role across the metal-metal bond in these "internal vibrations."

It seems that the mutual influence of metal π-symmetry d-orbitals (34) is more successful in predicting that the d_o-d_o' interactions should be larger than the d_i-d_i' interactions. This mechanism would be more effective in the axial mode (d_o-d_o') than the radial mode (d_i-d_i'), if perturbations in bond order are due primarily to changes in Mn→CO π back-bonding

rather than changes in Mn←CO σ bonding. This is because there are more d-orbitals involved which are appropriately aligned for interaction across the Mn--Mn bond for the axial-CO ligands than the radial-CO ligands.

In Part III it will be shown in a study of Raman intensity measurements that the role of the metal-d⟶π*CO back-bonding system becomes increasingly important relative to the role of the CO⟶metal σ bonding system in determining changes in bonding electron density for the series $Mn(CO)_5Cl$, $Mn(CO)_5Br$, $Mn(CO)_5I$, and $Mn_2(CO)_{10}$. These independent findings would seem to favor changes in the Mn d-orbitals arising primarily through perturbations in the d-Mn⟶ π*CO system.

The compliance constant for $(A_1)_\gamma$ is actually larger than the value of $C_{13,13}$ for $(B_2)_\gamma$. This is probably due to the misassignment of $(B_2)_{\psi-\delta}$ mentioned earlier; reassigning this mode to a higher frequency in accordance with the discussion on page 146 would have the desirable effect of raising the value of $C_{13,13}$.

A_2 and B_1 Symmetry Blocks

Calculations for the $(A_2)_\beta$ and $(B_1)_\beta$ MCO bending

TABLE 28

Frequency Calculation for A_2 Symmetry Block								
$\{C_{8,8} = 1.85$ (held fixed) $\quad F_{8,8} = .54$ (held fixed)$\}$								
$Mn_2(^{12}C^{16}O)_{10}$			$Mn_2(^{13}C^{16}O)_{10}$			$Mn_2(^{12}C^{18}O)_{10}$		
$\nu_{obsd.}$	$\nu_{calcd.}$	Δ	$\nu_{obsd.}$	$\nu_{calcd.}$	Δ	$\nu_{obsd.}$	$\nu_{calcd.}$	Δ
---	441.3	---	---	427.8	---	---	435.9	---

Frequency Calculation for B_1 Symmetry Block								
$C_{9,9} = 1.85$ (held fixed) $\quad F_{9,9} = .54$ (held fixed)								
$C_{10,10} = 10.0$ (" ") $\quad F_{10,10} = .1$ (" ")								
$C_{9,10} = 0$ (" ") $\quad F_{9,10} = 0$ (" ")								
$Mn_2(^{12}C^{16}O)_{10}$			$Mn_2(^{13}C^{16}O)_{10}$			$Mn_2(^{12}C^{18}O)_{10}$		
$\nu_{obsd.}$	$\nu_{calcd.}$	Δ	$\nu_{obsd.}$	$\nu_{calcd.}$	Δ	$\nu_{obsd.}$	$\nu_{calcd.}$	Δ
---	448.8	---	---	434.8	---	---	443.6	---
---	42.3	---	---	42.0	---	---	40.4	---

modes utilized a direct transfer of compliance constants from $Mn(CO)_5Br$.

A compliance constant of 10.0 (i.e. a force constant of 0.1) was arbitrarily chosen for the torsional mode $(B_1)_\tau$. The calculated frequencies are presented in Table 28.

E_2 Symmetry Block

The components of these degenerate modes are localized on one or the other $Mn(CO)_5$ group, therefore no interaction constants across the metal-metal bond exist for this block.

The calculations are quite similar to the B_1 and B_2 blocks for $Mn(CO)_5Br$. Off-diagonal C_{ij} between E_2 modes were transferred directly from these calculations and it was found necessary to alter only $C_{25,27}$ to obtain a satisfactory fit.

C_{ij} were constrained equal to zero for those pairs of elements in which one mode was analogous to a B_1 $Mn(CO)_5Br$ mode and the other a B_2 $Mn(CO)_5Br$ mode. The resulting C matrix had the following form:

	$(E_2)_{ri}$ $(\rightarrow B_1)$	$(E_2)_{\gamma}$ $(\rightarrow B_1)$	$(E_2)_{\beta}$ $(\rightarrow B_2)$	$(E_2)_{di}$ $(\rightarrow B_1)$	$(E_2)_{\alpha}$ $(\rightarrow B_2)$	$(E_2)_{\psi-\delta}$ $(\rightarrow B_1)$
$(E_2)_{ri}$ $(\rightarrow B_1)$	$C_{23,23}$	$C_{23,24}$	0	$C_{23,26}$	0	$C_{23,28}$
$(E_2)_{\gamma}$ $(\rightarrow B_1)$		$C_{24,24}$	0	$C_{24,26}$	0	$C_{24,28}$
$(E_2)_{\beta}$ $(\rightarrow B_2)$			$C_{25,25}$	0	$C_{25,27}$	0
$(E_2)_{di}$ $(\rightarrow B_1)$				$C_{26,26}$	0	$C_{26,28}$
$(E_2)_{\alpha}$ $(\rightarrow B_2)$					$C_{27,27}$	0
$(E_2)_{\psi-\delta}$ $(\rightarrow B_1)$						$C_{28,28}$

TABLE 29

Compliance and Force Constant[a] Calculation for E_2 Symmetry Block

$C_{25,25}$	= .0615	$F_{25,25}$	= 16.58
$C_{26,26}$	= .802	$F_{26,26}$	= 1.44
$C_{27,27}$	= 2.73	$F_{27,27}$	= .369
$C_{28,28}$	= .349	$F_{28,28}$	= 2.94
$C_{29,29}$	= 1.21	$F_{29,29}$	= .83
$C_{30,30}$	= 2.34	$F_{30,30}$	= .50
$C_{26,28}$	= -.167	$F_{26,28}$	= .05

[a] Force constants were derived from elements of $\underline{C^{-1}}$.

TABLE 29 continued

Frequency Calculation for E Symmetry Block								
$Mn_2(^{12}C^{16}O)_{10}$			$Mn_2(^{13}C^{16}O)_{10}$			$Mn_2(^{12}C^{18}O)_{10}$		
$\nu_{obsd.}$	$\nu_{calcd.}$	Δ	$\nu_{obsd.}$	$\nu_{calcd.}$	Δ	$\nu_{obsd.}$	$\nu_{calcd.}$	Δ
2018.7	2019.8	-1.1	1974.1	1973.0	1.1	----	1973.8	---
672.7	675.6	-2.9	658.3	655.4	2.9	---	666.8	---
481.8	483.6	-1.8	466.2	465.6	.6	---	482.1	---
419.0	419.4	-.4	413.0	412.5	.5	---	404.6	---
131.3	131.9	-.6	129.8	131.6	-1.8	---	124.7	---
95.2	94.9	.3	93.7	94.0	-.3	---	90.7	---

The full value of these calculations will be realized only when less approximate values for the potential constants of the remaining symmetry blocks are obtained making it possible to determine the internal coordinate potential constants as was done for $Mn(CO)_5Br$.

As large uncertainties exist in the assignments of $(E_2)_\gamma$, $(E_2)_\alpha$, and $(E_2)_{\psi-\delta}$, further discussion of these calculations is thus unwarranted at this time. It is noted in closing that the values expected for this block should be close to the B_1 and B_2 calculations as the analogous E_2 frequencies are not shifted too far from the position of the $Mn(CO)_5Br$ modes.

E_1 and E_3 Symmetry Blocks

The calculations for these blocks were extremely unsatisfactory as no good fit of the three MCO bending modes and the MC stretching mode could be obtained by adjusting only the diagonal C_{ii}.

Apparently $(E_1)_\gamma$ and $(E_3)_\gamma$ have shifted to lower energy while $(E_1)_{d_i}$ and $(E_3)_{d_i}$ have shifted to higher energy. Mixing among the γ, ϕ, and d_i coordinates is expected to be even more extensive than for $Mn(CO)_5Br$.

It is unreasonable at this point to offer explanations for the large shifts of the γ and d_i modes relative to their counterparts in $Mn(CO)_5Br$ due to the uncertainties regarding the potential field of the simpler molecule (see pps. 93 to 97).

Potential constants were calculated for CO stretching modes yielding values of $C_{17,17} = .0596$, $C_{31,31} = .0616$, $F_{17,17} = 17.21$, and $F_{31,31} = 16.67$. From these we deduce $\Delta C_{ii} = -.0020$ and $\Delta F_{ii} = +.54$. These result in numerical values for the internal coordinate splitting constants $C_{ri,45}$, $C_{ri,135}$, $F_{ri,45}$, and $F_{ri,135}$ when combined with results from the A_1 - B_2 block results.

this work	this work	(5)	(31)
$C_{ri,45} = -.0010$	$F_{ri,45} = .27$	.33	.22
$C_{ri,135} = -.0002$	$F_{ri,135} = .08$	0	.03

These values are in fair agreement with the results of Bor (31) and indicate that the assumption by Cotton (5) that $F_{ri,135} = 0$ was fairly good.

Conclusions

1. From the observed frequency shifts and calculated potential constants it is seen that all C--O bonds are more compliant in $Mn_2(CO)_{10}$ than in $Mn(CO)_5Br$ while the reverse is true for all Mn--C bonds.

2. These changes in bond order may best be explained by the increasing importance of Mn-d$\longrightarrow\pi^*$CO back-bonding from $Mn(CO)_5Br$ to $Mn_2(CO)_{10}$. The more covalent nature of the Mn--C bonds in the binuclear species due to the negligible induced positive charge on the Mn atoms will lead to a relatively greater expansion of the Mn d-orbitals and consequent greater Mn-d$\longrightarrow\pi^*$CO back-bonding.

3. Splittings of A_1 and B_2 modes by interaction constants across the Mn--Mn bond offer very strong evidence that CO-C'O' interactions arise primarily through electrostatic effects while MnC-Mn'C' interactions come about by mutual repulsion of the Mn d-orbitals of π symmetry.

4. Mixing of the metal-metal stretching coordinate with ligand-metal-ligand deformation coordinates is quite large and serious errors in the estimation of F_Δ for various metal-metal bonded systems may arise if this mixing is not taken into account.

III.

RAMAN AND ELECTRONIC ABSORPTION STUDIES OF $M(CO)_5X^{n-}$ COMPOUNDS

CHAPTER 1

RAMAN SPECTRA OF $M(CO)_5X^{n-}$ COMPOUNDS

$M(CO)_5X^- \cdot N(C_2H_5)_4^+$ Compounds

These compounds were prepared in accordance with the literature method (44); commercially available $M(CO)_6$ (M = Cr, Mo, or W) is reacted with $N(C_2H_5)_4X$ (X = Cl or Br; no iodides were prepared in this study) in hot diglyme for approximately one hour, then filtered from the remaining solids consisting of unreacted salts and decomposition products. The complex in solution was then precipitated by the addition of petroleum ether.

At this point large amounts of impurities were present in most of the complexes prepared (except for the $Cr(CO)_5Br^-$ derivative) as evidenced by their infra-red spectra in the 2100 to 1800cm^{-1} region. Before any experimental measurements were undertaken, the compounds were purified by recrystallization or by separation in CH_2Cl_2 or $CHCl_3$.

Intensity Studies of Raman Modes

As shown in Table 30 there is evidence for a reversal of the trend in intensity ratios for the

metal--carbon stretching modes $(A_1)_{d_o}/(A_1)_{d_i}$ going from the Cr subgroup pentacarbonyl halides to the Mn pentacarbonyl halides.

For the Mn compounds the trend seems to be an increase in this ratio for the halide order I < Br < Cl while the intensity of the radial A_1 M--C stretching mode seems to remain constant with respect to the intensities of the C--O stretching modes.

Thus the major change in intensity may be seen to be occurring in the vibration of the Mn--C bond trans to the halide atom. This is accompanied by an increase in the frequency of this mode in the order I< Br < Cl.

As the intensity of this mode increases with the electronegative character of the halide ion, it is suggested that the mechanism responsible for these changes is primarily an increasing stabilization of the axial-MnC σ-bond by the induction of an increasing positive charge on the Mn atom. The increased electron density in the σ-bond would then give rise to a greater change in polarization on vibration, $\partial\alpha/\partial Q_{d_o}$, which in turn is responsible for the intensity of this Raman mode.

This induction of a positive charge also implies a shrinkage effect in the metal π-symmetry d-orbitals which in turn must reduce the amount of metal-ligand

TABLE 30

Raman Intensities for CO and MC Stretching Modes: $M(CO)_5X^{n-}$

M	X	ν	Assignment	Intensity Relative to A_1(MC-rad)[a]	
Cr	Cl	387	A_1(MC-rad)	1.00	
"	"	498	A_1(MC-ax)	.50	
"	"	1857	A_1(CO-ax)	not msrd.	
"	"	not msrd.	B_1(CO-rad)	" "	
"	"	2062	A_1(CO-rad)	.18	
Cr	Br	387	A_1(MC-rad)	1.00	(1.00)
"	"	498	A_1(MC-ax)	.70	(.56)
"	"	1856	A_1(CO-ax)	not msrd.	(.58)
"	"	1969	B_1(CO-rad)	not msrd.	(.63)
"	"	2060	A_1(CO-rad)	.19	(.20)
Mn	Cl	389	A_1(MC-rad)		(1.00)

[a]For CH_2Cl_2 Solution; Values in parentheses for Solid

TABLE 30 continued

M	X	ν	Assignment	Intensity relative to A_1(MC-rad)	
Mn	Cl	479	A_1(MC-ax)		(.44)
"	"	1989	A_1(CO-ax)		(.65)
"	"	2080 + 2095	B_1(CO-rad)		(1.26)
"	"	2151	A_1(CO-rad)		(.51)
Mn	Br	384	A_1(MC-rad)	1.00	(1.00)
"	"	473	A_1(MC-ax)	.24	(.34)
"	"	1989	A_1(CO-ax)	.10	(.54)
"	"	2080	B_1(CO-rad)	.17	(.90)
"	"	2137	A_1(CO-rad)	.25	(.50)
Mn	I	389	A_1(MC-rad)		(1.00)
"	"	464	A_1(MC-ax)		(.19)
"	"	2005	A_1(CO-ax)		(.68)
"	"	2073	B_1(CO-rad)		(.98)
"	"	2131	A_1(CO-rad)		(.53)

$d\pi \longrightarrow \pi^*CO$ bonding. This effect seems to be secondary to the σ effect in the Mn compounds; however, for the case of $Cr(CO)_5Cl^-$ and $Cr(CO)_5Br^-$ it seems that the importance of the σ- and π-electron effects is reversed. This trend was also observed for the case of $Mo(CO)_5Cl^-$ and $Mo(CO)_5Br^-$ but the data were deemed not as reliable as those for the Cr compounds due to the large amount of impurities present and the rapid decomposition of the material in solution. Only the $W(CO)_5Br^-$ derivative was prepared which obviously eliminates the observation of any trends for the tungsten series.

It is suggested here that the increasing dipole induced in these M(0) compounds for Br to Cl is governed by the π back-bonding destabilization effect thus causing a <u>net</u> decrease in electron density within the axial Cr--C bond and a corresponding decrease in the intensity ratio of the Raman bands.

Although one must necessarily have reservations about this interpretation until the $M(CO)_5I^-$ compounds are prepared and measured, the trend is also reflected in the fact that there is now no increase in the frequency of $(A_1)_{d_o}$ mode going from Br to Cl. Further research must establish the relation of these M--C

stretching intensities to the intensities of other molecular vibrations (as was done above for the Mn compounds).

Intensity ratios for the Cr compounds were determined with respect to only one C--O stretching vibration, and thus it is deemed that further work with purer starting substances would be necessary to more fully substantiate these conclusions.

It would also be helpful to extend the series of compounds to include the hydride derivative, $M(CO)_5H^{n-}$, and possibly the binuclear species $M(CO)_5\text{--}\left[M(CO)_5\right]^{2n-}$. It was found that the intensity ratio of $(A_1)_{d_o}/(A_1)_{d_i}$ for $Mn_2(CO)_{10}$ fitted into the series $Mn(CO)_5 < I < Br < Cl$; however, here the shift in $(A_1)_{d_o}$ could not be directly compared with the other compounds due to a change in symmetry and frequency shifts due to interaction potential constants across the metal-metal bond.

To summarize briefly, Raman studies indicate that the halide atom's influence in the Cr subgroup compounds is felt primarily through the M--C π-bonding system. Further, the influence of the halide ion in the Mn compounds is most obvious in the M--C σ-bonding system. This also implies the relative amount of π-bonding increases from $Mn(CO)_5X$ to $Cr(CO)_5X^-$.

CHAPTER 2

ELECTRONIC ABSORPTION SPECTRA OF $M(CO)_5Br^{n-}$

Recording of the Spectra

The observed electronic absorption spectra of $Cr(CO)_5Br[N(C_2H_5)_4]$ and $Mn(CO)_5Br$ in various solvents are illustrated in figures 30, 31, and 32. The band positions (with molar extinction coefficients for the Mn(I) compound in parenthesees) are given in Table 31. These spectra were obtained with a Cary 14 spectrometer specially modified for low temperature work.

The difficulties with impurities and rapid decomposition of the Cr compound which were experienced in the Raman experiments were met with here also. The compound seemed especially unstable in the pure hydrocarbons used as solvents for $Mn(CO)_5Br$, hence only the $CHCl_3$ solution data are presented here.

Due to the impurities present (even following recrystallization) only a rough estimate of the concentration of the Cr compound in solution could be made and this is listed in figure 32.

The observed spectra will be assigned on the basis of two possible models discussed below: the

tetragonally distorted ligand field model (TDLF) and the pseudo octahedral ligand field model (POLF).

Ligand Field Models for $M(CO)_5Br^{n-}$

When the symmetry of a metal hexacarbonyl molecule is lowered from O_h to C_{4v} on going to a $M(CO)_5X^{n-}$ complex the e_g and t_{2g} ligand field levels are split as follows:

$$e_g \longrightarrow a_1(d_z2) + b_1(d_x2 - y2)$$
$$t_{2g} \longrightarrow e(d_zx,yz) + b_2(d_xy)$$

In the complex under discussion the X group is the σ-electron acceptor Br. It may be argued that replacement of a CO group by a Br atom would considerably stabilize the $a_1(d_z2)$ level relative to the $b_1(d_x2 - y2)$ level. This results in a ligand field which is substantially different from the octahedral case and gives rise to the TDLF model.

X-ray diffraction studies have shown, however, that the axial Mn--C bond is shorter than the radial Mn--C bonds for both $Mn(CO)_5H$ (28) and $Mn_2(CO)_{10}$ (39). Presumably this is also the case for $Mn(CO)_5Br$ and thus it may be surmised that the tighter bonding of the axial-CO group will largely destabilize the $a_1(d_z2)$ level causing the a_1 - b_1 splitting to be

considerably smaller than expected in the TDLF model. This is the basis of POLF model.

In (45) Slater-Condon energy parameters were calculated for various electronic configurations of d^6 $M(CN)_5X^{n-}$ complexes with a strong crystal field. These are listed below:

Electron Configuration	Designation	Slater-Condon[a] energy (+ 15 F_o)
$e^4b_2^2$	$^1A_1$	- 30 F_2 - 60 F_4
$e^4b_2b_1$	$^1A_2$	- 30 F_2 - 95 F_4
$e^4b_2a_1$	$^1B_2$	- 14 F_2 - 175 F_4
$e^3b_2^2a_1$	$^1E(1)$	- 26 F_2 - 115 F_4
$e^3b_2^2b_1$	$^1E(2)$	- 18 F_2 - 155 F_4

[a] Configuration interaction between $^1E(1)$ and $^1E(2)$ is neglected.

On the basis of electron repulsion the $^1A_2$ and $^1E(1)$ transitions are expected to be the lowest observed ligand field bands. In the case of the TDLF model we expect the $^1A_2$ transition to lie at higher energy than the $^1E(1)$ band due to the large splitting of d_{z^2} and $d_{x^2-y^2}$. On the basis of the POLF framework we expect the $^1A_2$ and $^1E(1)$ transition might occur at quite similar energies. Due to the unfavorable electron repulsion terms for $^1B_2$ and $^1E(2)$, both these bands are expected at higher energies.

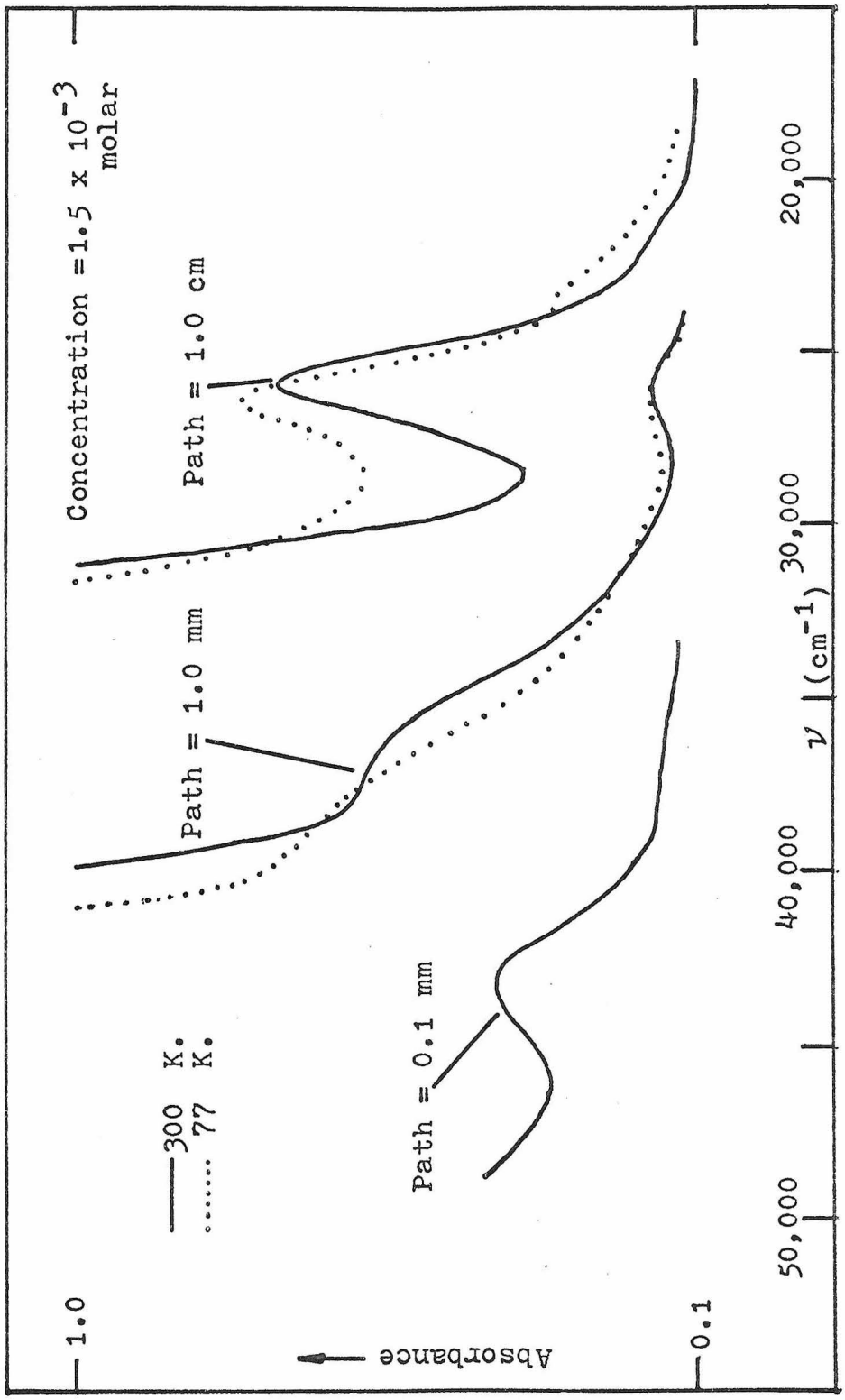

Figure 30. Electronic Absorption Spectrum of $Mn(CO)_5Br$ in 6/1 Pentane/Isopentane Solution

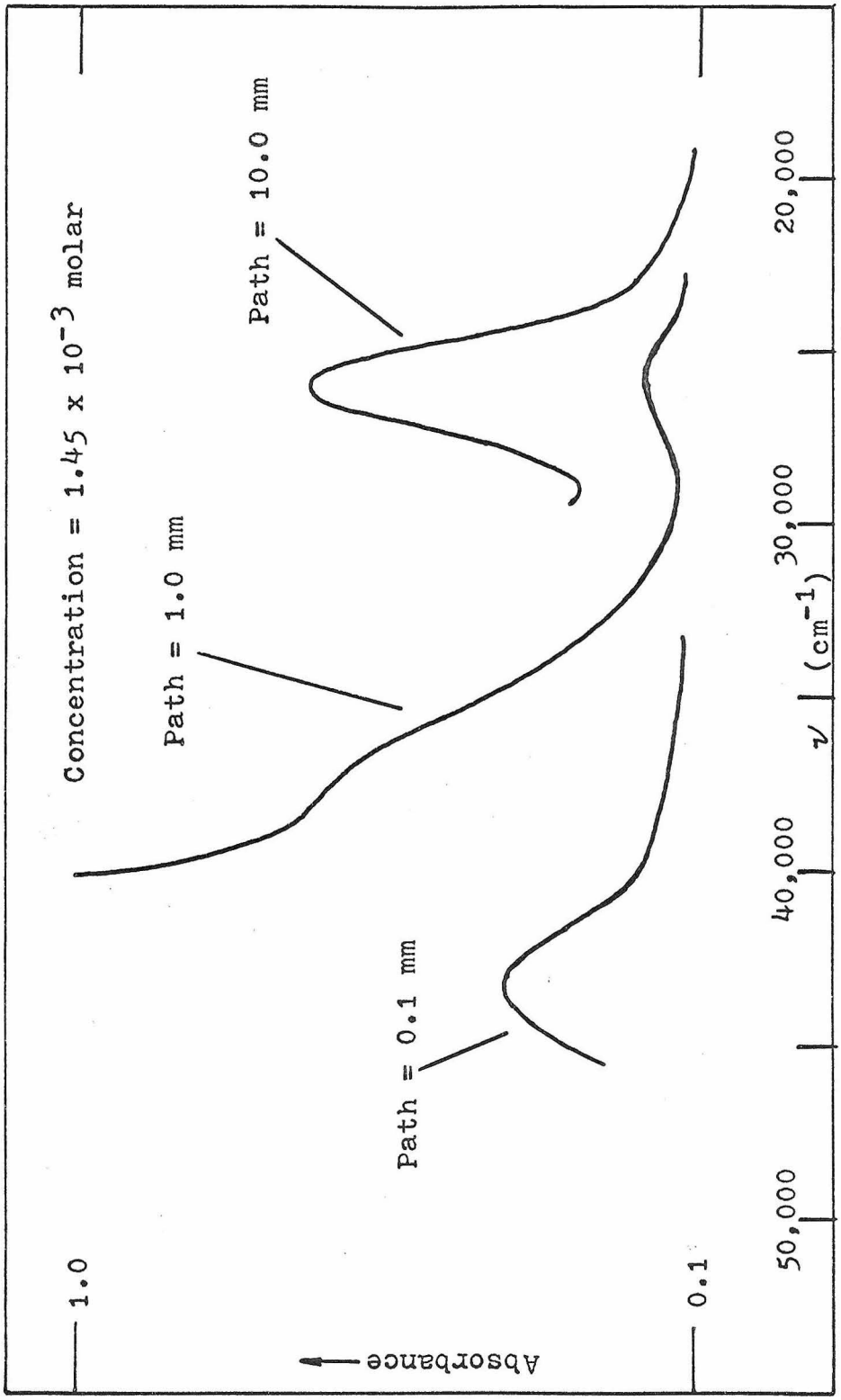

Figure 31. Electronic Absorption Spectrum of $Mn(CO)_5Br$ in $CHCl_3$ Solution

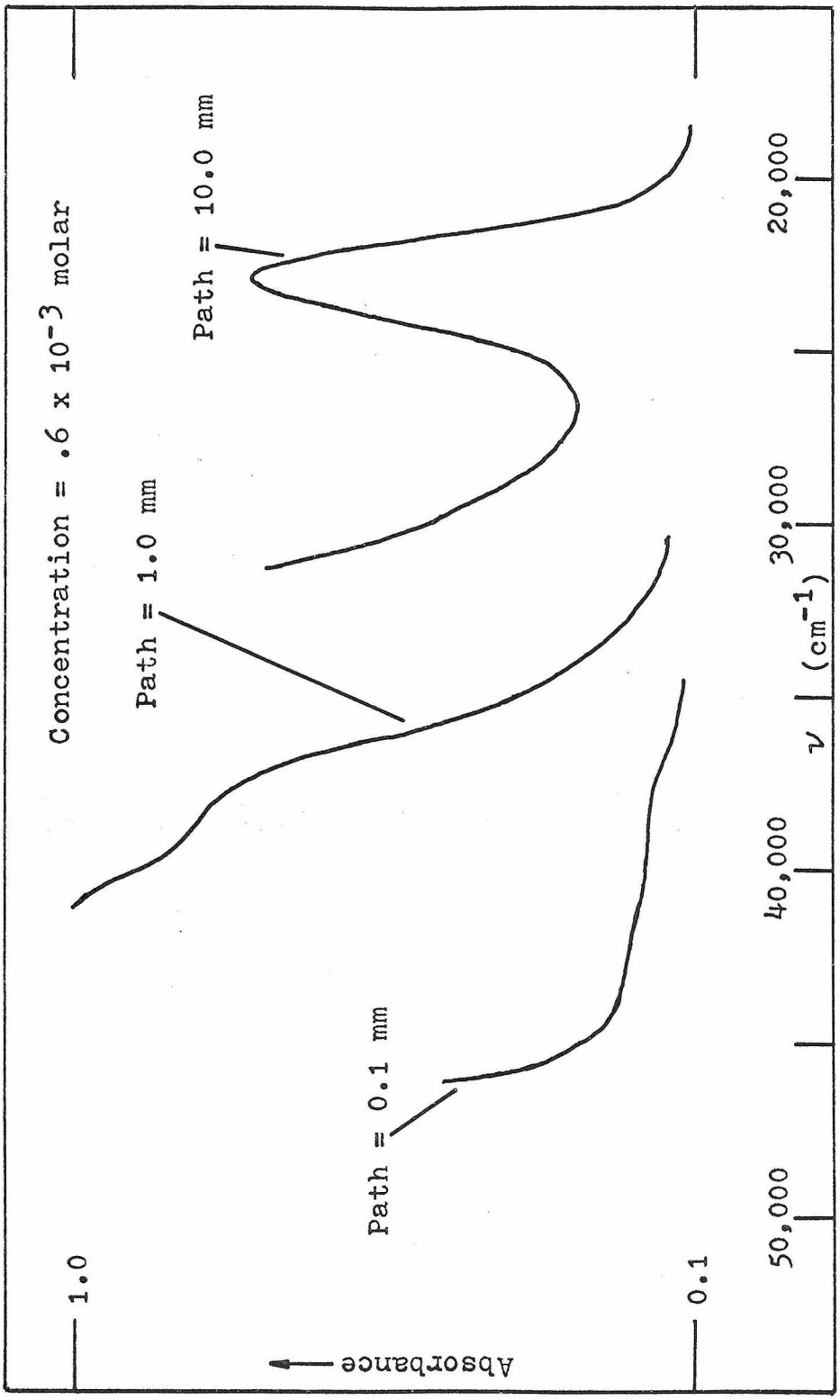

Figure 32. Electronic Absorption Spectrum of $(Et_4N)Cr(CO)_5Br$ in $CHCl_3$ Solution

TABLE 31

Electronic Absorption Spectra of $M(CO)_5X^{n-}$ in $CHCl_3$, cyclohexane, 6/1 pentane/isopentane solutions

Assignment	$CHCl_3$ soln (300° K)	cyclohexane soln (300°K)	6/1 pentane/isopentane soln (77°K)
		$Mn(CO)_5Br$	
$^1A_1 \rightarrow {}^1E(3)$	43,100 (19,000)	42,600	not msrd.
$^1A_1 \rightarrow {}^1E(2)$	36,600sh (600)	36,700	37,600
$^1A_1 \rightarrow {}^1B_2$	not obsd.	not obsd.	not obsd.
$^1A_1 \rightarrow {}^1E(1)$	25,600 (390)	25,800	26,300
$^1A_1 \rightarrow {}^1A_2$	21,600 v wk, br (30)	22,000	23,100
		$Cr(CO)_5Br^-$	
$^1A_1 \rightarrow {}^1E(4)$	41,800	not msrd.	not msrd.
$^1A_1 \rightarrow {}^1E(3)$	37,500	"	"
$^1A_1 \rightarrow {}^1E(1)$	22,900	"	"
$^1A_1 \rightarrow {}^1A_2$	not obsd.	"	"

The spacing of these ligand field levels should be represented by the following diagram:

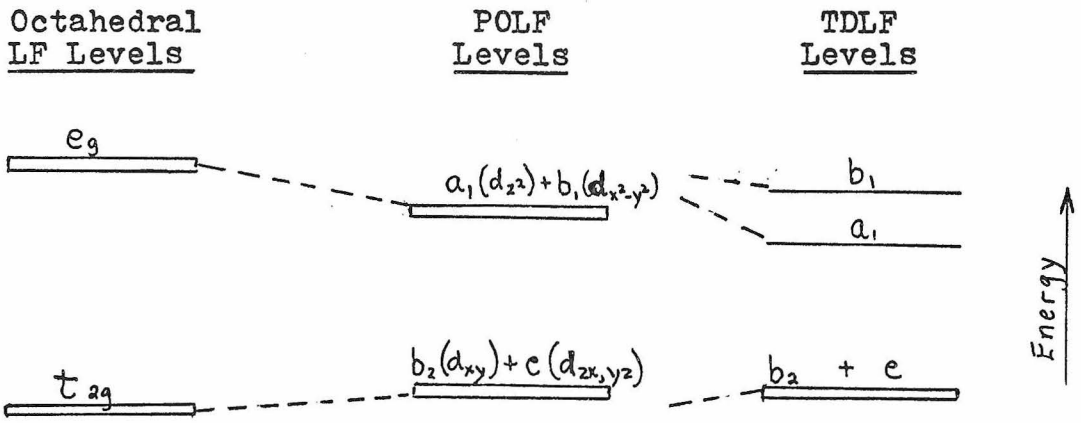

Band Assignments for $Mn(CO)_5Br$

The first intense band in the $Mn(CO)_5Br$ spectrum is found at 25,600cm^{-1} and is assigned to the $^1E(1)$ d-d transition. Recent work on the $Mn(CO)_6^+$ complex by Gray and Beach (46) has made untenable a very early assignment (47) of this band as part of the Mn→π*CO charge transfer system.

The second intense band is a shoulder at 36,600cm^{-1} which is assigned to $^1E(2)$. This is close to the observed value of 38,500cm^{-1} for $^1A_{1g} \rightarrow {}^1T_{1g}$ in $Mn(CO)_6^+$ (46).

An extremely intense band at 43,100cm^{-1} is assigned as the first Mn⟶π*CO charge transfer band, probably

of ^1E symmetry due to its very large ϵ value.

A very weak and broad feature at $\sim 21{,}600 cm^{-1}$ was observed clearly at liquid nitrogen temperature at $23{,}100 cm^{-1}$. The two possible assignments for this band are $^1A_1 \longrightarrow {}^1A_2$ or $^1A_1 \longrightarrow {}^3E(1)$ as its low intensity indicates that it should be either orbitally or spin forbidden. The third possibility $^1A_1 \longrightarrow {}^1B_2$ is rejected on the basis of the very large electron repulsion as discussed above.

The assignment of this weak band is crucial as it allows us to ascertain the relative importance of both TDLF and POLF models in this system. If the TDLF model is predominant this must be a singlet-triplet transition as the $^1A_2$ state would be expected at a higher energy than the observed $^1E(1)$ band; if the POLF model is predominant the nearness of this weak absorption to the $^1E(1)$ band would indicate the very small splitting of the $a_1(d_{z2})$ and $b_1(d_{x2} - y^2)$ levels.

To confirm either assignment the spectrum of the analogous Re complex should be obtained. Considerable enhancement of this band (as was the case (46) for the absorption at ca. $29{,}000 cm^{-1}$ in $Mo(CO)_6$ and $W(CO)_6$) would tend to favor its assignment as the spin-forbidden

$^1A_1 \longrightarrow {}^3E(1)$ transition. A comparable intensity ($\epsilon \sim 30$) would support the $^1A_2$ assignment.

It is of interest to note that a POLF model is compatible with the ligand field spectra in the $Co(CN)_5X^{3-}$ system (48). This type of model has also been invoked to account for the magnetic properties of the $Fe(CN)_5X^{3-}$ system (49).

Band assignments for $Cr(CO)_5Br^-$

The lower positive charge on the metal atom going from Mn(I) to Cr(0) will result in a considerable energy lowering of the charge transfer system. Thus the two intense bands at 41,800 and 37,500cm^{-1} are both assigned as d-Cr$\longrightarrow\pi^*$CO charge transfer bands. Due to this lowering $^1E(2)$ is not observed in $Cr(CO)_5Br^-$ as it is expected to fall underneath the lowest charge transfer band.

E(1) was observed at 22,900cm^{-1} but the weak band expected at slightly lower energy was not seen. This may be due to either very low intensity or accidental degenracy with $^1E(1)$.

Discussion

The electronic structure of metal carbonyl complexes has just recently become the subject of many

thorough theoretical and experimental electronic structural investigations including electronic absorption spectral and electron impact experiments (7, 46, 50, 51), and molecular orbital calculations (46, 52, 53). It is thus of considerable interest to determine what insight into these problems the foregoing vibrational analyses contribute.

The conclusions reached in Part I favor the POLF model discussed above for the following reasons:

1. It was found that the calculated interaction constants agree very well with equivalent constants from the $Cr(CO)_6$ octahedral system. This tallies quite well with the observation that although considerable changes in bonding from $M(CO)_6$ have taken place, these changes have been complementary in such a way that the ligand field of $Mn(CO)_5Br$ has remained very nearly octahedral.

2. Those interaction constants which show a large change from their octahedral equivalents are involved with coordinates whose atomic motion is along or parallel to the four-fold axis of $Mn(CO)_5Br$. The relative magnitudes of these constants and the orientation of their coordinates indicate that they may be electrostatic in nature; these differences may thus be thought of as <u>external</u> to the resultant ligand field.

3. The repeatedly emphasized importance of σ-bonding effects in the interpretation of trends in potential constants from $M(CO)_6$ to $Mn(CO)_5Br$ may be taken as evidence that the changes in π bonding and charge distribution caused by substitution of a Br for a CO group are being compensated for, and the departure from an octahedral field for this molecule may be quite small indeed.

CHAPTER 3

FINAL SUMMARY AND EVALUATION OF RESULTS

As were outlined in the Introduction, the main goals of this work were (1) the evaluation of the assumptions underlying the many approximate force fields presented for metal carbonyls of the form $M(CO)_5X$ in the literature since about 1962; (2) the relation of $M(CO)_5X$ systems to $M(CO)_6$ systems regarding changes in bonding, also the determination of the highly debated nature of vibrational interactions across the metal-metal bond in $M_2(CO)_{10}$ systems; (3) and finally the evaluation of several calculations of the metal-metal stretching force constant in $Mn_2(CO)_{10}$ to determine their relative merits in light of a full normal coordinate analysis and to establish a minimum set of requirements for calculations on other $M_2(CO)_{10}$ systems and more complicated polynuclear carbonyls. The main conclusions on these points are summarized below.

1. The assumptions involved in the force field proposed by Cotton and Kraihanzel (1) to account for the observed infra-red C--O stretching modes have been found in this work to be unjustifiable. The approximation in (1) that $F^c_{r_i,r_i} = 0.5\ F^t_{r_i,r_i}$ is contrasted with the

present value $F^{c}_{r_i,r_i} \cong 4\ F^{t}_{r_i,r_i}$. Although this does not discount the results of many later studies which make use of the relative values of these parameters for a series of $M(CO)_5X$ derivatives, any discussion of the absolute values of these parameters or their dependance on changes in the metal back-bonding d-π orbitals as formulated in (1) is incorrect.

2. The fact that $F^{c}_{r_i,r_i}$ is much larger than $F^{t}_{r_i,r_i}$ and that $F_{r_i,45}$ is much larger than $F_{r_i,135}$ and $F_{r_o,j}$ for $Mn_2(CO)_{10}$ indicates that interactions among the various CO ligands are primarily electrostatic in nature.

The opposite behavior is observed for the metal--carbon stretching coordinates, d_i and d_o, where $|F^{t}_{d_i,d_i}| \gg |F^{c}_{d_i,d_i}|$ for $Mn(CO)_5Br$ and likewise $|F_{d_o,j}| \gg |F_{d_i,45} + F_{d_i,135}|$ for $Mn_2(CO)_{10}$. These results support an interaction mechanism involving changing electron populations in the metal d-orbitals of π symmetry as proposed in (5).

Raman intensity studies and electronic absorption investigations show that considerable changes in the σ-bonding system of $M(CO)_5X^{n-}$ have occured from $M(CO)_6^{(n+1)-}$; the substitution of a halide atom for a CO group is apparently responsible for these effects and they appear to play a major role in the transmission of metal-ligand

stretching interactions.

These Raman intensity studies reveal further that changes in metal d$\longrightarrow\pi^*$CO back-bonding are the dominant factors in transmitting metal-ligand stretching interactions across the metal-metal bond in $Mn_2(CO)_{10}$. This is analogous to the mechanism of Cotton (5) which was incorrectly applied to interactions among the CO stretching modes.

Both the vibrational and electronic spectral studies indicate a striking similarity in the ligand field of the $Mn(CO)_5Br$ molecule to the octahedral $Cr(CO)_6$ and $Mn(CO)_6^+$ systems. Apparently the changes in σ-bonding mentioned above on the substitution of Br for CO compensate to a large degree for changes in the π electronic structure. It is hoped that this satisfactory correlation of results will serve as an incentive for further combined spectral studies in this field.

3. A large amount of interest exists today in the nature of the metal-metal bonding in polynuclear carbonyls. The calculation of accurate metal-metal stretching potential constants is thus of major importance in the interpretation of these systems.

This work has shown that the metal-metal stretching coordinate, Δ, is highly mixed with the C--M--C bending

coordinate of A_1 symmetry. Comparison of the value calculated here, $F = 1.26$ md/A, with that of Spiro (37), $F_{Mn-Mn} = .59$ md/A, indicates that a mere estimate of this mixing is insufficient to obtain accurate potential constants. Both A_1 modes must be definitely assigned and the mixing constant $F_{\Delta,\psi-\delta}$ allowed to vary for the most accurate fit.

Values for these parameters in the $Tc_2(CO)_{10}$, $Re_2(CO)_{10}$, and $MnRe(CO)_{10}$ systems should definitely be re-evaluated on the basis of polarized Raman solution spectra before any trends in the metal-metal bonding of these systems or more complicated polynuclear systems are discussed.

B I B L I O G R A P H Y

BIBLIOGRAPHY

1. F. A. Cotton and C. S. Kraihanzel, Inorg. Chem., 2, 533 (1963).

2. F. A. Cotton, ibid., 3, 702 (1964).

3. N. Flitcroft, D. K. Huggins, and H. D. Kaesz, ibid., 3, 1123 (1964).

4. J. C. Hielman, D. K. Huggins, and H. D. Kaesz, ibid., 1, 933 (1962).

5. F. A. Cotton and R. M. Wing, ibid., 4, 1328 (1965).

6. H. D. Kaesz, R. Bau, D. Hendrickson, and J. M. Smith, J. Am. Chem. Soc., 89, 2844, (1967).

7. E. W. Abel, et al., J. Molecular Spec., 30, 29 (1969).

8. H. Haas and R. K. Sheline, J. Chem. Phys., 47, 2996 (1967).

9. I. J. Hyams, D. Jones, and E. R. Lippincott, J. Chem. Soc. (A), 1967, 1987.

10. L. H. Jones, R. S. MacDowell, and M. Goldblatt, J. Chem. Phys., 48, 2663 (1968).

11. K. L. Watters, J. N. Brittain, and W. M. Risen, Inorg. Chem., 8, 1347 (1969).

12. I. J. Hyams and E. R. Lippincott, Spectrochimica Acta, 25A, 1845 (1969).

13. W. F. Edgell, J. W. Fisher, G. Asato, and W. M. Risen, Inorg. Chem., 8, 1103 (1969).

14. L. H. Jones, R. S. MacDowell, and M. Goldblatt, ibid., 8, 2349 (1969); and L.H. Jones, private communication.

15. (a) W. A. G. Graham, Inorg. Chem., 7, 315 (1968); (b) R. P. Stewart and M. D. Treichel, ibid., 7, 1942 (1968).

16. F. A. Cotton and G. Wilkinson, Advanced Inorganic Chemistry, 2nd Ed., Interscience Publishers, New York City, N. Y., 1966, p. 728ff.

17. Abel and Wilkinson, J. Chem. Soc. (A), 1959, 1501.

18. F. A. Cotton, A. Musco, and G. Yagupsky, Inorg. Chem., 6, 1357 (1967).

19. I. S. Butler and H. K. Spendjian, Canad. J. Chem. 47, 4117 (1969).

20. (a) R. J. H. Clark and B. C. Crosse, J. Chem. Soc. (A), 1969, 224.
(b) D. M. Adams and A. Squire, ibid., 1968, 2817.

21. V. Valent, et al., Inorg. Nucl. Chem. Letters, 3, 237 (1967).

22. G. Herzberg, Infrared and Raman Spectra, D. Van Norstrand Co., Inc., Princeton, N.J., 1945.

23. L. H. Jones, Inorg. Chem., 6, 1269 (1967).

24. J. H. Schachtschneider, SD-9032-I and SD-9032-VII, Shell Development Corp.

25. E. B. Wilson, Jr., J. C. Decius, and P. C. Cross, Molecular Vibrations, McGraw-Hill Book Co., New York, N. Y., 1955.

26. J. C. Decius, J. Chem. Phys., 38, 241 (1963).

27. L. H. Jones and R. R. Ryan, ibid., 52, 2003 (1970).

28. S. J. la Placa, et al., Inorg. Chem., 8, 1928 (1969).

29. M. A. El-Sayed and H. D. Kaesz, J. Molecular Spec., 9, 310 (1962).

30. D. J. Darensbourg and T. L. Brown, Inorg. Chem., 7, 959, (1968).

31. G. Bor, Chem. Communications, 1969, 641.

32. J. Lewis, A. R. Manning, and J. R. Miller, J. Chem. Soc. (A), 1966, 845.

33. D. J. Parker and M. H. B. Stiddard, ibid., 1966, 695.

34. J. M. Smith, Ph. D. Dissertation, University of California, Los Angeles, Cal., 1966.

35. G. P. Ceasar, R. A. Levenson, and H. B. Gray, J. Am. Chem. Soc., 91, 772 (1969).

36. R. Levenson, private communication.

37. C. O. Quicksall and T. G. Spiro, Inorg. Chem., 8, 2363, (1969).

38. J. Lewis, et al., Nature, 207, 142 (1965).

39. L. F. Dahl and R. E. Rundle, Acta Cryst., 16, 419 (1963).

40. H. M. Gager, J. Lewis, and M. J. Ware, Chem. Communications, 1966, 616.

41. G. O. Evans, W. T. Wozniak, and R. K. Sheline, Inorg. Chem., 9, 979 (1970).

42. H. J. Svec and G. A. Junk, J. Am. Chem. Soc., 89, 2836 (1967).

43. S. L. Segel, J. Chem. Phys., 51, 848 (1969).

44. Abel, Butler, and Reid, J. Chem. Soc. (A), 1963, 2068.

45. H. B. Gray and C. J. Ballhausen, J. Chem. Phys., 36, 1151 (1962).

46. N. A. Beach and H. B. Gray, J. Am. Chem. Soc., 90, 5713 (1968).

47. H. B. Gray, E. Billig, A. Wojcicki, and M. Farona, Canad. J. Chem., 41, 1281 (1963).

48. D. F. Gutterman and H. B. Gray, to be published.

49. D. F. Gutterman and H. B. Gray, to be published.

50. D. R. Lloyd and E. W. Schlag, Inorg. Chem., 8, 2544 (1969).

51. R. E. Sullivan and R. W. Kiser, J. Chem. Phys., 49, 1978 (1968).

52. I. H. Hillier, J. Chem. Phys., 52, 1948 (1970).

53. A. F. Schreiner and T. L. Brown, J. Am. Chem. Soc., 90, 3366 (1968).

P R O P O S I T I O N S

PROPOSITIONS

I.

It is proposed to study the adsorption, reaction, and desorption mechanisms of several simple diatomic and triatomic gases on various transition metals and their oxides by means of isotopic fractionation analysis.

II.

Oriented single crystal Raman experiments are proposed to unequivocably assign the observed spectrum of $M_2(CO)_{10}$ and $M_2(CO)_8X_2$ (where M = Mn or Re and X = Cl, Br, or I).

III.

Metal-metal interactions have been suggested to explain the observed Raman spectrum of $Bi_6(OH)_{12}^{6+}$; it is proposed here to further elucidate the nature of any Bi--Bi interactions through the use of nuclear quadrupole resonance experiments.

IV.

The reaction mechanisms for the pyrolysis and disproportionation of the simple silanes and halosilanes is very incompletely understood. Fundamental research on this topic is proposed using the techniques of isotopic fractionation analysis of ^{28}Si ^{30}Si isotopic molecules.

V.

It is proposed to obtain the polarized Raman and infra-red spectra of single crystals of $K_4Mo(CN)_8 \cdot H_2O$. Accurate assignment of these vibrational spectra will be very beneficial in the characterization of numerous poorly understood derivatives of the eight-coordinate $Mo(CN)_8^{4-}$ ion.

PROPOSITION I

(1) Isotopic fractionation study of the catalytic hydrogenation of carbon monoxide.

There has been very little use made of isotopic fractionation as a tool for studying reactions catalyzed by metal and metal oxide surfaces. It seems reasonable that since isotopic fractionations are characteristic of the detailed structure of the reactants and intermediates during the course of chemical reactions, investigations dealing with isotopic fractionations should give information regarding the structural details of various heterogeneous catalytic processes.

The simple reaction of $CO + 2\ H_2 \longrightarrow CH_4 + H_2O$ as catalyzed by Co and Ni metal subgroups affords an opportunity to investigate the isotopic fractionations associated with the reaction of all three elements: H, C, and O. These are elements whose isotopic ratio variations may be measured to within $\pm 0.01\%$ for carbon and oxygen and $\pm 0.1\%$ for hydrogen with contemporary high precision mass spectrometers.

Research may be initiated by determining fractionation factors for the adsorption of CO and H_2 separately on the metal catalysts mentioned above. This data may then be used in conjunction with the available studies

on chemisorbed H and CO species in interpreting fractionation experiments as H_2-CO mixtures are catalytically reacted to form CH_4 and H_2O.

The values of the fractionation factors, α, for each element and their temperature dependence should indicate the relation of rate of adsorption to the rate of reaction on the surface; this is due to the fact that the value of α can be expected to vary depending on whether the adsorption of H_2 and CO is in equillibrium with the gas phase or whether the adsorption of one or the other gas is the rate determining step.

A study of the temperature dependence of the fractionation involved in each step would provide a measure of the activation energy of that step, and it might also indicate the presence of more than one mechanism by changes in the slope of temperature versus α, or an "impossible" increase of α observed with increasing temperature as was found in Reference (1).

Previous work (2,3,4) indicates the rate determining step of this process is the formation of H-COH complexes on the surface of the catalyst and it would be very interesting to see how the isotopic fractionation work will compare with this.

Even more interesting would be the fractionations involved in the products CH_4 and H_2O. This data will be

a key to the mechanisms involved in the reactions of the adsorbed complexes themselves.

For even a simple system as this the problems in analysis of the resulting data will still be immense; it is therefore desirable to do precise determinations of α_H, α_C, and α_O, simultaneously, thus utilizing all the available information from these systems. This multiple approach to the problem may in turn lead to the definite acceptance or rejection of certain of the mechanisms proposed in the literature.

(2) Isotopic fractionation study of the catalytic decomposition of nitrogen oxides.

A parallel study is anticipated on the decomposition of NO and N_2O on metal oxides such as Cr_2O_3, Fe_2O_3, NiO, CuO, and ZnO at somewhat elevated temperatures with the formation of N_2 and O_2. Analysis of the mechanism occurring on the catalyst surface will be more complex than in the preceding case due to interaction (and thus possible fractionation effects) between the oxygen atoms of the nitrogen oxides and metal oxides.

Very interesting studies are possible here in terms of examining various layers of the catalyst after reaction for evidence of O^{18}/O^{16} fractionation. Also,

comparison experiments using the analogous metal sulfides would be an intriguing avenue of research; noticeable differences in O^{18}/O^{16} fractionation on the catalyst surface would be valuable in deducing the role of the surface oxygen anions in the adsorption and decomposition mechanisms (as in the recent EPR experiment (5) indicating the existence of the species NO_2^- in NO adsorbed on ZnO and the absence of NO_2^- in NO adsorbed on ZnS).

BIBLIOGRAPHY

1. Brown, Dole, and Lane; J. Chem. Phys. 27, 251 (1957).
2. Vlasenko, et al.; Kinet. Kataliz. 5, 337 (1964).
3. Kozub, et al.; ibid. 6, 244 (1965).
4. Vlasenko, Yuzefovich, and Rusov; ibid. 6, 688 (1965).
5. Lunsford; J. Chem. Phys. 72, 2141 (1968).

PROPOSITION II

A most interesting consequence of the vibrational analysis of polynuclear metal carbonyl systems would be the evaluation of interaction parameters which define the amount of coupling between vibrations originating on different metal centers.

This has stimulated much interest and a number of papers have appeared dealing with the metal-metal or metal-bridging group(s)-metal vibrations of these systems. (1-5) These results unfortunately yield only an idea of the strength of the bond between metallic centers and no knowledge of the electron distribution about them.

The evaluation of vibrational coupling constants acting between the metallic centers will provide important information through their magnitude and symmetry indicating which molecular orbitals may be instrumental in transmitting vibrational effects from one metallic center to the other.

These calculations of coupling constants depend on precise assignment of fundamental vibrations if any accurate conclusions are to be drawn at all; and this has stymied workers in this area for some time as the very interesting and complex polynuclear carbo-

nyl complexes possess correspondingly interesting and complex vibrational spectra.

However, with a highly polarizable laser light source available on contemporary Raman spectrometers and the known crystal structures of many of these systems, one may obtain polarized Raman spectra of their various single crystals; (6-13) The rigid selection rules which obtain for these systems will provide unequivocal assignment as to symmetry type for most observed modes and thus furnish an excellent starting point for vibrational calculations on these complicated systems.

A case in point are the $M_2(CO)_{10}$ and $M_2(CO)_8X_2$ (M = Mn or Re; X = Cl, Br, or I) complexes; the former involves a direct metal-metal bond and the latter a metal-bridging halogens-metal system. Both types form regular shaped monoclinic crystals (14,15), and preliminary experiments by myself and Mr. Jeffery Hare of this laboratory have produced highly polarized Raman spectra for crystals of $Mn_2(CO)_{10}$, $Re_2(CO)_{10}$, and $Mn_2(CO)_8Br_2$.

The main difficulty in definitive experiments will be the determination of the crystals' precise orientation in the spectrometer's laser beam. The individual $M_2(CO)_{10}$ and $M_2(CO)_8X_2$ molecules possess almost exact

D_{4d} and D_{2h} point symmetry, respectively, and are arranged in the crystal lattice as shown below:

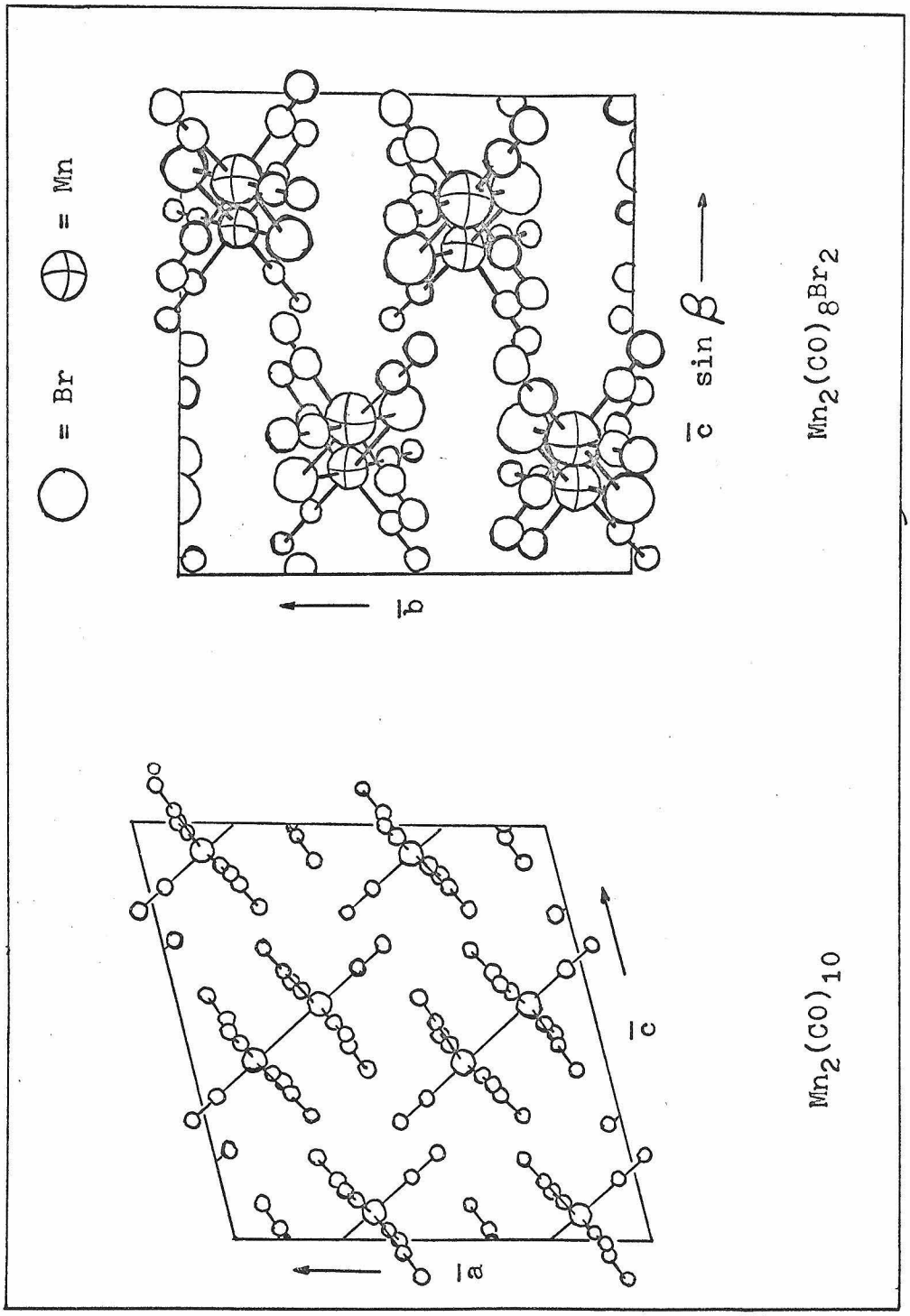

Figure 1. Projection of Unit Cells of $Mn_2(CO)_{10}$ and $Mn_2(CO)_8Br_2$

Since the M—M axes and the M<X X>M axes, respectively, lie parallel to one another in the crystal, one may ignore as a first approximation the lower symmetry of the unit cell's factor group and derive selection rules for the molecular vibrations directly from the molecular point symmetry involved. These follow from the appropriate character tables:

TABLE I

D_{4d}			D_{2h}		
A_1		$\alpha_{xx} + \alpha_{yy}, \alpha_{zz}$	A_{1g}		$\alpha_{xx}, \alpha_{yy}, \alpha_{zz}$
A_2	R_z		B_{1g}	R_z	α_{xy}
B_1			B_{2g}	R_y	α_{zx}
B_2	T_z		B_{3g}	R_x	α_{yz}
E_1	T_x, T_y		A_u		
E_2		$\alpha_{xx} - \alpha_{yy}, \alpha_{xy}$	B_{1u}	T_z	
E_3	R_x, R_y		B_{2u}	T_y	
			B_{3u}	T_x	

Thus if the appropriate orientation of the crystals is achieved, simply rotating the plane of polarization of the incident laser beam relative to a polaroid film used to "analyze" the scattered radiation previous to its entering the spectrometer should produce the following polarization effects:

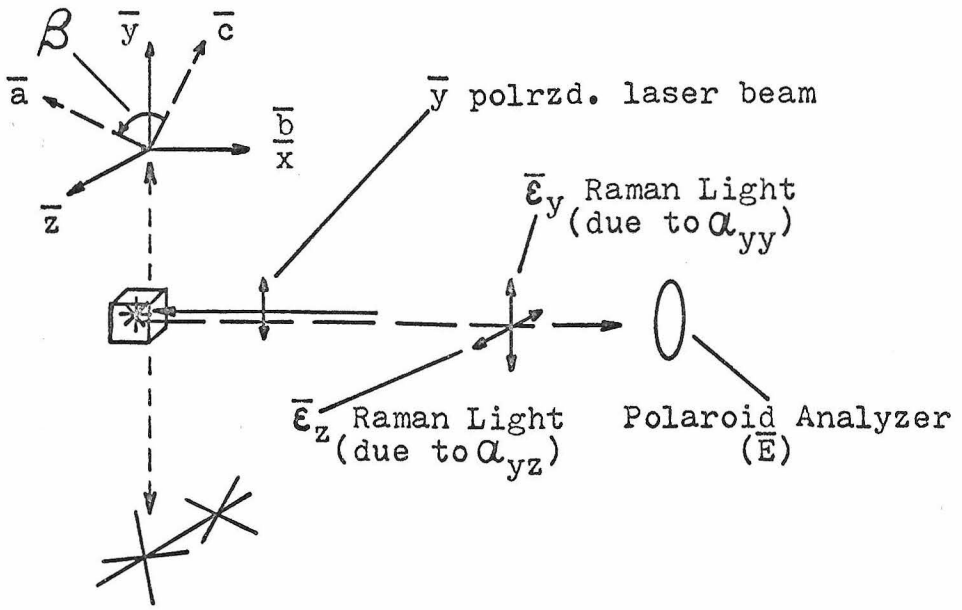

Figure 2. Single Crystal Raman Set-Up for $Mn_2(CO)_{10}$

In this figure the molecular orientation in the crystal is given by the $\bar{x}$, $\bar{y}$, and $\bar{z}$ axes, and the crystallographic axes are indicated by $\bar{a}$, $\bar{b}$, and $\bar{c}$. The polaroid analyzer will pass Raman scattered light $\bar{\varepsilon}_y$ or $\bar{\varepsilon}_z$ depending on the orientation of $\bar{E}$.

To indicate the various experimental orientations involved we use the standard notation given in Reference (8); this is $X(ij)\bar{X}$ where

X = direction of propagation of laser beam
i = orientation of electric vector of laser
j = " " " Raman light
$\bar{X}$ = direction of propagation of Raman light

Considering then only Raman active modes under D_{4d} symmetry we have:

A_1 --- active for x(yy)x and x(zz)x. If $Intensity_{x(yy)x} > Intensity_{x(zz)x}$ then $\alpha_{yy} > \alpha_{zz}$ for the particular mode involved which gives information as to the axial or radial character of the vibration.

--- inactive for x(yz)x.

E_2 --- inactive for x(yy)x, x(zz)x, and x(yz)x.

E_3 --- active for x(yz)x.

--- inactive for x(yy)x and x(zz)x.

In the case of the $M_2(CO)_8X_2$ systems one must modify figure 2 so that the $\bar{a}$ crystallographic axis now lies parallel to the laser beam's direction of propagation. This again will align the $M\langle{}^{X}_{X}\rangle M$ axes perpendicular to the $\bar{x}$ axis, and under D_{2h} symmetry the following selection rules for Raman active modes may be derived:

A_g --- active for x(yy)x and x(zz)x. The same argument above for the intensities of the two orientations will apply here also.

--- inactive for x(yz)x.

B_{1g} --- inactive for x(yy)x, x(zz)x, and x(yz)x.

B_{2g} --- inactive for x(yy)x, x(zz)x, and x(yz)x.

B_{3g} --- active for x(yz)x.

--- inactive for x(yy)x and x(zz)x.

BIBLIOGRAPHY

1. F. A. Cotton and R. M. Wing; Inorg. Chem. 4, 1328 (1965).

2. I. J. Hyams, D. Jones, and E. R. Lippincott; J. Chem. Soc. (London) 1967A, 1987.

3. C. O. Quicksall and T. G. Spiro; Inorg. Chem. 8, 2363 (1969).

4. F. J. Farrell, V. A. Maroni, and T. G. Spiro; Inorg. Chem. 8, 2638 (1969).

5. G. O. Evans, W. T. Wozniak, and R. K. Sheline; Inorg. Chem. 9, 979 (1970).

6. L. Couture-Mathieu and J.-P. Mathieu; Acta Cryst. 5, 571 (1952).

7. P. J. Hendra and E. R. Lippincott; Nature 212, 1448 (1966).

8. T. C. Damen, S. P. S. Porto, and B. Tell; Phys. Rev. 142, 570 (1966).

9. V. Ananthanarayanan; J. Chem. Phys. 48, 573 (1968).

10. L. Colombo; ibid. 49, 4688 (1968).

11. I. Nakagawa and J.L. Walter; ibid. 51, 1389 (1969).

12. B. Fanconi, et. al.; ibid. 51, 3993 (1969).

13. R. K. Khanna, C. W. Brown and L. H. Jones; Inorg. Chem. 8; 2195 (1969).

14. L. F. Dahl and R. E. Rundle; Acta Cryst. 16, 419 (1963).

15. L. F. Dahl and C.-H. Wei; ibid. 16, 611 (1963).

PROPOSITION III

Recently a localized molecular orbital scheme was proposed (1) for the $Bi_6(OH)_{12}^{6+}$ cluster compound; the basis for this was a vibrational analysis which indicated that a substantial amount of metal-metal bonding was present. The structure of this cation has been deduced (2) by X-ray scattering from a 5.1 molar aqueous solution of its ClO_4^- salt and this is illustrated in figure 1.

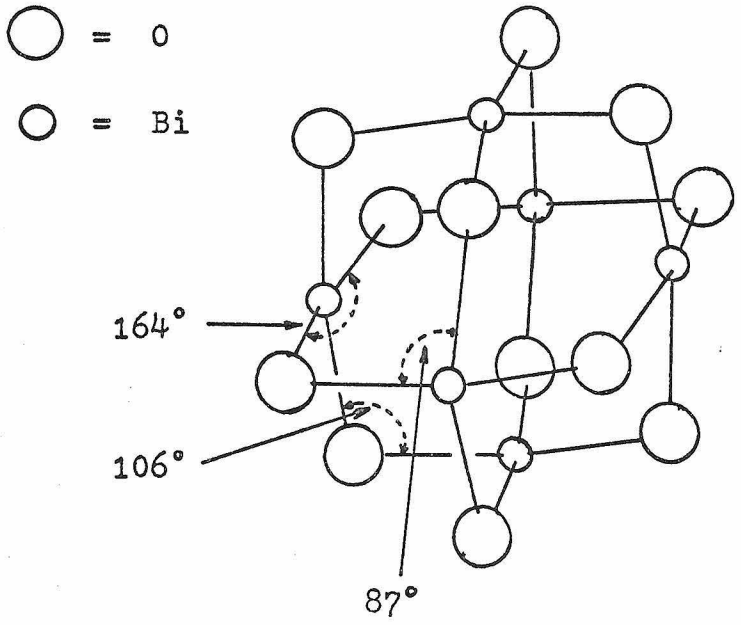

Bond Distances:

Bi-Bi = 3.71 A

Bi-O = 2.33 A

Figure 1. Structure of $Bi_6(OH)_{12}^{6+}$ in Aqueous Solution

The M.O. scheme outlined in (1) is similar in terms of bonding orbitals to that proposed for $Ta_6Cl_{12}^{2+}$ (3) differing in that there are fewer complications in the Bi compound due to the completely filled 5d shell in contrast to the transition metal complex.

Thus the bonding in the Bi--OH cluster may be discussed as a first approximation in terms of M.O.'s constructed solely from the Bi $[6s]$ and $[6p]$ orbitals. The empty $[6p_x]$ and $[6p_y]$ orbitals are used to form the slightly bent (164°) bonds with the OH^- ions while the remaining $[6s]$ and $[6p_z]$ orbitals are hybridized to form 6 bonding orbitals which interact at the center of the Bi_6 cage.

This interpretation is at variance with the usual behavior of the $Bi^{(III)}$ ion (4) which may be described in terms of an "inert" pair of electrons in the $[6s]$ orbital. This is due primarily to the rather large energy separation of 8.8 e.v. between the $[6s]$ and $[6p]$ levels in the free Bi^{3+} ion (5). However, sufficient stabilization might arise from the metal-metal interaction to promote some $s\text{-}p_z$ hybridization. To estimate this quantity it is proposed to obtain and interpret the nuclear quadrupole resonance (NQR) spectrum of $Bi_6(OH)_{12}(ClO_4)_6$.

A fair amount of success has been obtained in the interpretation of NQR results for various metal-halide systems (excluding fluorides) using the "p-shell hole"

theory of Townes and Dailey (6). In brief, they showed that the major contribution to the electric field gradient (EFG) about a nucleus exhibiting an NQR spectrum was due to an imbalance in the number of p valence electrons for that nucleus. Effects arising from s-electrons and all filled shells were zero due to their spherical symmetry, and contributions from d- and f-wave functions were judged to be neglegible. This is assumed to be the case here also in view of the equally large energy separation of the $\left[6p\right]$ and $\left[6d\right]$ levels.

The ^{209}Bi nucleus has a spin of $I = 9/2$ and thus it will exhibit an NQR spectrum of 4 lines corresponding to the splittings of the spin states by the EFG:

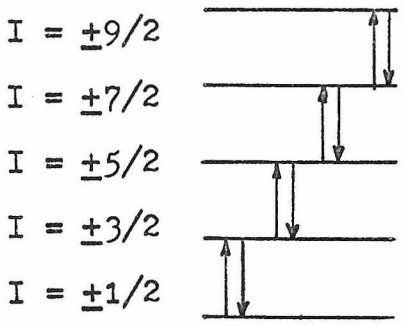

(The selection rules for obsd. NQR frequencies are $\Delta I = \pm 1$.)

The separation of these frequencies yields the quadrupole coupling const. eQq_{zz} (where eQ = the nuclear quadrupole moment and q_{zz} = EFG in an axially symmetric field). In the case of axial symmetry we have also $q_{xx} = q_{yy}$, and the imbalance in p-electrons is

$$Up = \left(\frac{Np_x + Np_y}{2} - Np_z\right) = (Np_{x,y} - Np_z)$$

Up = unbalanced p-electrons

Np_x = No. of electrons in Px, etc.

and it can be shown (6) that $eQq_{zz} = UpeQq_{zz}(p)$ where $eQq_{zz}(p)$ is the coupling constant arising from 1 unbalanced p-electron. In reference (7) this was calculated from atomic hyperfine structure to be $eQq_{zz}(p) = 1500$ mc/sec.

However, before estimating the amount of s-p hybridization, one must consider changes in Up due to the fact that $Np_{x,y} \neq 0$; i.e., the Bi--O bond is far from being completely ionic. It may be estimated from Pauling (8) that the ionic character of this bond is 47%; thus $Np_{x,y} = (1.00 - 0.47) = 0.53$, and $Up = 0.53 - Np_z$.

The s-p bonding orbital's wave function may be written as

$$\frac{1}{(1 + \lambda^2)^{1/2}} (\lambda[6s] + [6p])$$

where λ is the fraction of s hybridization; as each s-p hybridized bonding orbital will be filled, the final expression for Up is estimated to be

$$Up = 0.53 - \frac{2}{(1 + \lambda^2)^{1/2}}$$

and expressing the ratio of coupling constants as

$$eQq_{zz}/eQq_{zz}(p) = \rho$$

we may write $Up = 0.53 - \frac{2}{(1 + \lambda^2)^{1/2}} = \rho$

This expression is plotted in figure 2 for values of λ from .1 to 4.0. This encompasses a fractional s character of 9% to 80% (or consequently a fractional p character of 91% to 20%). If the p character should fall below 20% then the function is no longer analytic due to the ambiguity of the sign in Up. Thus one must be continually more cautious in regard to interpretation of the amount of hybridization as the value of ρ falls toward 0.

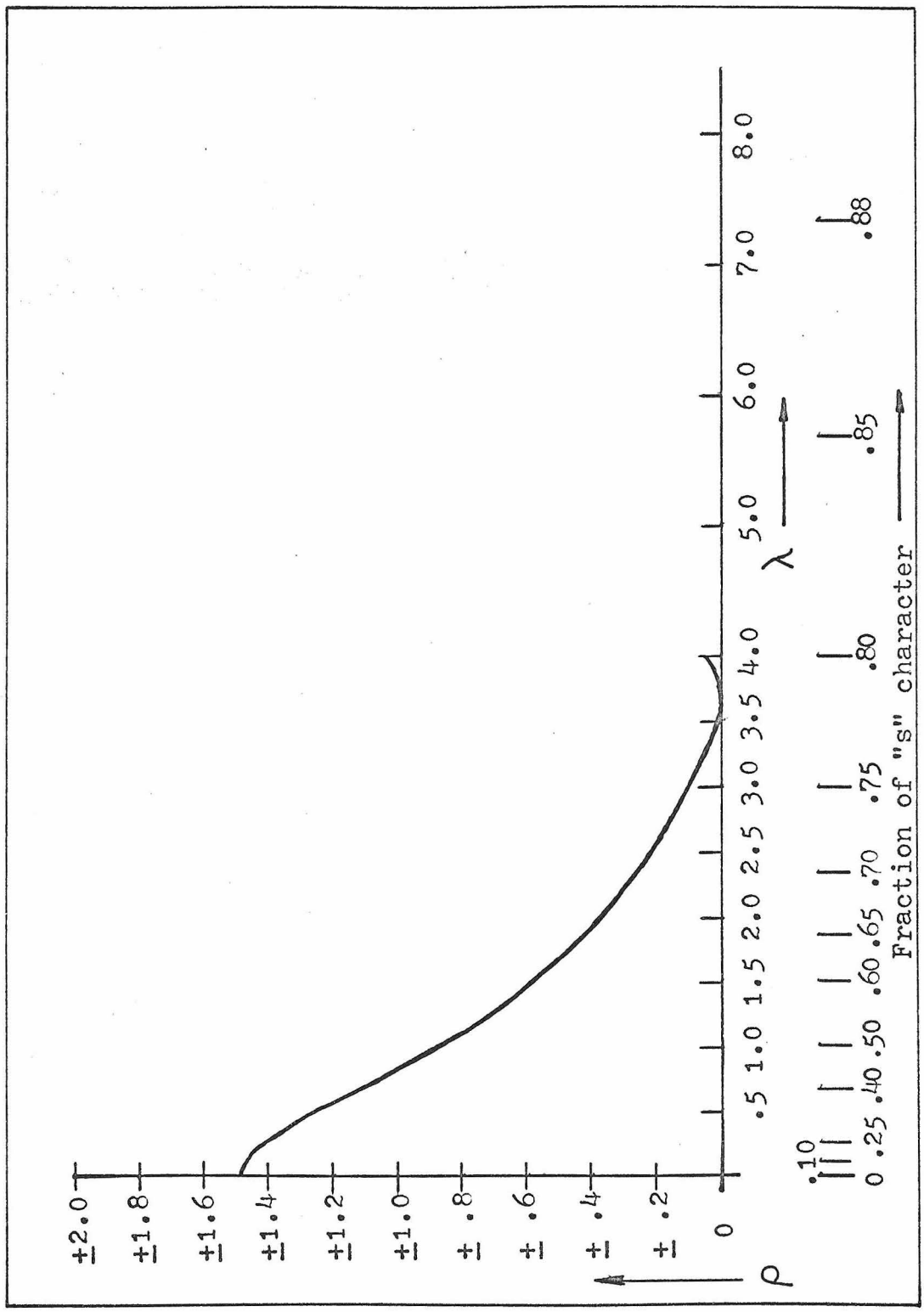

Figure 2. λ versus ρ

BIBLIOGRAPHY

1. V. A. Maroni and T. G. Spiro; Inorg. Chem. 7, 183 (1968).

2. H. A. Levy, M. D. Danford, and P. A. Agron; J. Chem. Phys. 31, 1458 (1959).

3. F. A. Cotton and T. E. Haas; Inorg. Chem. 3, 10 (1964).

4. L. E. Orgel; J. Chem. Soc. (London) 1959, 3815.

5. C. E. Moore, "Atomic Energy Levels," Vol. III, Circular No. 467, N.B.S., U.S. Govt. Printing Office, Washington, D.C., 1958.

6. C. H. Townes and B. P. Dailey; J. Chem. Phys. 17, 782 (1949).

7. H. G. Robinson, H. G. Dehrnelt, and W. Gordy; Phys. Rev. 89, 1305 (1953).

8. L. Pauling, "Nature of the Chemical Bond," 3rd Ed., Cornell Univ. Press; Ithica, N. Y., 1960.

PROPOSITION IV

Although the chemistry of silanes and their derivatives has been in existence for approximately 100 years, surprisingly little is known regarding the mechanisms involving breaking of Si--H or Si--Si bonds. The smaller silanes and their halogen derivatives are either gases at room temperature or extremely volatile liquids. As such they lend themselves well to mass spectrometric studies, and it is proposed to initiate isotopic fractionation studies of reactions involving these molecules to elucidate the nature of the operative reaction mechanisms.

This approach utilizes only natural isotopic abundances and thus avoids the stigma of entirely changing the nature of the system under investigation which is the fate of isotopic enrichment studies. One may also take advantage of the relatively large amount of ^{30}Si ($\sim 5\%$) and obtain fractionation factors, α, not only for D/H ratios, but also for $^{28}Si/^{30}Si$ ratios.

One motivation for this proposal is a recent publication (1) indicating very large differences in α_{Si} for lunar and terrestial silicates as compared with the Si material contained in fossilized organisms (2,3).

These differences are on the order of 5‰ with an experimental error of $\pm$ .08 ‰. As of yet, however,

the characterization by means of isotopic fractionation of even the simplest reactions in Si chemistry has not been done.

A logical starting place would be with the pyrolysis reaction of monosilane

(1) $2SiH_4 \xrightarrow{\Delta} Si_2H_6 + H_2$

and the disproportionation of monohalo derivatives of monosilane

(2) $2SiH_3X \xrightarrow{liq.} SiH_4 + SiH_2X_2$

Current mass spectrometric research (4) on reaction 1 has included an isotopic enrichment study involving equimolar mixtures of SiH_4 + SiD_4 in order to distinguish between 2 proposed mechanisms (5,6) involving, first, the silyl radical

$SiH_4 \longrightarrow SiH_3\cdot + H\cdot$

$H\cdot + SiH_4 \longrightarrow SiH_3\cdot + H_2$

$2SiH_3\cdot \longrightarrow Si_2H_6$

and, second, the silane diradical (analogous to carbene)

$SiH_4 \longrightarrow :SiH_2 + H_2$

$:SiH_2 + SiH_4 \longrightarrow Si_2H_6$

By the absence of SiH_3--SiD_3 in the final product they eliminate the first mechanism; however, a large amount of HD is present which should not be according to the second mechanism. This difficulty and the fact that isotopic enrichment itself may have significantly altered

the reaction mechanism make isotopic fractionation studies extremely attractive. Also, a large amount of disagreement (7,8,9) over the dissociation energy of the Si--Si bond has existed, thus the $\alpha_{^{30}Si/^{28}Si}$ will be quite interesting in view of the fact that a Si--Si bond is being formed. The dependence of α on temperature will be a function of the different activation energies for Si--H bond breaking or Si--Si bond forming depending on which step is the rate determining process.

A similar amount of conjecture exists for reaction 2; the commonly accepted mechanism for this process (10) involves a polynuclear intermediate

$$2SiH_3X \longrightarrow H_3Si\begin{matrix}X\\H\end{matrix}SiH_2X \longrightarrow SiH_4 + SiH_2X_2$$

This does not, however, explain the complication that this reaction (where X = F) is catalyzed by HF (11). Changes in α factors for the reaction with and without HF present could indicate that a second preferential mechanism is operative when HF is in the system.

Hopefully studies of this nature may yield a firmer understanding of Si--H, Si--X, and Si--Si bond breaking and formation processes and can be extended to the higher silanes and their derivatives, and to reaction in more complicated systems.

BIBLIOGRAPHY

1. S. Epstein and H. P. Taylor; Science 167, 533 (1970).
2. J. Reynolds; Geochim. et Cosmochim. Acta 3, 224 (1953).
3. D. Tilles; Geophys. Research 66, 3003 (1961).
4. M. A. Ring, et al.; Inorg. Chem. 8; 2033 (1969).
5. H. Niki; J. Phys. Chem. Phys. 37, 207 (1962).
6. B. H. Mahan and R. Mandal; J. Cham. Phys. 37, 207 (1962).
7. S. R. Gunn and L. G. Green; J. Phys. Chem. 65, 779 (1961).
8. I. M. T. Davidson and I. L. Stephanson; J. Chem. Soc. (London), A, 282 (1968).
9. W. C. Steele and F. G. A. Stone; J. Am. Chem. Soc. 84, 3599 (1962).
10. MacDiarmid; Advan. Inorg. Chem. Radiochem. 3, 207 (1961).
11. J. K. Wolfe and N. C. Cooke; Abstr. 128th Meeting A. C. S. Minneapolis, 1955, 48M.

PROPOSITION V

The $Mo(CN)_8^{4-}$ ion has been of continued interest to the inorganic chemist as it is one of the few examples of a stable eight-coordinate complex involving unidentate ligands. Further, a large number of related eight-coordinate compounds have been prepared from $Mo(CN)_8^{4-}$ by the substitution of one or more ligands (1, 2, 3, 4). This provides a large potential knowledge to be gained concerning the energetics of the eight-coordinate state.

Unfortunately this potential has largely been unrealized due to the difficulties encountered in characterizing these systems. Vibrational spectroscopy which is usually a great aid in structural characterizations has so far been of only limited value in these investigations due to the large uncertainties surrounding the vibrational spectrum of the parent $Mo(CN)_8^{4-}$ ion. It is therefore proposed to undertake a complete normal coordinate analysis of this system with the aid of ^{13}C and ^{15}N substitution and appropriate polarized vibrational spectra in the solid crystalline state.

The structure of $K_4Mo(CN)_8.2H_2O$ has been solved and refined by X-ray diffraction (5, 6) and the structure of the anion is shown below in figure 1.

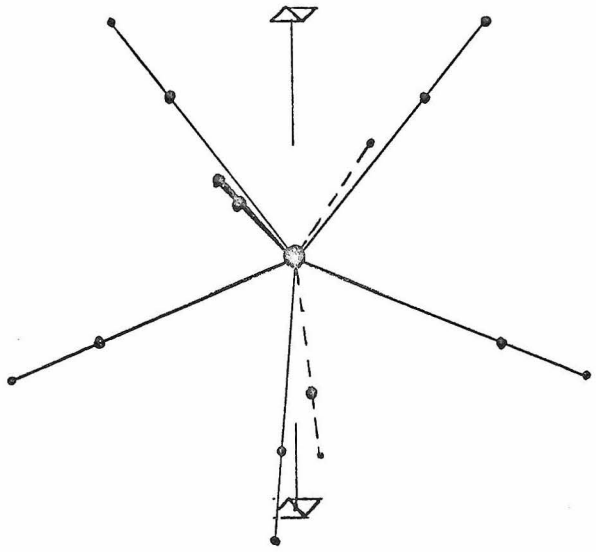

Figure 1. Structure of the $Mo(CN)_8^{4-}$ Ion.

The molecular symmetry is D_{2d} and it is found that the spectra of the CN stretching region (6 expected Raman bands and 4 expected I. R. bands) may be assigned under this symmetry (7, 8, 9, 10, 11). This indicates that interactions between ions in the unit cell may be ignored thus considerably simplifying the effective spectroscopic selection rules which would obtain for the D_{2h} symmetry of the unit cell's space group (12).

It was shown in (9) that excellent crystals of this material may be grown from aqueous solution and it is thus a simple matter to obtain the polarized Raman spectrum (the workers in Reference 9 observed by accident that two of the CN stretching modes showed strong polarizations for their particular experimental orientation, but these results were not discussed or

pursued further).

On the basis of the prevailing D_{2d} symmetry it will be possible to distinguish between A_1, B_2, and E modes. A_2 modes are totally inactive and the remaining B_1 modes will polarize similar to the A_1 modes.

It was also noted in (9) that attempts to obtain polarized I. R. data were hampered by crystals which were too thick. A new technique which is applicable in the case of large crystals is Attenuated Total Reflectance (ATR) spectroscopy (13) which analyzes reflected I. R. light from the surface of a crystal thus making its thickness immaterial. On this basis it will be possible to assign the B_2 and E I. R. active modes.

Very useful structural information may be obtained from the MCN bending and MC stretching regions of the spectrum which lie from 600 to 250 cm^{-1} in general (14). Although modes in this region are very susceptible to intermixing with one another they do possess the advantage of occupying a large energy region compared to the approximately 60cm^{-1} span in which the CN stretching modes are found.

The symmetries of these lower energy modes may be determined from the polarization experiments above, however frequency shifts from isotopic substitution will be necessary to determine the MCN-bend or MC-stretch character of each individual vibration.

Substitution of $^{13}CN^-$ will be most helpful regarding frequency shifts for MCN-bends which should be about $15cm^{-1}$ to lower energy; MC-stretching modes will shift only about $6cm^{-1}$ to lower energy (14). Substitution of $C^{15}N^-$ will aid especially in the determination of MC-stretching character of a given mode as the expected shifts are approximately $6cm^{-1}$ for these vibrations while MCN bending motions should shift only about $2cm^{-1}$ (14).

With this information in hand a reasonable calculation of the normal coordinates of vibration for $K_4Mo(CN)_8.H_2O$ may be obtained. Vibrational spectroscopy may then possibly realize a fuller role in the characterization of this and other related systems.

BIBLIOGRAPHY

1. W. R. Bucknell and W. Wardlaw, J. Chem. Soc. (A), 1927, 2981.

2. A. W. Adamson and J. R. Perumareddi, Inorg. Chem., 4, 247 (1965).

3. J. R. Perumareddi, Z. Naturforch., 21b, 22 (1966).

4. G. Rossman, private communication.

5. J. L. Hoard and H. H. Nordsieck, J. Am. Chem. Soc., 61, 2853, (1939).

6. J. L. Hoard and J. V. Silverton, Inorg. Chem., 2, 235 (1963).

7. S. F. A. Kettle and R. V. Parish, Spectrochimica Acta, 21A, 1087 (1965).

8. R. V. Parish, ibid., 22A, 1191 (1966).

9. K. O Hartman and F. A. Miller, ibid., 24A, 669 (1968).

10. V. H. Stammreich and O. Sala, Z. Elektrochem., 64, 741, (1960).

11. V. H. Stammreich and O. Sala, ibid., 65, 149 (1960).

12. W. B. White and B. A. de Angelis, Spectrochimica Acta, 23A, 985 (1967).

13. A. M. Deane, E. W. T. Richards, and I. G. Stephen, Spectrochimica Acta, 22A, 1253 (1966).

14. L. H. Jones, Inorg. Chem., 4, 1472 (1965).